Model Predictive Control for UAGV Path Tracking in the Presence of Wheel Slip

Author:
Wang, Xu

Publication Date:
2017

DOI:
https://doi.org/10.26190/unsworks/19845

Model Predictive Control for UAGV Path Tracking in the Presence of Wheel Slip

Xu Wang

Thesis submitted for the degree of
Master of Engineering (Research)

School of Mechanical and Manufacturing Engineering
The University of New South Wales

25 July, 2017

PLEASE TYPE

THE UNIVERSITY OF NEW SOUTH WALES
Thesis/Dissertation Sheet

Surname or Family name: Wang

First name: Xu

Other name/s: Annie

Abbreviation for degree as given in the University calendar: ME

School: Mechanical and Manufacturing Engineering

Faculty: Engineering

Title: Model Predictive Control for UAGV Path Tracking in the Presence of Wheel Slip

Abstract 350 words maximum: (PLEASE TYPE)

Investigation of Unmanned Agricultural Ground Vehicles (UAGVs) has been on the increase in recent decades as UAGVs have great potential in agricultural applications and thus are expected to rule farms in the future. The use of UAGVs benefit from not only replacing human operators to do tiresome and even hazardous work and thus reduce danger, but also significantly improving the efficiency to solve food shortages due to the dramatic growth of world. Path Tracking has been an important topic in the development of UAGVs, however the automatic guidance of farm vehicle becomes more difficult and challenging than that of standard mobile robots as farm vehicles are subjected to significant disturbances due to rough terrain and ground engaging operations. The controller of autonomous farm vehicles is required to be sufficiently robust to both guarantee high path tracking accuracy and stability.

This thesis mainly researches path tracking control methods for three kinds of UAGVs in the presence of significant wheel slip. In path tracking, UAGVs are guided to follow a desired path from an initial position while the controller keeps minimizing offsets with respect to the reference path. To achieve the accuracy required in agriculture, this work utilizes offset models derived based on kinematic models, which take both lateral and longitudinal slips into account. A model predictive controller with receding min-max optimization is then proposed to address the problem of wheel slip in UAGVs. This adaptive min-max model predictive controller provides both robustness and adaptation for path tracking.

The superior performance of the proposed controller is verified by kinematic simulation, dynamic simulation as well as field testing, compared to that of the classical model predictive control. Then, the proposed controller is also compared with a well-known robust sliding mode controller and a well-performing backstepping controller, which is carried out by implementing controllers on a UAGV at Elizabeth Macarthur Agricultural Institute. Results from simulations and experiments validate that the proposed adaptive min-max model predictive controller ensures the required accuracy and robustness in the presence of wheel slip without any slip estimation or estimation.

FOR OFFICE USE ONLY

Date of completion of requirements for Award:

COPYRIGHT STATEMENT

'I hereby grant the University of New South Wales or its agents the right to archive and to make available my thesis or dissertation in whole or part in the University libraries in all forms of media, now or here after known, subject to the provisions of the Copyright Act 1968. I retain all proprietary rights, such as patent rights. I also retain the right to use in future works (such as articles or books) all or part of this thesis or dissertation.

I also authorise University Microfilms to use the 350 word abstract of my thesis in Dissertation Abstract International (this is applicable to doctoral theses only).

I have either used no substantial portions of copyright material in my thesis or I have obtained permission to use copyright material; where permission has not been granted I have applied/will apply for a partial restriction of the digital copy of my thesis or dissertation.'

Signed

Date

AUTHENTICITY STATEMENT

'I certify that the Library deposit digital copy is a direct equivalent of the final officially approved version of my thesis. No emendation of content has occurred and if there are any minor variations in formatting, they are the result of the conversion to digital format.'

Signed

Date

ORIGINALITY STATEMENT

'I hereby declare that this submission is my own work and to the best of my knowledge it contains no materials previously published or written by another person, or substantial proportions of material which have been accepted for the award of any other degree or diploma at UNSW or any other educational institution, except where due acknowledgement is made in the thesis. Any contribution made to the research by others, with whom I have worked at UNSW or elsewhere, is explicitly acknowledged in the thesis. I also declare that the intellectual content of this thesis is the product of my own work, except to the extent that assistance from others in the project's design and conception or in style, presentation and linguistic expression is acknowledged.'

Signed

Date

I would like to dedicate this thesis to my loving parents and my husband.

Acknowledgements

During the writing of this thesis, there were many people who have provided valuable suggestions and encouragement for me. I would like to take this chance to give my immense gratitude to them.

To my supervisor, Associate Professor Jayantha Katupitiya for providing me with not only academic support for my research but also emotional support for my life. His professional knowledge and experiences eased the process of completing this research.

To Javad Taghia who was always there to answer my questions and help me figure out programming problems. He is also a very important friend in life and always helps me out when I feel unconfident.

To our 'Lunch Group' members Lingling Shi and Sharmila Kayastha who are not just my lab partners but also close friends at UNSW. In particular, I would like to appreciate them for revising parts of my thesis.

To Dr. Mark Witty who was willing to talk with me and gave me precious advice on my future study.

To Dr. Ngai Ming Kwok who gave me advice on the improvement of my English.

To Xuesong Li who took time from his busy schedule to read my thesis.

To all my colleagues in the Mechatronics group at UNSW, Penglei Dai, Scarelett Liu, Shilong Liu, Hiranya Jayakody, Michael Woods who mentored me during the study.

To Xue Sun, my best friend, who is always encouraging me when I doubt myself.

Finally to my parents and my husband for their invaluable love.

Abstract

Investigation of Unmanned Agricultural Ground Vehicles (UAGVs) has been on the increase in recent decades as UAGVs have great potential in agricultural applications, and thus UAGVs are expected to rule farms in the future. The use of UAGVs benefits from replacing human operators to do tiresome as well as hazardous work, thus reducing the risk. It can also significantly improve the efficiency to solve food shortages due to the dramatic growth of world. Path Tracking has been an important topic in the development of UAGVs, however the automatic guidance of farm vehicle becomes more difficult and challenging than that of standard mobile robots as farm vehicles are subjected to significant disturbances due to rough terrain and ground engaging operations. The controller of autonomous farm vehicles is required to be sufficiently robust to both guarantee high path tracking accuracy and stability.

This thesis mainly researches path tracking control methods for three kinds of UAGVs in the presence of significant wheel slip. In path tracking, UAGVs are guided to follow a desired path from an initial position while the controller keeps minimizing offsets with respect to the reference path. To achieve the accuracy required in agriculture, this work utilizes offset models derived based on kinematic models, which take both lateral and longitudinal slips into account. A model predictive controller with receding min-max optimization is then proposed to address the problem of wheel slip in UAGVs. This adaptive min-max model predictive controller provides both robustness and adaptation for path tracking.

The superior performance of the proposed controller is verified by kinematic simulation, dynamic simulation as well as field testing, compared to that of the classical model predictive control. Then, the proposed controller is also compared with a well-known robust sliding mode controller and a well-performing backstepping controller, which is carried out by implementing controllers on a UAGV at Elizabeth Macarthur Agricultural Institute. Results from simulations and experiments validate that the proposed adaptive min-max model predictive controller ensures the required accuracy and robustness in the presence of wheel slip without any slip measurement or estimation.

Table of Contents

List of Figures

List of Tables

Chapter 1

Introduction

1.1 Background and Motivation

The development of Unmanned Ground Vehicles (UGV) has been the hot subject for many years due to great potential for applications in mining, defence and industrial production. In these applications, UGVs not only take over the work of humans to operate in dangerous or inconvenient environments, but also see an improvement in the operational efficiency. The above factors have led to a rapid development of efficient and effective UGVs, and researchers keep investigating applications of UGVs in more areas to perform more complex and challenging work.

In the near future, UGVs are expected to revolutionize the whole farming system worldwide, which can perform farming tasks now done by humans. For example, Unmanned Agricultural Ground Vehicles (UAGVs) that can accurately follow predefined paths can be used to plant the crop and then repeatedly revisit the growing crop accurately for crop management including growth monitoring and fertilizer, herbicides and pesticide application. Highly accurate autonomous machines can apply fertilizers, herbicides, and pesticides with greater spatial precision leading up to plant level care instead of field level care thereby bringing in significant cost savings due to reduced fertilizer and chemical usage. In addition, the use of autonomous vehicles addresses the skilled operator shortage, reduces the labour costs and improves occupational health and safety standards of operators [77].

Path tracking is one of the most important tasks for UAGVs. It controls the UAGV to follow a predefined reference path from an initial position under certain conditions. However, ensuring accurate operation of autonomous agricultural vehicles is a challenging and complex task. The primary reason is that UAGVs operate on rough terrain, which at times can be sloping and undulating. Moreover, they carry out ground engaging operations such as ploughing. These conditions often lead to inevitable slip at the front and rear wheels in both lateral and longitudinal directions which can result in poor performance. Currently, many path tracking systems do not take this sliding phenomenon into account when designing path tracking controllers so the desired accuracy is difficult to achieve. Therefore it is important to design a robust controller for UAGVs to address the problem brought by high level of uncertainties in the fields.

Generally, there are two kinds of UAGVs, Tractor only and Tractor with Implements. In the past decades, research on the Tractor only system was carried out more, whereas recently the demand on the tractor-trailer system is increasing due to its broader applications. For example, seeding is an agricultural application which cannot be well implemented by a tractor only system. However, most of previous studies related to tractor-trailer type vehicles only concentrated on passive implement. In fact, most of farming tasks are carried out by the implement (trailer) rather than the leading vehicle (tractor), which indicates that path tracking accuracy of the implement plays a more important role. Thus, path tracking control of the tractor-trailer model needs to be researched further.

1.2 Objectives

The main objectives of this research completed are listed as follows:

1. To propose a new control approach in the presence of slip for farm vehicle path tracking so that the accuracy can be guaranteed although vehicles traverse the farmland with the high-level of uncertainties.

2. To extend the proposed method to three different types of farm vehicles, namely tractor, tractor-trailer and tracked vehicle-trailer.

3. To validate the proposed control method and compare it with other well functioning control methods through both simulation and field experiments.

1.3 Contributions

A novel robust model predictive controller is proposed to address the problem of wheel slip in three kinds of farm vehicles. Classical model predictive controller is improved to an adaptive min-max model predictive controller which can provide robustness as well as adaptation. The superior performance of the proposed controller is verified in both simulation and field experiments in comparison to that of the classical model predictive control method. Then, the proposed controller is compared with a well-known adaptive and robust sliding mode controller and also with a well-performing backstepping controller reported in the literature. These comparisons are carried out by implementing the controllers on a farm tractor in field experiments. The experimental results show that the proposed adaptive min-max model predictive controller ensures the accuracy and robustness in the presence of wheel slip. Furthermore, the autonomous technologies presented in this thesis can be employed in other industries such as road construction in civil engineering, mining and defence.

The following papers have been published or submitted during the production of this thesis:

1. X. Wang, J. Taghia and J. Katupitiya, “Robust model predictive control for path tracking of a tracked vehicle with a steerable trailer in the presence of slip”. In 5^{th} IFAC Conference on Sensing, Control and Automation Technologies for Agriculture(AGRICONTROL 2016), Seattle, WA, USA, August 14-17, 2016.

2. J. Taghia, X. Wang, S. Lam and J. Katupitiya, “A sliding mode controller with a nonlinear disturbance observer for a farm vehicle operating in the presence of wheel slip”, Autonomous Robots, vol.41, no.1, pp.71-88, 2017.

3. Q. F. Tan, X. Wang, J. Taghia and J. Katupitiya, “Force Control of 2WS4WD Vehicles Using MPC and SQP for Improved Path Tracking”, International Journal of Advanced Robotic Systems, conditionally accepted.

4. X. Wang, J. Taghia and J. Katupitiya, “Adaptive min-max model predictive control for field vehicle guidance in the presence of wheel slip”, a book chapter in Robotics and Mechatronics for Agriculture by CRC Press/Taylor & Francis Group, submitted.

1.4 Thesis Outline

This thesis is organised into chapters as follows:

Chapter 2 provides a thorough review of previous literature in terms of the future of farming, farm vehicle model as well as control methods including PID control, robust control and model predictive control.

Chapter 3 proposes an adaptive min-max model predictive controller for path tracking control of tractor in the presence of slip. The performance of the proposed controller is evaluated with extensive simulation incorporating kinematic simulation, dynamic simulation and real field experiments in which the performance of the AMM-MPC is compared with that of the classical MPC. Moreover, the proposed controller is compared with two successful implementations of other forms of robust nonlinear controllers in field experiments on a typical farm.

Chapter 4 extends and applies the proposed control method developed in Chapter 3 to a tractor-trailer system used in autonomous farming in the presence of slip. The proposed controller is validated by comparing its performance with the performance of the trailer in the absence of controller as well as the performance of the classical model predictive controller.

Chapter 5 presents a robust and adaptive MPC controller for path tracking control of a tracked vehicle pulling a steerable trailer in the presence of slip. The kinematic model of a tracked vehicle pulling a trailer is linearised by a method different from previous two chapters. A realistic dynamic simulation platform is used to evaluate the performance of the proposed controller that is compared with the performance of min-max MPC and SMC.

Finally, Chapter 6 summarizes the work performed in the production of this thesis and provides suggestions for the direction of future work that could be explored.

Chapter 2

Literature Review

This chapter gives an extensive review of past contributions to path tracking for UGVs. Section 2.1 surveys the future of farming in terms of using autonomous technology. This is then followed in Section 2.2 by a review of two common models of UAGVs. A survey of the current control methods of guidance control for UAGVs is presented in Section 2.3. Finally, in Section 2.4, a summary is presented that no effective solution has yet been produced which fully achieves the objective of this thesis.

2.1 Future of Farming

Food and agriculture are fundamental to human survival and it was the birth of agriculture that laid down the basis for human civilisation. However, it is predicted that the world will face widespread food shortages due to the dramatic growth of world population without a comparable increase in farmworkers in the near future [23]. The research predicted that the world population will be 34 percent higher than today's population, reaching 9.1 billion by 2050. Therefore, agricultural efficiency has to be improved through farm machinery and equipment. Unmanned Agricultural Ground Vehicles(UAGVs) are seen as an effective strategy that pushes forward high efficiency production by using high technology such as observing and measuring in crops, thus becoming an trigger for the development of UAGVs.

Besides above, the second trigger would be the high labour cost in farming, especially for Australia, since Australian farm labour costs are relatively higher than any other countries worldwide. To cope with this issue, the usage of UAGVs is expected to reduce the amount of human labour and meanwhile improve the overall efficiency of the production process. Finally, UAGV drivers are usually exposed to fatigue and long driving hours in harsh weather which is a risk factor in agricultural vehicle accidents, whereas self-driving vehicles will increase driver safety. Therefore, all reasons above make the research of UAGVs become more and more important. The meaning of UAGVs is summarized as follows:

1. Compared with limited human ability, automatic farming can implement more accurate operation.

2. Autonomous operation can reduce required human labour on the field.

3. The labour cost can be reduced while the efficiency can be increased in farms.

4. Safety can be improved in accomplishing hazardous tasks, e.g. handling and spraying poisonous pesticides.

5. The overlap of fertilizer spraying can be solved by increasing guidance accuracy, which is environmental-friendly.

Actually, autonomous mobile robots have been widely and successfully used in various fields such as military, mining, transportation and industry fields to provide services. The research of autonomous mobile robots in mining can be found in [62] which proposed an autonomous navigation system - opportunistic localization for a 30 tonne Load-Haul-Dump truck. Bagnell [8] designed a navigation algorithm for a military vehicle named Crucher. In this study a vision system was used to provide perception of the terrain. Ch.K. Volos

[78] presented a chaotic path planning generator based on a nonlinear circuit, which was implemented in military autonomous mobile robots to cover a terrain. Duff [17] used an autonomous vehicle in mining industry where an underground autonomous mining vehicle was operated in an uncertain and hazardous environment of mines. Autonomous vehicles used for the surveillance of terrains can be found in [48, 49], and a floor-cleaning robot in domestic environments was researched in [55]. Recently, a number of guidance and auto steering systems have been commercially adopted in industry. For example, one Chinese courier company started using auto-steering robots to efficiently sort and carry parcels at the warehouse [47]. Kawasaki robotics made autonomous robots which are specifically designed for cleaning the room as well as auto-steering robot arms used in industries. Considering benefits brought by these robots, demand for auto steering systems is expected to rise worldwide during the forecast period from now to 2020. The success of autonomous mobile robots in these areas laid the foundation for the research on unmanned vehicles in agriculture.

In the field of farming, the research has shown many possible applications of autonomous vehicles, such as harvesting, weeding, fertiliser spraying, seeding and hoeing. E.J. Van Henten et al. [76] reported a concept of an autonomous vehicle used for harvesting cucumbers in greenhouse. Moreover, harvesting not only includes picking fruits but also the transportation of large quantities of fruits to the main storage area. The experimental results showed the autonomous vehicle can pick more than 80% of the cucumbers in greenhouse without human interference. R. Eaton et al. in [18, 20] presented a relatively complex precision autonomous farming system which was a foundation for precision seeding and weeding operation or setting guidelines for agricultural vehicles to follow, such as the most appropriate farm layout, dosage types as well as levels for levels for fertilizer, herbicides and pesticides. Astrand [5] studied row-following system based on computer vision for an autonomous agricultural machinery. Therefore, the potential for UAGVs to perform farm work is huge and this field needs more investigation.

Guidance for UAGVs is the main topic of this thesis. Although different automatic farm vehicles are used in different ways, all these vehicles contain the guidance part of farm vehicles which is the basic component of an autonomous vehicle. In general, farm vehicles guidance systems consist of at least three parts - sensor, controller and actuator. Sensor is used to measure the position of the tractor or the trailer for the system. Controller is then used to create an input such as a steering angle to control the vehicle. Finally, actuator is the component which is responsible for controlling the vehicle and trailer to move, such as the front and rear axle.

However, the task of farm vehicle guidance in highly uncertain and unknown environment is not trivial but rather difficult. One of the main difficulties is the uncertain wheel slip, which makes the control design very challenging. Consequently, building an accurate model and providing a robust and reliable controller which can be adaptive to environmental changes are very demanding. In addition to the above, safety and regulations are very challenging for autonomous operations. I know that a number of countries have established relevant departments to work on this area. For example, California's Department of Motor Vehicles (DMV) proposed regulations about operating autonomous vehicles in April, 2017. In fact, It is rather difficult to set up rules for autonomous vehicles due to rapid changes and diversity of autonomous technologies.

2.2 Farm Vehicle Model

The first step towards controller development is modelling. Two types of models can be used for controller development, the kinematic models or the dynamic models. Even though dynamic models are more complex, they actually are more accurate than kinematic models especially when the vehicles operate with high accelerations. However, dynamic models are more specific to a given system than kinematic models, which are more general and easy to use. Nevertheless, it has been shown that, for vehicles operating at low speeds with low accelerations such as UAGVs, the kinematic models are accurate enough for designing path following controllers [81]. Thus, kinematic models of two types of UAGVs will be investigated in this section.

2.2.1 Tractor

To fulfil the accuracy of guidance in agricultural applications, the tractor position should be precise enough which is usually achieved by installing Real-time Kinematic Global Positioning Systems(RTK-GPS) sensors. Details can be found in the literature [9, 24, 41]. Then, whether the vehicle model is accurate or not is another factor related to the guidance accuracy. A number of kinematic models of tractor systems based on non-slip assumption have been derived in previous research [51, 66, 74, 82]. However, this is not a valid assumption in the agricultural environment because slip is significant and inevitable. Afterwards, researchers started to take sliding phenomena into account but modelling of the slip is very challenging in terms of agricultural fields. It is because slip is not only affected by the terrain properties but also other parameters such as the speed and the curvature of the desired path. As an initial approach, in [43, 44], Lenain et al. proposed an extended kinematic model incorporating a rear side slip angle, and a front side slip angle to take the slip effects into account. Although the longitudinal slip velocity was not included in the model, there was a useful strategy in this study that was the estimation of front side sliding angle parameters by use of an "Internal Model Adaptive Scheme". A more comprehensive kinematic model was then introduced by Fang et al. in [22]. In this model, a lateral slip velocity perpendicular to the velocity of the field vehicle was added to the front wheels as a steering bias. The new sliding parameter was able to include the neglected longitudinal tires' sliding. As a further extension, a kinematic model in [30] was derived with three slips - lateral slip velocity, longitudinal slip velocity and steering slip angle. An offset model was then proposed which was an extended form from the kinematic model. The error model was the result of the lateral and orientation difference between the desired path and the actual position, which was a more realistic kinematic model for a tractor.

2.2.2 Tractor-trailer

In recent decades, the demand of tractor-trailer systems is increasing as the implement or trailer has more possibilities in performing farm tasks. The trailer can be either installed in the front of a tractor or pushed by the tractor. However, in this thesis, only trailers placed at back are discussed. In a tractor-trailer system, the tractor is to deliver a high tractive force for the purposes of pulling the trailer. Generally, there are two kinds of trailer: passive trailer and active trailer. 'Passive' means no steering capabilities on the side of the trailer or the implement side. The driving force is applied just on the tractor side; so, there is no propulsion on the trailer side. By contrast, an active trailer means that it can deal with an extra steering mechanism, which is on the trailer side of the system. Adding steering capabilities on the trailer side increases manoeuvre of the vehicle in the field also increases the stability and robustness of the path following in agricultural environment.

Ridley et al. [61] developed a kinematic model for a Load haul Dump vehicle used for underground mining operations such as transporting ore in dangerous environment. The vehicle was operating with a low speed of 10 km/h and cyclically travelling along a round path by controlling the hitch angle. The control design was based on a linear kinematic model without slip involved. The simulation results showed the feasibility of this autonomous vehicle under the low speed. In [4], A. Astolfi et al. proposed a path tracking controller for a tractor pulling a passive trailer to follow rectilinear and circular paths. However, it only reported simulation results of the circle reference path which does not fit the situation in agriculture. In [15], DeSantis et al. presented development of a tractor-trailer model.

In this work, there were two new states: steering angle which is equal to the propulsion for steering control and vehicle velocity that is equal to combination of mass, geometrical parameters, forces of the vehicle. Then, in [16], path tracking control for a tractor-trailer (on-axle)-trailer (off-axle) were developed by DeSantis et al and forward as well as reverse motion were considered in this work. In [6], Backman et al. developed a path tracking control method for the tractor-trailer system where the drawbar of the trailer was controlled by a hydraulically active joint. However, this research assumed that the ground is ideal and sliding effects do not exist, which is not true in the real world. Then, the work presented in [7], took the wheel slip into account and used extended Kalman filter to compensate for the slippage. However, this approach was not robust due to the assumption of the Gaussian distribution of slip, which was not a reliable assumption. In [65], a steerable trailer was considered, similar to [11, 54], and still there was no slip considered in the modelling. In [54], a multi-steered n-trailer is considered by OConnor et al. The kinematic model was derived for the n-trailer scenario and there was no slip involved in the derivation. Although this study was interesting for covering concept of multi-steerable n-trailers, the linearisation technique presented in this paper was not applicable in our study. As indicated before, the slip parameters must be included in the modelling and our control strategy. There are also studies on dynamic modelling for tractor-trailer systems. In [33], Keymasi et al. proposed a dynamic model in the presence of uncertainties for a wheeled mobile robot towing a trailer. Finally, the work carried out by Campion et al. [12] gave classification of kinematic as well as dynamic models for wheeled mobile robots.

In this work, the offset model presented in [30] is used to design the path tracking controller. Slip is considered as slip velocity in the kinematic model. The tractor had three slips, longitudinal slip at rear wheels, lateral slip at rear wheels and slip angle at front wheels, while the trailer had a lateral slip velocity at rear wheels which are steerable.

2.3 Control Methods

After reviewing vehicle modelling, another key objective is designing a path tracking controller for UAGVs in this thesis. The quality of the controller plays an important role in the accuracy of automatic guidance. As can be seen in last section, the kinematic models of UAGVs are highly nonlinear and complex. Moreover, UAGVs are affected by inevitably significant disturbances during tracking the desired path. Based on both factors, advanced and robust control methods are suggested. In this section, control approaches will be reviewed in three parts: linear control, robust control, model predictive control.

2.3.1 Linear control

A Proportional-Integral-Derivative (PID) controller is the most famous linear controller, benefiting from its simple structure and fast response [56]. It has been proved to be feasible in plenty of industrial applications such as controlling industrial robot arms [63], governing the industrial steam turbine [29], the control of industrial hydraulic actuator [64]. A review on applications of classical PID controllers can be found in [39]. In [53], Julio E. Normey-Rico et al. presented a robust PID controller for path tracking of a mobile robot which benefited from the tuning of this simple controller. In [1], Auday Al-Mayyahi proposed a PID controller with an optimal control technique - Particle Swarm Optimization (PSO) to solve the problem of path tracking. In this research, kinematic model as well as dynamic model was utilized and the simulation results showed the error was minimized and the system is globally asymptotically stable. In [2], a simple PID controller and an optimal preview controller were combined to improve precision guidance performance and robustness. Although some improvement were made, disadvantages arose because the slip phenomenon was not considered in the design of control system presented in this study.

However, there are some limitations in these PID controllers. For example, optimal control is generally not provided by PID control and optimization needs to be obtained by using other techniques, which may produce poor performance in controlling. Also, PID control is normally used for the single-input single-output (SISO) case and not applicable for the multi-inputs-multi-outputs case. As a result, the control method in this thesis was expected to be a more advanced control design method.

2.3.2 Robust control

As mentioned before, wheel slip is the interaction between soil and wheels, and affected by tyres as well as speed of UAGVs, terrain properties, and path curvatures. In specific agricultural applications, 5 centimetres accuracy with respect to the reference path is required, although farm vehicles are moving on slope and undulating ground [43]. As the experimental results shown in [42], classical control without considering the sliding deviated the farm tractor from the desired path. To be specific, the highest lateral offset during the slope was 30 cm while errors during the curve varied from 40 cm to 60 cm. The effect brought by slip in field is significant, and cannot be ignored definitely. Thus, robust control is expected to be a good choice for path tracking in agriculture as this control method has the capability to deal with uncertainties and disturbances. Generally speaking, robust control approaches take advantage of the bounds of errors to manage disturbances. The bounds are usually grouped into polytopic and multi-model paradigm [36].

Sliding mode control (SMC) and back stepping control (BSC) are two well-performing robust control methods, and have been widely used in many industrial applications [35, 69, 83]. Both control methods are based on Lyapunov stability analysis, and they perform successfully in the presence of uncertainties and disturbances [37, 68]. A good overview of robust approaches based on their historical time line and importance is provided by Kokotovic [34, 35]. In [14], M.L. Corradini and G.Orlando tackled the problem of trajectory tracking for a two driving wheels mobile robot in the presence of uncertainties. A discrete time sliding mode controller was proposed based on the dynamic model of the robot. In

[28], a sliding mode controller was proposed to enhance the tracking performance of a two-degree-of-freedom robotic manipulator which was subject to external disturbances. In [46], a backstepping controller was designed for a quadrotor helicopter, and simulation results showed this controller stabilized the quadrotor. In [84], L. Z. Li et al. proposed a backstepping controller combined with the direct fuzzy logic system for the turbine steam valve control.

Besides above, research has also been focused on applying robust control in controlling autonomous vehicles. In [71], J. Taghia and J. Katupitiya proposed a sliding mode controller with a disturbance observer for a steerable tractor-trailer with slip effects accounted. The controller contained an on-line estimation algorithm called recuMrsive least squares (RLS) of slip velocities during the tractor-trailer traverses the farmland, which brought robustness as well as adaptation ability. The tractor-trailer in this work traversed at a low speed of 3 m/s and the absolute value of lateral offsets in the simulation were within 2 cm. However, there was no estimation about the trailer and this approach is sensitive to unmatched uncertainties in the system model. In [31], V. Huynh et al. presented a PI and backstepping controller for a tractor-steerable trailer system which was guided in both lateral and longitudinal directions by using offset models. It was assumed that the lateral slip velocity at the rear of the trailer was larger than it at the tractor side. However, in this work, sliding parameters were selected as constant value which was not correct in the real world. From the simulation results, it could be seen that the error of trailer was a constant value around 40 cm. In [22], H. Fang et al. proposed a robust adaptive control for the kinematic model with slip of the farm tractor. This work introduced two slip parameters, the lateral sliding velocity at and bias of the steering angle at front wheels whereas the longitudinal tire sliding was neglected. However, when the reference path changed to a trajectory used in the real agriculture application, the lateral offsets were almost 52 cm at the curve, and the lateral offsets at the straight lines were larger than 12 cm. As a result, accuracy at both straight lines and curves needs to be improved in the path tracking of UAGVs.

2.3.3 Model predictive control

A very promising control method for achieving high precision path tracking is Model Predictive Control (MPC) due to its receding optimization and predictive ability. In the past, MPC has been mainly used in many industrial applications especially chemical fields such as oil-refining and power systems, while recently, MPC is also found to be a successful controller in the area of food processing, automation and aerospace areas due to its feasibility, stability and good performance [52]. For MPC technology, [27] is a very comprehensive books, which introduces linear and nonlinear MPC knowledge in detail. In [58], J. Richalet described two classical applications of model based on predictive control. One was a typical crude oil distillation tower which was a slow process unit; the other was a two degree freedom servo turret. In [57], S. Joe Qin and Thomas A. Badgewell gave an overview of MPC technology, and the industrial survey showed the number of MPC applications has almost doubled in four years from 1995 to 1999. In [3], M. Arnold and G. Andersson proposed a MPC strategy for multi-carrier energy systems to keep the consequences of forecast uncertainties at acceptable levels. The operation costs were reduced by implementing the controller.

In the recent years, researchers have shown an interest in applying MPC to path tracking control in agriculture, whereas research results are not satisfactory. One of the major problems is the absence of managing wheel slip in farming environments. Moreover, classical MPC is not inherently robust [25], therefore it is necessary to design a MPC algorithm taking the wheel slips into account. In [82], MPC was developed for controlling a mobile robot, where the path tracking errors were penalized by a quadratic cost function. In [7, 32], Backman et al. presented a MPC law to direct a tractor-trailer kinematic model without slips accounted. Again, model without slips was not very good in realistic applications. In [26] , Garcia presented a controller based on MPC for a commercial vehicle and also observed with the EKF filter, not including slips. Then, the work presented in [43], developed a model predictive controller for wheeled farm tractor path tracking in the presence of slip. The control design was starting from a nonlinear control approach taking slip into account. The rear side slip angle and the front side slip angle were estimated by a difference value which was only brought by slip. This difference was the error between the actual position measured by RTK-GPS and the predicted position computed by kinematic models without slip. Then a predictive controller was added to reduce the transient overshoots brought by actuation delays and vehicle large inertia. The experimental results showed the maximum value of lateral offset was around 20 cm and most of guidance accuracy stayed in the range between -15 cm and 15 cm during the path tracking. However, the noise levels on the two estimated slip angles were problematic and the objective function of the model predictive control law was only to ensure the convergence of lateral offset to zero whereas there is also an orientation offset which can affect the accuracy of path following.

The work reviewed above was only using a classical model predictive controller, whereas in [13] proposed a robust MPC method which incorporated robustness into MPC without online estimation. The strategy was called minimax which means the worst-case considers all possible disturbances including the worst case. However, at times, this method may cause overcompensation because the worst case does not occur always. To avoid overcompensation, Scokaert et al. in [67] proposed a min-max feedback MPC control method for a linear system. Although this method leads to a better performance than min-max MPC, it is computationally intensive. In [45], J. Löfberg proposed a robust model predictive control for uncertain constrained linear discrete-time systems. In [60], Arthur proposed two different robust model predictive control methods involving imperfect information. One was robust output feedback MPC, the other was robust MPC with time delay. Both were proved feasible in this study. In [40], a robust MPC achieved by using tube was proposed and it can benefit linear and time-invariant systems. For details, a brief review of robust MPC formulation was given in [59].

2.4 Summary

This chapter has surveyed the future of farm, farm vehicle models and different control approaches for path tracking. The review of farming in the future shows that UAGVs are expected to be a powerful tool to solve food shortages due to the dramatic growth of world's population in the future. The development of UAGVs is not only meaningful in increasing efficiency but also reducing the labour cost as well as being environmental-friendly.

The review of farm vehicle models shows the importance of the accurate vehicle model for the performance of the controller. Though dynamic models are more accurate, kinematic models are chosen because it is easy to implement and good enough when vehicles operate at low speeds with low accelerations. Thus, the review was focused on kinematic models of farm vehicle. There have been several contributions on kinematic modelling made by researchers, although some disadvantages exist in some way, e.g. no slip considered in the model.

Finally, the review of control methods shows the importance of having robustness in order to deal with significant disturbances in fields. The review is conducted from linear control to model predictive control. Linear control is not suitable for highly nonliear vehicle models although this method is simple and has fast response. Then, SMC and BSC are two robust control methods based on Lyapunov functions against uncertainties, however, the accuracy is not satisfactory in terms of path tracking in agriculture. Compared with MPC which does not have robustness, robust model predictive control has more potential to be a good path tracking controller in achieving high accuracy of path tracking due to the receding optimization as well as robustness.

Chapter 3

Model Predictive Control for Tractor Path Tracking

In general, autonomous guidance is classified into two categories: path tracking and trajectory tracking. In path tracking, UAGVs are driving along a predefined path starting from a given initial position without a timing law, while in trajectory tracking control, UAGVs must follow a geometric trajectory with a specified timing law. In the auto-farming applications, path tracking can fulfil more production duties than trajectory tracking, thus research presented in this thesis focuses on path tracking.

As mentioned before, accurate path tracking control for UAGVs is very challenging in farm environment, as UAGVs are subject to significant disturbances from rough soil. Hence, path tracking control of UAGVs requires the controller to be sufficiently robust to guarantee high path tracking accuracy and stability. By considering above requirements, model predictive control is found to be a very promising control method to acquire high precision due to its receding optimization and predictive algorithm. However, when the vehicle is suffering from significant external disturbances, the accuracy goes beyond reasonable limits. For example, errors in the curves can be over 50 cm and errors in the straight lines can be over

20 cm. To bring any improvement, an adaptive min-max model predictive controller was proposed to provide robustness and adaptation in guidance control.

This chapter presents two path tracking control algorithms for a tractor system, classical MPC and robust MPC. The structure of this chapter is that, in Section 3.1, a kinematic model of a tractor that takes into account sliding and an offset model extended from this kinematic model are built. In Section 3.2 feedback linearisation is used to linearise the highly nonlinear offset model. In Section 3.3 previous work about classical model predictive control design is reviewed. The classical model predictive controller will later be improved to deliver better performance. In Section 3.4, presence of a new predictive controller, by considering the significant sliding phenomenon, an adaptive min-max model predictive control (AMM-MPC) is derived and comparative simulation as well as experiments are presented to validate the proposed control law.

3.1 System Modelling and Description

The vehicle in this chapter is a 2WD2WS tractor, and it is presented as a bicycle model where two front steered wheels are simplified into one steered wheel shown in Figure 3.1. The vehicle wheelbase is l_t ,and the tractor is driven at rear wheels with a longitudinal velocity v while steered at the front wheel with a steering angle δ. Other related variables as well as parameters are shown in Table 3.1.

3.1.1 Kinematic model

The tractor's states are defined by a vector $\mathbf{p}_t = [x_t, y_t, \theta_t]^T$, where ($x_t$,$y_t$) represents the position of the tractor (middle point O') in the global coordinate xOy and θ_t represents the heading of the tractor. As shown in Figure 3.1, the tractor is subject to three wheel slips, lateral slip velocity v_{sr}, longitudinal slip velocity v_{lr} and slip angle β_f. In detail, the lateral

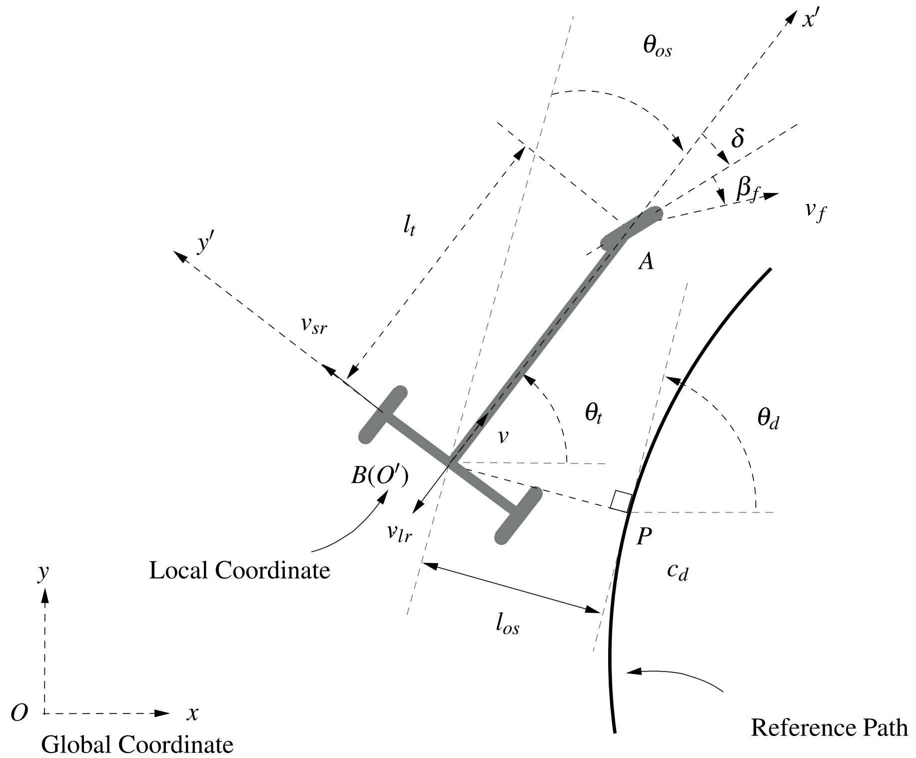

Fig. 3.1 Tractor kinematic model and the reference path.

slip velocity v_{sr} and the longitudinal slip velocity v_{lr} are both located at the rear wheels of the tractor while the slip angle β_f is located at the front wheels of the tractor.

The kinematic equations of the tractor in the presence of slips are derived by using the kinematic model introduced in [30],

$$
\begin{aligned}
\dot{x}_t &= (v - v_{lr})\cos\theta_t - v_{sr}\sin\theta_t, \\
\dot{y}_t &= (v - v_{lr})\sin\theta_t + v_{sr}\cos\theta_t, \\
\dot{\theta}_t &= \frac{v - v_{lr}}{l_t}\tan(\delta + \beta_f) + \frac{v_{sr}}{l_t}.
\end{aligned}
\tag{3.1}
$$

3.1.2 Offset model

In Figure 3.1, path tracking errors between the position of the tractor and the reference path are represented by path offset l_{os} and heading offset θ_{os}. The path offset l_{os} is defined as the

Table 3.1 System description

Variables	Description
c_d	curvature of the reference path
x_t	x-coordinate of point O' in the xOy coordinate
y_t	y-coordinate of point O' in the xOy coordinate
θ_t	heading of the tractor in the xOy coordinate
$\mathbf{v}$	driving velocity vector at point B in the xOy coordinate, $v = \|\mathbf{v}\|$
$\mathbf{v}_f$	front wheel velocity, $v_f = \left\|\mathbf{v}_f\right\|$
θ_d	desired heading angle
δ	steering angle
l_{os}	path offset
θ_{os}	heading offset
$\mathbf{v}_{sr}$	lateral slip velocity at point B, $v_{sr} = \|\mathbf{v}_{sr}\|$
$\mathbf{v}_{lr}$	longitudinal slip velocity at point B, $v_{lr} = \|\mathbf{v}_{lr}\|$
β_f	front wheel slip angle
l_t	vehicle wheelbase
Points	**Description**
A	center of the front axle
B	center of the rear axle
O	origin of global coordinate frame
O'	origin of local coordinate frame (coincides with B)
P	point of intersection of normal from B to the reference path

distance $O'P$ while θ_{os} is defined as the angle $\theta_{os} = \theta_d - \theta_t$. Thus, based on [30], an offset model is as follow,

$$\begin{aligned} \dot{l}_{os} &= -\sigma|v - v_{lr}|\sin\theta_{os} - \sigma\zeta v_{sr}\cos\theta_{os}, \\ \dot{\theta}_{os} &= \frac{v - v_{lr}}{l_t}\tan(\delta + \beta_f) + \frac{v_{sr}}{l_t} - \\ &\quad \sigma|v - v_{lr}|\frac{c_d\cos\theta_{os}}{1 + c_d l_{os}} + \sigma\zeta v_{sr}\frac{c_d\sin\theta_{os}}{1 + c_d l_{os}}, \end{aligned} \tag{3.2}$$

where σ is a direction coefficient. If σ is -1, the vehicle tracks the reference path in a clockwise direction. If σ is +1, the tractor tracks the reference path in a counterclockwise direction. Another coefficient added to the model is ζ which is +1 when the tractor moves forward and -1 when the vehicle moves backward. In this chapter, the tractor is assumed to move forward only, and therefore ζ is always +1.

Compared to the kinematic model (3.1), the offset model (3.2) creates an immediate connection between the position of the tractor and the reference path. Two path tracking errors l_{os} and θ_{os} are controlled by the steering angle δ. According to [43], both l_{os} and θ_{os} can be measured based on a RTK GPS. Thus, this model can be later used for designing a path tracking controller.

3.2 Feedback Linearisation

As seen in Section 3.1.2, the model (3.2) is highly nonlinear, and therefore directly using it in control design is tedious. In order to apply the MPC law developed by using a linear state-space model [79], feedback linearisation based on [34] is thus carried out to convert the highly nonlinear system to a linear system.

To implement feedback linearisation, two assumptions are considered as follows.

Assumption 1 *The longitudinal velocity of the tractor $v > 0$ and satisfies $v > |v_{lr}|$.*

Assumption 1 is valid because the tractor is expected to move forward despite slipping. Based on Assumption 1, the absolute part $|v - v_{lr}|$ in (3.2) is simplified as

$$\sigma|v - v_{lr}| = -\sigma(v - v_{lr}). \tag{3.3}$$

Assumption 2 *The side slip angle β_f at the front wheel of the tractor is small compared to $\delta + \beta_f$.*

Assumption 2 is valid because β_f is generally a small value in practical situations, usually between 0° and 5° [22, 31]. Based on Assumption 2, $\tan(\delta + \beta_f)$ is written as

$$\tan(\delta + \beta_f) \approx \tan\delta + \tan\beta_f. \tag{3.4}$$

Then the overall disturbances d_1 and d_2 are defined, the model (3.2) are rewritten as,

$$\begin{aligned} \dot{l}_{os} &= -\sigma v \sin\theta_{os} + d_1, \\ \dot{\theta}_{os} &= \frac{v}{l_t}\tan\delta - \sigma v \frac{c_d \cos\theta_{os}}{1 + c_d l_{os}} + d_2, \end{aligned} \tag{3.5}$$

where

$$\begin{aligned} d_1 &= \sigma v_{lr} \sin\theta_{os} - \sigma v_{sr} \cos\theta_{os}, \\ d_2 &= -\frac{v_{lr}}{l_t}\tan\delta + \frac{v - v_{lr}}{l_t}\tan\beta_f + \frac{v_{sr}}{l_t} + \sigma v_{lr}\frac{c_d\cos\theta_{os}}{1 + c_d l_{os}} + \sigma v_{sr}\frac{c_d \sin\theta_{os}}{1 + c_d l_{os}}. \end{aligned} \tag{3.6}$$

For cancelling the nonlinearity in (3.5), two new state variables z_1, z_2 and one new control input u_k are defined as

$$\begin{aligned} z_1 &= l_{os}, \\ z_2 &= -\sigma v \sin\theta_{os}, \\ u_k &= -\sigma v \cos\theta_{os}\left(\frac{v}{l_t}\tan\delta - \sigma v \frac{c_d\cos\theta_{os}}{1 + c_d l_{os}}\right). \end{aligned} \tag{3.7}$$

then

$$\begin{aligned} \dot{z}_1 &= z_2 + \omega_1, \\ \dot{z}_2 &= u_k + \omega_2, \end{aligned} \tag{3.8}$$

where

$$\begin{aligned} \omega_1 &= d_1, \\ \omega_2 &= -\sigma v \cos\theta_{os} d_2. \end{aligned} \tag{3.9}$$

Finally, two vectors $\mathbf{z}_k = [z_1 \ z_2]^T$ and $\omega_k = [\omega_1 \ \omega_2]^T$ are defined so that a state-space model is obtained as,

$$\begin{aligned} \dot{\mathbf{z}}_k &= \mathbf{A}_c\mathbf{z}_k + \mathbf{B}_c u_k + \mathbf{D}_c\omega_k, \\ y_k &= \mathbf{C}_c\mathbf{z}_k. \end{aligned} \tag{3.10}$$

where

$$\mathbf{A}_c = \begin{bmatrix} 0 & 1 \\ 0 & 0 \end{bmatrix}, \mathbf{B}_c = \begin{bmatrix} 0 \\ 1 \end{bmatrix},$$

$$\mathbf{C}_c = \begin{bmatrix} \alpha\,\mathrm{sign}(l_{os}) & \gamma\,\mathrm{sign}(\theta_{os}) \end{bmatrix}, \mathbf{D}_c = \begin{bmatrix} 1 \\ 1 \end{bmatrix}.$$

In (3.10), $\mathbf{z}_k$ is the current state; u_k is the control input; and ω_k is the disturbance in the state-space model, where $\mathbf{A}_c$, $\mathbf{B}_c$ and $\mathbf{D}_c$ are defined as above. Moreover, this model has y_k as the output, which is used to represent path tracking errors. In detail, the output y_k depends on the values of α and γ which are gains on l_{os} and θ_{os}, respectively, which means that the output is the summation of two offsets and can change by the proportion of two offsets. For instance, if $\alpha = 1$ and $\gamma = 0$, y_k contains only l_{os} contribution, so the controller solely sends l_{os} to zero. Note that, sign() in $\mathbf{C_c}$ guarantees errors l_{os}, θ_{os} or their combination base on α and γ to be diminished regardless of the signs of l_{os} and θ_{os}.

3.3 Classical MPC for Tractor Path Tracking

3.3.1 Augmented discrete-time state-space model

According the literature [38, 75], the classical MPC algorithm is based on the assumption of pure rolling without sliding, and thus disturbances in the model (3.10) is ignored as

$$\begin{aligned} \dot{\mathbf{z}}_k &= \mathbf{A}_c\mathbf{z}_k + \mathbf{B}_c u_k, \\ y_k &= \mathbf{C}_c\mathbf{z}_k. \end{aligned} \tag{3.11}$$

where

$$\mathbf{A}_c = \begin{bmatrix} 0 & 1 \\ 0 & 0 \end{bmatrix}, \mathbf{B}_c = \begin{bmatrix} 0 \\ 1 \end{bmatrix}, \mathbf{C}_c = \begin{bmatrix} \alpha \operatorname{sign}(l_{os}) & \gamma \operatorname{sign}(\theta_{os}) \end{bmatrix}.$$

The continuous-time state-space model in (3.11) then needs to be discretized as,

$$\begin{aligned} \mathbf{z}_{k+1} &= \mathbf{A}_d \mathbf{z}_k + \mathbf{B}_d u_k, \\ y_k &= \mathbf{C}_d \mathbf{z}_k, \end{aligned} \tag{3.12}$$

where $\mathbf{A}_d$, $\mathbf{B}_d$, $\mathbf{C}_d$ are discrete counterparts of $\mathbf{A}_c$, $\mathbf{B}_c$, $\mathbf{C}_c$ with respect to sampling interval Δt.

Then the linear state-space model in (3.12) is converted to an augmented model with an embedded integrator based on [79] as follows,

$$\Delta \mathbf{z}_k = \mathbf{z}_k - \mathbf{z}_{k-1},\ \Delta u_k = u_k - u_{k-1}, \tag{3.13}$$

then the augmented model is obtained as,

$$\begin{bmatrix} \Delta \mathbf{z}_{k+1} \\ y_{k+1} \end{bmatrix} = \begin{bmatrix} \mathbf{A}_d & \mathbf{o}_d^T \\ \mathbf{C}_d \mathbf{A}_d & 1 \end{bmatrix} \begin{bmatrix} \Delta \mathbf{z}_k \\ y_k \end{bmatrix} + \begin{bmatrix} \mathbf{B}_d \\ \mathbf{C}_d \mathbf{B}_d \end{bmatrix} \Delta u_k, \tag{3.14}$$

where $\mathbf{o}_d = [0\ 0]$.

To simplify, the vector $\mathbf{x}_k = [\Delta \mathbf{z}_k^T\ y_k]^T$ is defined and (3.14) is rewritten as,

$$\begin{aligned} \mathbf{x}_{k+1} &= \mathbf{A}\mathbf{x}_k + \mathbf{B}\Delta u_k, \\ y_k &= \mathbf{C}\mathbf{x}_k, \end{aligned} \tag{3.15}$$

where

$$\mathbf{A} = \begin{bmatrix} \mathbf{A}_d & \mathbf{o}_d^T \\ \mathbf{C}_d \mathbf{A}_d & 1 \end{bmatrix}, \mathbf{B} = \begin{bmatrix} \mathbf{B}_d \\ \mathbf{C}_d \mathbf{B}_d \end{bmatrix}, \mathbf{C} = \begin{bmatrix} \mathbf{o}_d & 1 \end{bmatrix}.$$

In (3.15), $\mathbf{x}_k \in \mathbb{R}^{3\times1}$, $y_k \in \mathbb{R}^{1\times1}$, $\Delta u_k \in \mathbb{R}^{1\times1}$ denote the state, the controlled output, the augmented control input, respectively.

3.3.2 Prediction of state and output variables

The basic idea of model predictive control is to calculate the future outputs together with the future control inputs by using the current states that are measurable and minimizing an objective function to obtain the optimal control trajectory.

This whole process is shown in Figure 3.2. To begin with, at the sampling time k, $k \geq 0$, the current state is assumed as $\mathbf{x}_{k|k}$, which is the same as $\mathbf{x}_k$ mentioned earlier. Using $\mathbf{x}_{k|k}$, the future states are predicted for N_p sample times which is called the prediction horizon. The state $\mathbf{x}_{k+n|k}$ denotes the predicted state at $k+n$, predicted using $\mathbf{x}_{k|k}$ at sampling instant k. The number of control inputs to obtain the future outputs is N_c which is called the control horizon. Note that, $N_p \geq N_c$, preferably, $N_p > N_c$.

To obtain a convenient notation, vectors are introduced to denote future states $\mathbf{X}$, future outputs $\mathbf{Y}$, future control inputs $\Delta\mathbf{U}$ as,

$$\begin{aligned}
\mathbf{X} &= \left(\mathbf{x}_{k+1|k}\ \mathbf{x}_{k+2|k}\ \mathbf{x}_{k+3|k}\ \cdots\ \mathbf{x}_{k+N_p|k}\right)^T \\
\mathbf{Y} &= \left(y_{k+1|k}\ y_{k+2|k}\ y_{k+3|k}\ \cdots\ y_{k+N_p|k}\right)^T \\
\Delta\mathbf{U} &= \left(\Delta u_{k|k}\ \Delta u_{k+1|k}\ \Delta u_{k+2|k}\ \cdots\ \Delta u_{k+N_c-1|k}\right)^T.
\end{aligned} \tag{3.16}$$

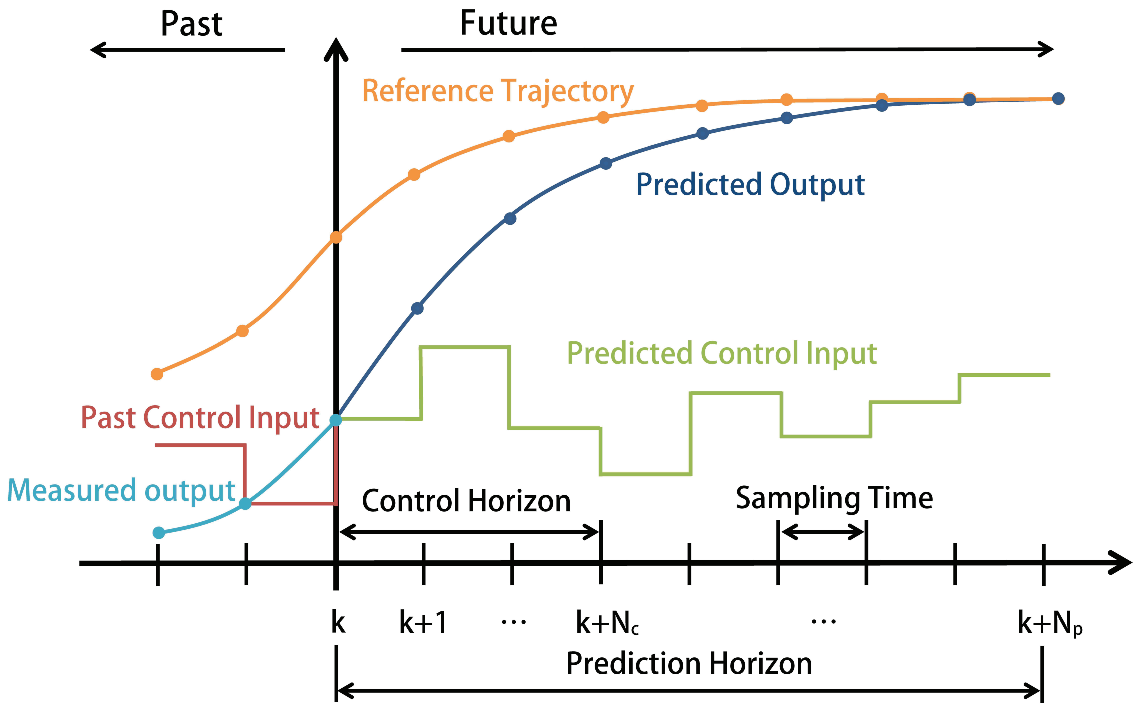

Fig. 3.2 Flowchart of the model predictive control algorithm.

Based on (3.15), the future states $\mathbf{X}$ are calculated successively by using the future control inputs $\Delta\mathbf{U}$,

$$\begin{aligned}
\mathbf{x}_{k+1|k} &= \mathbf{A}\mathbf{x}_k + \mathbf{B}\Delta u_k \\
\mathbf{x}_{k+2|k} &= \mathbf{A}\mathbf{x}_{k+1|k} + \mathbf{B}\Delta u_{k+1} \\
&= \mathbf{A}^2\mathbf{x}_k + \mathbf{A}\mathbf{B}\Delta u_k + \mathbf{B}\Delta u_{k+1} \\
&\vdots \\
\mathbf{x}_{k+N_p|k} &= \mathbf{A}^{N_p}\mathbf{x}_k + \mathbf{A}^{N_p-1}\mathbf{B}\Delta u_k + \mathbf{A}^{N_p-2}\mathbf{B}\Delta u_{k+1} + \cdots + \mathbf{A}^{N_p-N_c}\mathbf{B}\Delta u_{k+N_c-1}.
\end{aligned}$$

Then, the predicted output variables are calculated by substitution,

$$\begin{aligned}
\mathbf{y}_{k+1|k} &= \mathbf{C}\mathbf{A}\mathbf{x}_k + \mathbf{C}\mathbf{B}\Delta u_k \\
\mathbf{y}_{k+2|k} &= \mathbf{C}\mathbf{A}\mathbf{x}_{k+1|k} + \mathbf{C}\mathbf{B}\Delta u_{k+1} \\
&= \mathbf{C}\mathbf{A}^2\mathbf{x}_k + \mathbf{C}\mathbf{A}\mathbf{B}\Delta u_k + \mathbf{C}\mathbf{B}\Delta u_{k+1} \\
&\vdots \\
\mathbf{y}_{k+N_p|k} &= \mathbf{C}\mathbf{A}^{N_p}\mathbf{x}_k + \mathbf{C}\mathbf{A}^{N_p-1}\mathbf{B}\Delta u_k + \mathbf{C}\mathbf{A}^{N_p-2}\mathbf{B}\Delta u_{k+1} + \cdots + \mathbf{C}\mathbf{A}^{N_p-N_c}\mathbf{B}\Delta u_{k+N_c-1}.
\end{aligned}$$

Referring to (3.16), the output $\mathbf{Y}$ is obtained as follows,

$$\mathbf{Y} = \mathbf{F}\mathbf{x}_k + \mathbf{\Phi}\Delta\mathbf{U}, \tag{3.17}$$

where,

$$\mathbf{F} = \begin{bmatrix} \mathbf{CA} \\ \mathbf{CA}^2 \\ \mathbf{CA}^3 \\ \vdots \\ \mathbf{CA}^{N_p} \end{bmatrix}, \mathbf{\Phi} = \begin{bmatrix} \mathbf{CB} & 0 & 0 & \cdots & 0 \\ \mathbf{CAB} & \mathbf{CB} & 0 & \cdots & 0 \\ \mathbf{CA}^2\mathbf{B} & \mathbf{CAB} & \mathbf{CB} & \cdots & 0 \\ \vdots & \vdots & \vdots & \ddots & \vdots \\ \mathbf{CA}^{N_p-1}\mathbf{B} & \mathbf{CA}^{N_p-2}\mathbf{B} & \mathbf{CA}^{N_p-3}\mathbf{B} & \cdots & \mathbf{CA}^{N_p-N_c}\mathbf{B} \end{bmatrix}.$$

3.3.3 Receding optimization

The objective of the model predictive control system is to find the optimal control trajectory $\Delta\mathbf{U}$ such that the predicted output is as close as possible to the reference $\mathbf{R}_s$. This process can be implemented by minimizing a cost function J defined as,

$$J = (\mathbf{R}_s - \mathbf{Y})^T(\mathbf{R}_s - \mathbf{Y}) + \Delta\mathbf{U}^T\bar{\mathbf{R}}\Delta\mathbf{U}. \tag{3.18}$$

Then, we achieve

$$\begin{gathered}\min_{\Delta\mathbf{U}} J \text{ subject to} \\ \Delta\mathbf{U} \in \Delta\mathbf{U}^*,\end{gathered} \tag{3.19}$$

where $\Delta\mathbf{U}^*$ is constraint set, $\mathbf{Y} \in \mathbb{R}^{N_p\times 1}$ and $\Delta\mathbf{U} \in \mathbb{R}^{N_c\times 1}$. Moreover, the diagonal matrix $\bar{\mathbf{R}}$ is defined as $\bar{\mathbf{R}} = r_w\mathbf{I}_{Nc\times Nc}$ where $r_w \geq 0$ is a tuning parameter for penalizing the control input. When r_w is set to zero, the goal will be solely to make error as small as possible and no attention would be paid on how large $\Delta\mathbf{U}$ might be. For path tracking, $\mathbf{R}_s$ is always set to 0, as offsets are driven to zero. As a consequence, the cost function J can be simplified as,

$$\begin{aligned}&\min_{\Delta\mathbf{U}} \mathbf{Y}^T\mathbf{Y} + \Delta\mathbf{U}^T\bar{\mathbf{R}}\Delta\mathbf{U} \text{ subject to} \\ &\Delta\mathbf{U} \in \Delta\mathbf{U}^*,\end{aligned} \tag{3.20}$$

To minimized the cost function, the derivative of J is calculated,

$$J = (\mathbf{F}\mathbf{x}_k)^T(\mathbf{F}\mathbf{x}_k) + 2\Delta\mathbf{U}^T\boldsymbol{\Phi}^T(\mathbf{F}\mathbf{x}_k) + \Delta\mathbf{U}^T(\boldsymbol{\Phi}^T\boldsymbol{\Phi} + \bar{\mathbf{R}})\Delta\mathbf{U}, \tag{3.21}$$

the derivative of J with respect to $\Delta\mathbf{U}$ is obtained as

$$\frac{\partial J}{\partial \Delta\mathbf{U}} = 2\boldsymbol{\Phi}^T(\mathbf{F}\mathbf{x}_k) + 2(\boldsymbol{\Phi}^T\boldsymbol{\Phi} + \bar{\mathbf{R}})\Delta\mathbf{U}, \tag{3.22}$$

the minimum of J is to make above (3.22) zero

$$\frac{\partial J}{\partial \Delta \mathbf{U}} = 0, \tag{3.23}$$

then the optimal control trajectory will be

$$\Delta \mathbf{U} = -(\mathbf{\Phi}^T \mathbf{\Phi} + \bar{\mathbf{R}})^{-1} \mathbf{\Phi}^T (\mathbf{F} \mathbf{x}_k), \tag{3.24}$$

with the assumption that $(\mathbf{\Phi}^T \mathbf{\Phi} + \bar{\mathbf{R}})^{-1}$ exists.

As per the receding control principle, only the first element $\Delta u_{k|k}$ of $\Delta \mathbf{U}$ at sampling time k is implemented to the system model, thus

$$\begin{aligned} \Delta u_k &= \overbrace{[1\ 0\ \cdots\ 0]^T}^{N_c} \Delta \mathbf{U} \\ &= -\mathbf{K}_1 \mathbf{x}_k, \end{aligned} \tag{3.25}$$

where

$$\mathbf{K}_1 = \overbrace{[1\ 0\ \cdots\ 0]^T}^{N_c} (\mathbf{\Phi}^T \mathbf{\Phi} + \bar{\mathbf{R}})^{-1} (\mathbf{\Phi}^T \mathbf{F}). \tag{3.26}$$

Finally, the actual control input is,

$$\begin{aligned} u_k &= \Delta u_k + u_{k-1}, \\ \delta &= \arctan\{(\frac{l_t}{v})(u_k + \sigma |v| \frac{c_d \cos \theta_{os}}{1 + c_d l_{os}})\}. \end{aligned} \tag{3.27}$$

3.3.4 Simulation

The proposed controller above was used to control the kinematic model of a 2WD2WS tractor to follow a predefined path. The simulation platform was developed in MATLAB and the parameters were listed in Table 3.2. Note that parameters come from the John Deere 4210 Compact Utility Tractor-trailer in Figure 3.14, which also will be used for later simulation as well as experiments in Chapter 4 and Chapter 5. For all simulation and experiments, we chose the value of α is larger than the value of γ, as the path offset is considered more important in this thesis.

The reference path used in the simulation is shown in Fig. 3.3. This path has both straight and curved segments, and the curved segments have different curvatures. There are four curved segments labelled in the path, the sharpest curved segment is the fourth one. In the simulation, the vehicle travelled in the clock-wise direction starting around the first curved segment and travelled through the next three curved segments.

Table 3.2 Parameters for simulation and experiment.

Parameters	Value
Vehicle wheelbase l_t	1.7 m
Driving velocity v	3 m/s
Tuning parameter r_w	0.1
Prediction horizon N_p	5
Control horizon N_c	2
Tuning parameter for path offset α	1.5
Tuning parameter for heading offset γ	0.75
Steering angle $\lvert\delta\rvert$	$\leq 45°$

The comparison between the reference path and the actual path of classical MPC for path tracking is shown in Figure 3.4 while the path offset and heading offset are shown in Figure 3.5. From these two figures, we can see that MPC demonstrated perfect performance under assumption of pure rolling.

However, in real world, this assumption is invalid as the tractor definitely drives under the impact of slip in both lateral and longitudinal directions, namely slip velocities v_{sr}, v_{lr} and slip angle β_f in the kinematic model of tractor. Especially for UAGVs, slip will become

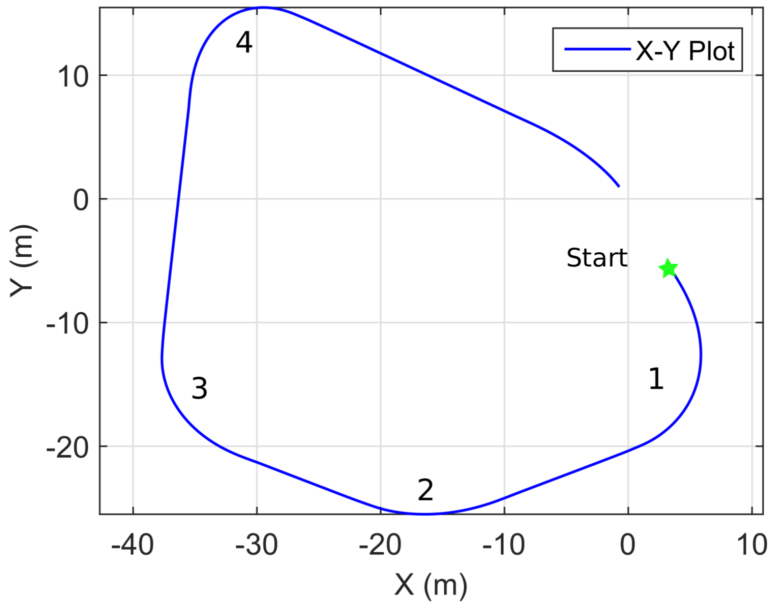

Fig. 3.3 The reference path. Starting point and the curve segments are labeled.

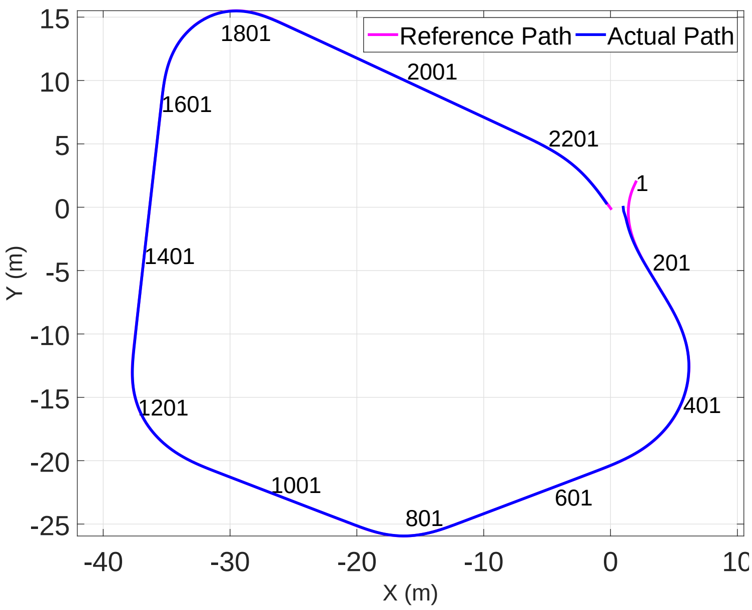

Fig. 3.4 Kinematic simulation: the X-Y plot of path tracking of the tractor based on MPC.

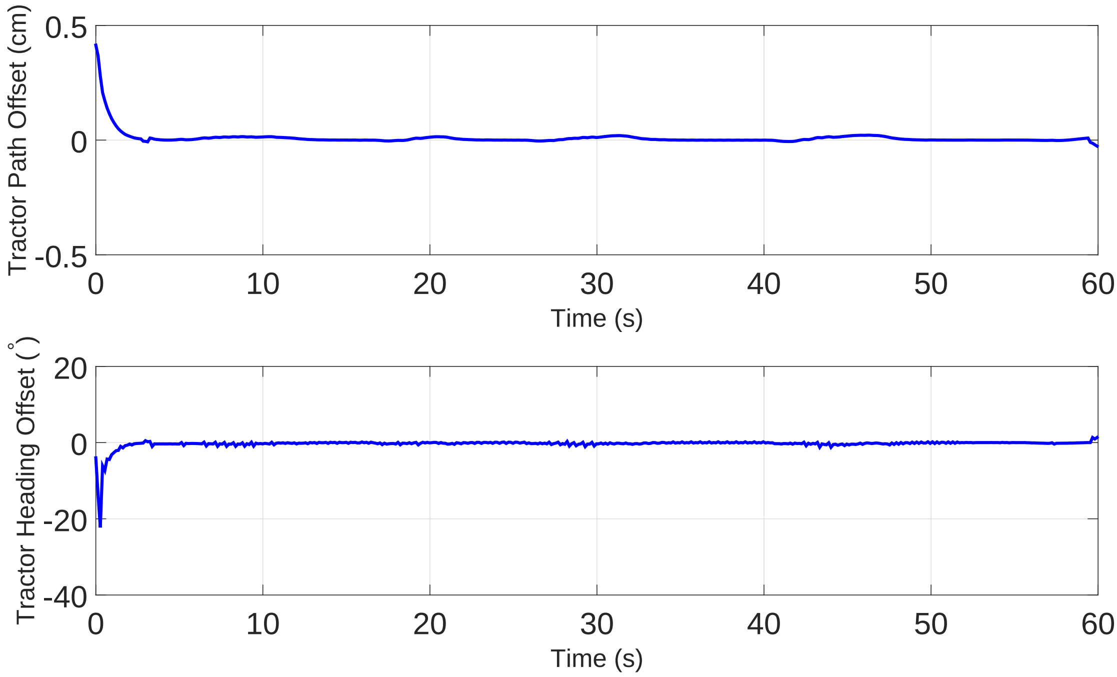

Fig. 3.5 Kinematic simulation: path offset and heading offset of the tractor based on MPC without slip.

more significant. Thus, we added slip phenomena to the kinematic platform and then tested the controller to see how significant an issue wheel slip is in path tracking of UAGVs.

In simulation, the lateral slip velocity v_{sr} and the longitudinal slip velocity v_{lr} are assumed to be less than 30% of the tractor velocity and generated by random numbers. Moreover, v_{sr} is more curvature varying while v_{lr} is more velocity varying, as per

$$\begin{aligned} v_{sr} &= -3(c_d \cos\delta + 0.2\delta)(\mathrm{Rand}() - 1), \\ v_{lr} &= 0.3v(\mathrm{Rand}() - 0.5) + \sin\delta, \end{aligned} \tag{3.28}$$

where Rand() is a uniform random number generator, generating numbers between 0 and 1. The steering slip angle β_f is defined as random numbers within the range -5° to 5°, and generated using

$$\beta_f = 10(\mathrm{Rand}() - 0.5). \tag{3.29}$$

As shown in Figure 3.6, the path offset was under significant influence brought by wheel slip, especially in the curve segments. The largest error was almost 16 cm occurring at the fourth corner. However, the accuracy in straight lines was close to zero, considered to be reasonable. To solve this significant problem, it is very necessary to create a control method which can deliver good robustness in the curves without affecting the accuracy in straight lines.

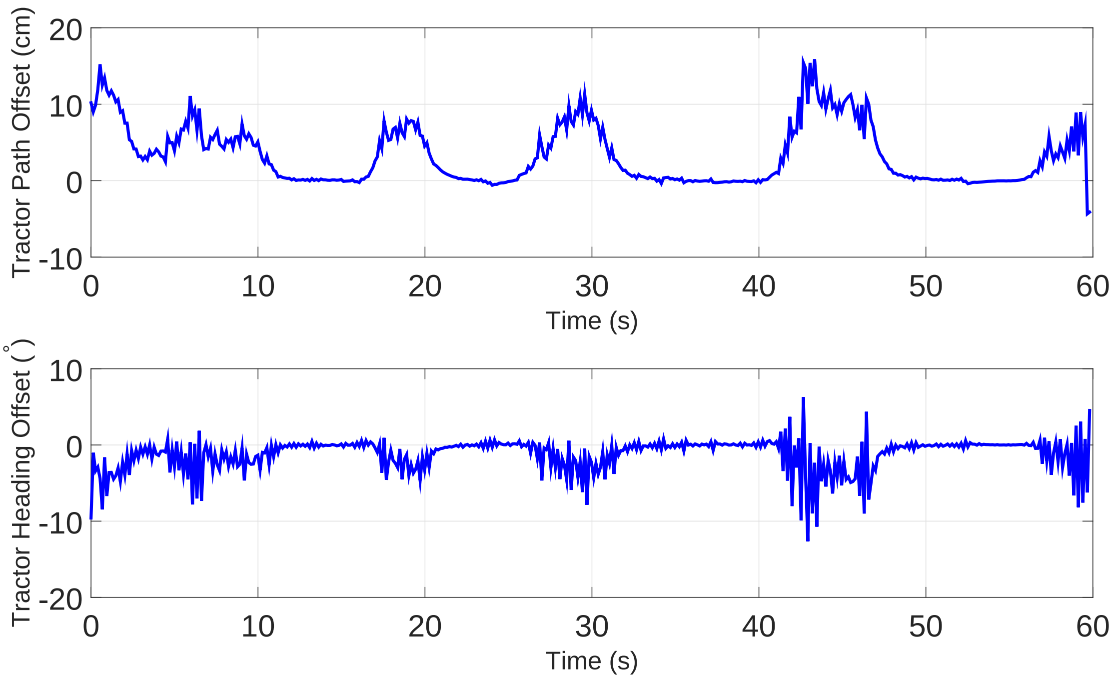

Fig. 3.6 Kinematic simulation: path offset and heading offset of the tractor based on MPC with slip.

3.4 AMM-MPC for Tractor Path Tracking

3.4.1 Augmented model with disturbances

As we need to consider the impact of disturbances, we first need to build an augmented models with disturbances based on above related work. The model in (3.10) is first discretized with respect time to sampling interval Δt as,

$$\begin{aligned} \mathbf{z}_{k+1} &= \mathbf{A}_d \mathbf{z}_k + \mathbf{B}_d u_k + \mathbf{D}_d \omega_k, \\ y_k &= \mathbf{C}_d \mathbf{z}_k, \end{aligned} \tag{3.30}$$

where $\mathbf{A}_d$, $\mathbf{B}_d$, $\mathbf{C}_d$ and $\mathbf{D}_d$ are discrete counterparts of $\mathbf{A}_c$, $\mathbf{B}_c$, $\mathbf{C}_c$ and $\mathbf{D}_c$.

The linear state-space model in (3.30) is then converted to an augmented model with disturbances. We define

$$\begin{aligned} \Delta \mathbf{z}_k &= \mathbf{z}_k - \mathbf{z}_{k-1}, \\ \Delta u_k &= u_k - u_{k-1}, \\ \Delta \omega_k &= \omega_k - \omega_{k-1} \end{aligned} \tag{3.31}$$

and obtain the augmented model as,

$$\begin{aligned} \begin{bmatrix} \Delta \mathbf{z}_{k+1} \\ y_{k+1} \end{bmatrix} &= \begin{bmatrix} \mathbf{A}_d & \mathbf{o}_d^T \\ \mathbf{C}_d \mathbf{A}_d & 1 \end{bmatrix} \begin{bmatrix} \Delta \mathbf{z}_k \\ y_k \end{bmatrix} + \begin{bmatrix} \mathbf{B}_d \\ \mathbf{C}_d \mathbf{B}_d \end{bmatrix} \Delta u_k + \begin{bmatrix} \mathbf{D}_d \\ \mathbf{C}_d \mathbf{D}_d \end{bmatrix} \Delta \omega_k, \\ y_k &= \begin{bmatrix} \mathbf{o}_d & 1 \end{bmatrix} \begin{bmatrix} \Delta \mathbf{z}_k \\ y_k \end{bmatrix}, \end{aligned} \tag{3.32}$$

where $\mathbf{o}_d = [0\ 0]$.

To simplify, we define $\mathbf{x}_k = [\Delta \mathbf{z}_k^T\ y_k]^T$ and rewrite (3.32) as,

$$\begin{aligned} \mathbf{x}_{k+1} &= \mathbf{A}\mathbf{x}_k + \mathbf{B}\Delta u_k + \mathbf{D}\Delta \omega_k, \\ y_k &= \mathbf{C}\mathbf{x}_k, \end{aligned} \tag{3.33}$$

where

$$\mathbf{A} = \begin{bmatrix} \mathbf{A}_d & \mathbf{o}_d^T \\ \mathbf{C}_d\mathbf{A}_d & 1 \end{bmatrix},$$
$$\mathbf{B} = \begin{bmatrix} \mathbf{B}_d \\ \mathbf{C}_d\mathbf{B}_d \end{bmatrix},$$
$$\mathbf{C} = \begin{bmatrix} \mathbf{o}_d & 1 \end{bmatrix},$$
$$\mathbf{D} = \begin{bmatrix} \mathbf{D}_d \\ \mathbf{C}_d\mathbf{D}_d \end{bmatrix}.$$

In (3.33), $\mathbf{x}_k \in \mathbb{R}^{3\times 1}$, $y_k \in \mathbb{R}^{1\times 1}$, $\Delta u_k \in \mathbb{R}^{1\times 1}$, $\Delta\omega_k \in \mathbb{R}^{2\times 1}$ denote the state, the controlled output, the augmented control input and the external disturbances, respectively.

3.4.2 Prediction of state and output variables with disturbances

We introduce an extra vector $\Delta\mathbf{W}$ for disturbance on the basis of (3.16) as,

$$\begin{aligned} \mathbf{X} &= \left(\mathbf{x}_{k+1|k}\ \mathbf{x}_{k+2|k}\ \mathbf{x}_{k+3|k}\ \cdots\ \mathbf{x}_{k+N_p|k}\right)^T \\ \mathbf{Y} &= \left(y_{k+1|k}\ y_{k+2|k}\ y_{k+3|k}\ \cdots\ y_{k+N_p|k}\right)^T \\ \Delta\mathbf{U} &= \left(\Delta u_{k|k}\ \Delta u_{k+1|k}\ \Delta u_{k+2|k}\ \cdots\ \Delta u_{k+N_c-1|k}\right)^T \\ \Delta\mathbf{W} &= \left(\Delta\omega_{k|k}\ \Delta\omega_{k+1|k}\ \Delta\omega_{k+3|k}\ \cdots\ \Delta\omega_{k+N_p-1|k}\right)^T. \end{aligned} \tag{3.34}$$

The future states with disturbances are then calculated successively by using the future control inputs:

$$
\begin{aligned}
\mathbf{x}_{k+1|k} &= \mathbf{A}\mathbf{x}_k + \mathbf{B}\Delta u_k + \mathbf{D}\Delta\omega_k \\
\mathbf{x}_{k+2|k} &= \mathbf{A}\mathbf{x}_{k+1|k} + \mathbf{B}\Delta u_{k+1} + \mathbf{D}\Delta\omega_{k+1} \\
&= \mathbf{A}^2\mathbf{x}_k + \mathbf{A}\mathbf{B}\Delta u_k + \mathbf{B}\Delta u_{k+1} + \mathbf{A}\mathbf{D}\Delta\omega_k + \mathbf{D}\Delta\omega_{k+1} \\
&\vdots \\
\mathbf{x}_{k+N_p|k} &= \mathbf{A}^{N_p}\mathbf{x}_k + \mathbf{A}^{N_p-1}\mathbf{B}\Delta u_k + \mathbf{A}^{N_p-2}\mathbf{B}\Delta u_{k+1} + \cdots + \mathbf{A}^{N_p-N_c}\mathbf{B}\Delta u_{k+N_c-1} \\
&+ \mathbf{A}^{N_p-1}\mathbf{D}\Delta\omega_k + \mathbf{A}^{N_p-2}\mathbf{D}\Delta\omega_{k+1} + \cdots + \mathbf{D}\Delta\omega_{k+N_p}
\end{aligned}
$$

Then, the predicted output variables are calculated by substitution:

$$
\begin{aligned}
\mathbf{y}_{k+1|k} &= \mathbf{C}\mathbf{A}\mathbf{x}_k + \mathbf{C}\mathbf{B}\Delta u_k + \mathbf{C}\mathbf{D}\Delta\omega_k \\
\mathbf{y}_{k+2|k} &= \mathbf{C}\mathbf{A}\mathbf{x}_{k+1|k} + \mathbf{C}\mathbf{B}\Delta u_{k+1} + \mathbf{C}\mathbf{D}\Delta\omega_{k+1} \\
&= \mathbf{C}\mathbf{A}^2\mathbf{x}_k + \mathbf{C}\mathbf{A}\mathbf{B}\Delta u_k + \mathbf{C}\mathbf{B}\Delta u_{k+1} + \mathbf{C}\mathbf{A}\mathbf{D}\Delta\omega_k + \mathbf{C}\mathbf{D}\Delta\omega_{k+1} \\
&\vdots \\
\mathbf{y}_{k+N_p|k} &= \mathbf{C}\mathbf{A}^{N_p}\mathbf{x}_k + \mathbf{C}\mathbf{A}^{N_p-1}\mathbf{B}\Delta u_k + \mathbf{C}\mathbf{A}^{N_p-2}\mathbf{B}\Delta u_{k+1} + \cdots + \mathbf{C}\mathbf{A}^{N_p-N_c}\mathbf{B}\Delta u_{k+N_c-1} \\
&+ \mathbf{C}\mathbf{A}^{N_p-1}\mathbf{D}\Delta\omega_k + \mathbf{C}\mathbf{A}^{N_p-2}\mathbf{D}\Delta\omega_{k+1} + \cdots + \mathbf{C}\mathbf{D}\Delta\omega_{k+N_p}
\end{aligned}
$$

Referring to (3.34), we can obtain the simple form as follows,

$$
\mathbf{Y} = \mathbf{F}\mathbf{x}_k + \mathbf{\Phi}\Delta\mathbf{U} + \Lambda\Delta\mathbf{W}, \tag{3.35}
$$

where

$$\mathbf{F} = \begin{bmatrix} \mathbf{CA} \\ \mathbf{CA}^2 \\ \mathbf{CA}^3 \\ \vdots \\ \mathbf{CA}^{N_p} \end{bmatrix}, \mathbf{\Phi} = \begin{bmatrix} \mathbf{CB} & 0 & 0 & \cdots & 0 \\ \mathbf{CAB} & \mathbf{CB} & 0 & \cdots & 0 \\ \mathbf{CA}^2\mathbf{B} & \mathbf{CAB} & \mathbf{CB} & \cdots & 0 \\ \vdots & \vdots & \vdots & \ddots & \vdots \\ \mathbf{CA}^{N_p-1}\mathbf{B} & \mathbf{CA}^{N_p-2}\mathbf{B} & \mathbf{CA}^{N_p-3}\mathbf{B} & \cdots & \mathbf{CA}^{N_p-N_c}\mathbf{B} \end{bmatrix},$$

$$\mathbf{\Lambda} = \begin{bmatrix} \mathbf{CD} & 0 & 0 & \cdots & 0 \\ \mathbf{CAD} & \mathbf{CD} & 0 & \cdots & 0 \\ \mathbf{CA}^2\mathbf{D} & \mathbf{CAD} & \mathbf{CD} & \cdots & 0 \\ \vdots & \vdots & \vdots & \ddots & \vdots \\ \mathbf{CA}^{N_p-1}\mathbf{D} & \mathbf{CA}^{N_p-2}\mathbf{D} & \mathbf{CA}^{N_p-3}\mathbf{D} & \cdots & \mathbf{CD} \end{bmatrix}.$$

3.4.3 Receding min-max optimization

The crucial point in this subsection is how to manage disturbances and then achieve robust MPC. In real practice, capturing all uncertainties is almost impossible but knowing the bounds of external disturbances is realistic as these disturbances are all physical variables. For example, in the simulation part of last section, the bound of the longitudinal slip velocity v_{lr} is 30% of the tractor vehicle velocity v. Therefore, utilizing bounds of disturbances is a competitive way to obtain robustness.

In path tracking control, we have three external disturbances in the model (3.2) so we define,

$$\sup||v_{lr}|| \leq v_{lr}^*,$$

$$\sup||v_{sr}|| \leq v_{sr}^*,$$

$$\sup||\beta_f|| \leq \beta_f^*,$$

where v_{lr}^*, v_{sr}^* and β_f^* are the bounds of the uncertainties, which are in fact the bounds of slip values. Now, substituting these bounds in (3.6) and (3.9), we obtain,

$$\begin{aligned}
\sup||\omega_1|| &\leq \omega_1^*, \\
\sup||\omega_2|| &\leq \omega_2^*, \\
\omega_k &\in \omega_k^*, \\
\Delta\omega_k &\in \Delta\omega_k^*, \\
\Delta\mathbf{W} &\in \Delta\mathbf{W}^*,
\end{aligned}$$

where ω_k^* and $\Delta\omega_k^*$ are bounded vectors of disturbances, and $\Delta\mathbf{W}^*$ is normally taken as a constant matrix that corresponds to the worst case scenario.

In terms of utilizing bounds of disturbances, an approach called min-max inspired by [45] is incorporated into the online optimization of MPC. To be specific, the 'min-max' means minimizing the worst case scenario. In our case, the worst-case is implemented by computing the cost function J using the bounds of external disturbances $\Delta\mathbf{W}^*$. Then the worst-case cost function is minimized to obtain the optimal control input. Hence, the cost function J can be represented as,

$$\begin{aligned}
&\min_{\Delta\mathbf{U}} \max_{\Delta\mathbf{W}} \mathbf{Y}^T\mathbf{Y} + \Delta\mathbf{U}^T\bar{\mathbf{R}}\Delta\mathbf{U} \ \text{ subject to} \\
&\Delta\mathbf{U} \in \Delta\mathbf{U}^*, \\
&\Delta\mathbf{W} \in \Delta\mathbf{W}^*.
\end{aligned} \tag{3.36}$$

However, in fact, this will cause overcompensation in most cases as the worst case does not occur all the time. Thus, it is very important to consider the field conditions to determine $\Delta\mathbf{W}^*$. For example, v_{sr} is a significant factor that makes the field vehicle deviate from the reference path, and it is generally larger during travel through high curvature segments of the path. However, it is insignificant during travel along straight segments. Thus, we can relate $\Delta\mathbf{W}^*$ to (i) the curvature of the reference path to provide robustness, (ii) the amount of errors in offset values to provide adaptation. Hence, we define

$$\Delta\mathbf{W}^* = \overbrace{[1\ 1\ \cdots\ 1]}^{N_p}{}^T (k_p c_d + k_q + k_t l_{os}), \tag{3.37}$$

where k_p is a value based on the worst case scenario when the curvature is not zero. The parameter k_q is a small positive constant at the worst case scenario representing zero curvature. The worst case scenario is decided by the bounds of v_{lr}, v_{sr} and β_f. The parameter k_t brings adaptive behaviour, which is based on the amount of the path offset. The path offset is selected to contribute in the adaptive part of the controller due to the importance of the path offset in comparison to the heading offset in path tracking control.

Through minimization of J, the control trajectory vector $\Delta\mathbf{U}$ is obtained, however, only the first control increment $\Delta u_{k|k}$ is applied as per MPC method, while other control inputs are ignored. Therefore,

$$\begin{aligned} \Delta u_k &= \overbrace{[1\ 0\ \cdots\ 0]}^{N_c}{}^T \Delta\mathbf{U} \\ &= -\mathbf{K}_1 \mathbf{x}_k - K_2, \end{aligned} \tag{3.38}$$

where

$$\mathbf{K}_1 = \overbrace{[1\ 0\ \cdots\ 0]}^{N_c}{}^T (\mathbf{\Phi}^T \mathbf{\Phi} + \bar{\mathbf{R}})^{-1} (\mathbf{\Phi}^T \mathbf{F}), \tag{3.39}$$

$$K_2 = \overbrace{[1\ 0\ \cdots\ 0]}^{N_c}{}^T (\mathbf{\Phi}^T \mathbf{\Phi} + \bar{\mathbf{R}})^{-1} (\mathbf{\Phi}^T \mathbf{\Lambda} \Delta\mathbf{W}). \tag{3.40}$$

Finally, from (3.7) and (3.31), the steering angle δ, which is the actual control input is calculated as,

$$\begin{aligned} u_k &= \Delta u_k + u_{k-1}, \\ \delta &= \arctan\{(\frac{l_t}{v})(u_k + \sigma|v|\frac{c_d \cos\theta_{os}}{1 + c_d l_{os}})\}. \end{aligned} \tag{3.41}$$

3.4.4 Kinematic simulation

To verify the performance of the proposed controller, the AMM-MPC algorithm was first tested in a kinematic simulation environment, controlling the kinematic model of the tractor to follow the reference path. In this simulation, the tractor was subjected to the same disturbances mentioned in Section 3.3.4, which aimed to compare with the results of MPC in Section 3.3.4.

Figure 3.7 shows the comparison of path offset as well as heading offset between AMM-MPC (Adaptive min-max model predictive control) (blue line) and Classical MPC (Model predictive control) (red line). As shown, the performance at four corners was significantly improved by AMM-MPC, even in the most challenging corner with the biggest error around 6 cm, decreasing by 10 cm compared with Classical MPC while errors in the rest of the corners dropped to 2 cm. Note that this outstanding improvement in the corners did not sacrifice the performance of AMM-MPC in the straight lines which was still negligible. On the other hand, the comparison of heading offset for between AMM-MPC (blue line) and Classical MPC (red line) indicated the heading error was decreased slightly.

To provide a better quantitative comparison, a box plot was used to depict two groups of numerical data, which included minimum, first quartile, median, third quartile, and maximum. In the box plot, the red lines indicate the median of the data, and the red points mean the outlier. The closer the red line is to zero, the better the result is. The upper and lower blue lines are first quartile and third quartile respectively. Figure 3.8 shows the box plot of path offset based on AMM-MPC and classical MPC. As shown, the median of AMM-MPC was very small, compared to that of classical MPC. Besides, most data of AMM-MPC was within 1cm while most data of Classical MPC was 6 cm. On the other hand, Figure 3.9 shows the box plot in heading offset of AMM-MPC and classical MPC. The median of AMM-MPC was still smaller than that of classical MPC. The better performance of AMM-MPC can be seen in the box plots. However, as shown in box plots, the improvement in

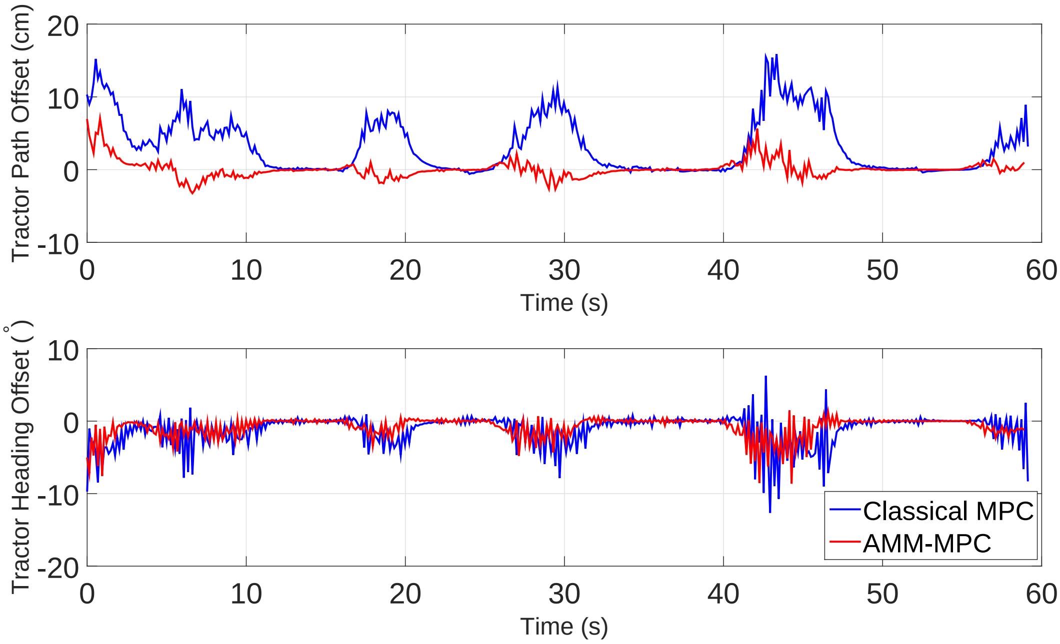

Fig. 3.7 Kinematic simulation: path offset and heading offset comparison between AMM-MPC and classical MPC. AMM-MPC shows improvement in path offset and heading offset, compared with classical MPC.

the heading offset is not as high as the improvement in the path offset. This is caused by the fact that the value of the path offset parameter α is chosen to be larger than the value of the heading offset parameter γ in the simulation. In the presented application, path offset is playing more important role than heading offset. As a result, the AMM-MPC algorithm successfully reduced the lateral errors and heading errors, especially the lateral offset.

3.4.5 Dynamic simulation

In the previous kinematic simulation, slip was considered as velocity such as $v_{sr}(m/s)$ but actually slip is a result of forces due to wheel-ground interaction. To investigate the performance of the controllers in the presence of slip forces, a more realistic simulation environment was built including a dynamic model of a tractor incorporating a wheel model generating the slip forces.

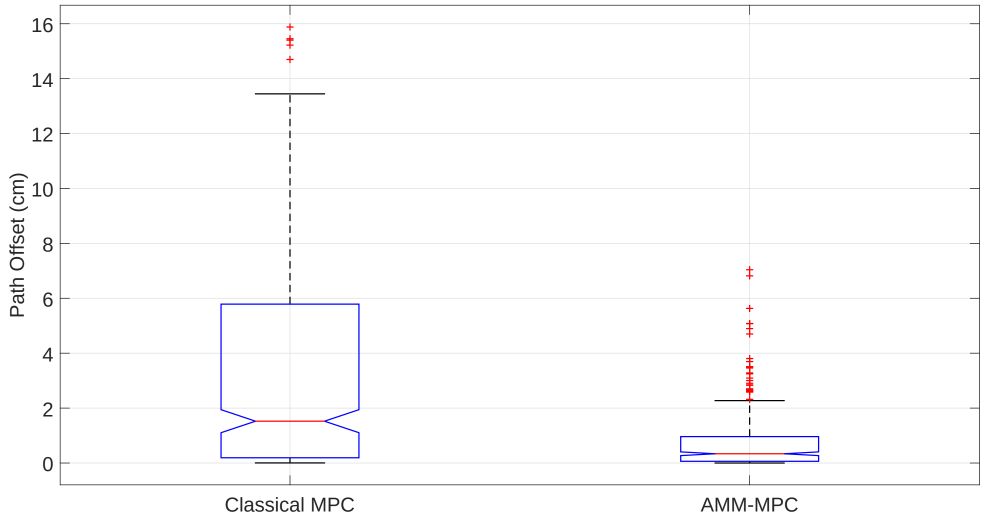

Fig. 3.8 Kinematic simulation: box plot of path offset comparison between AMM-MPC and classical MPC. AMM-MPC shows improvement in path offset and heading offset, compared with classical MPC.

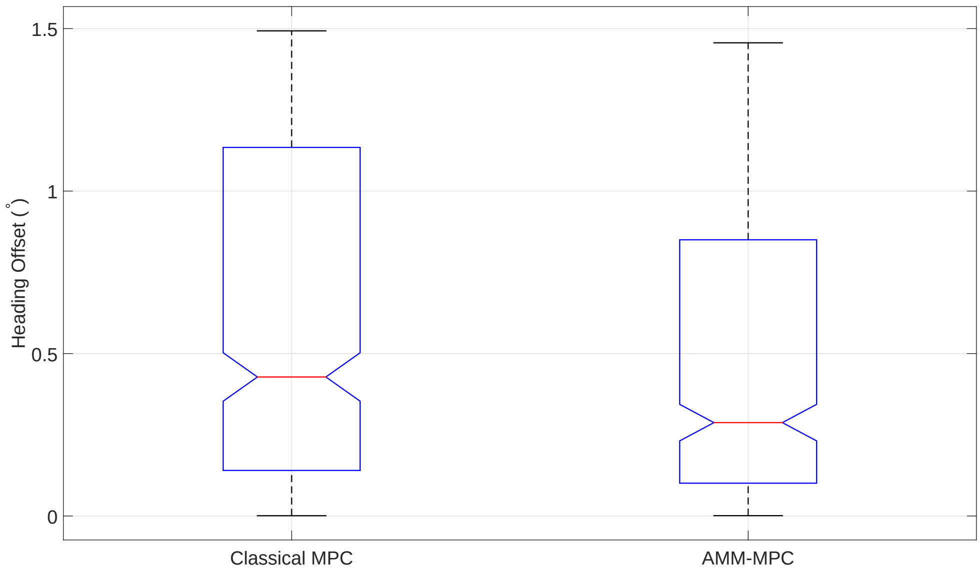

Fig. 3.9 Kinematic simulation: box plot of heading offset comparison between AMM-MPC and classical MPC. AMM-MPC shows improvement in heading offset, compared with classical MPC.

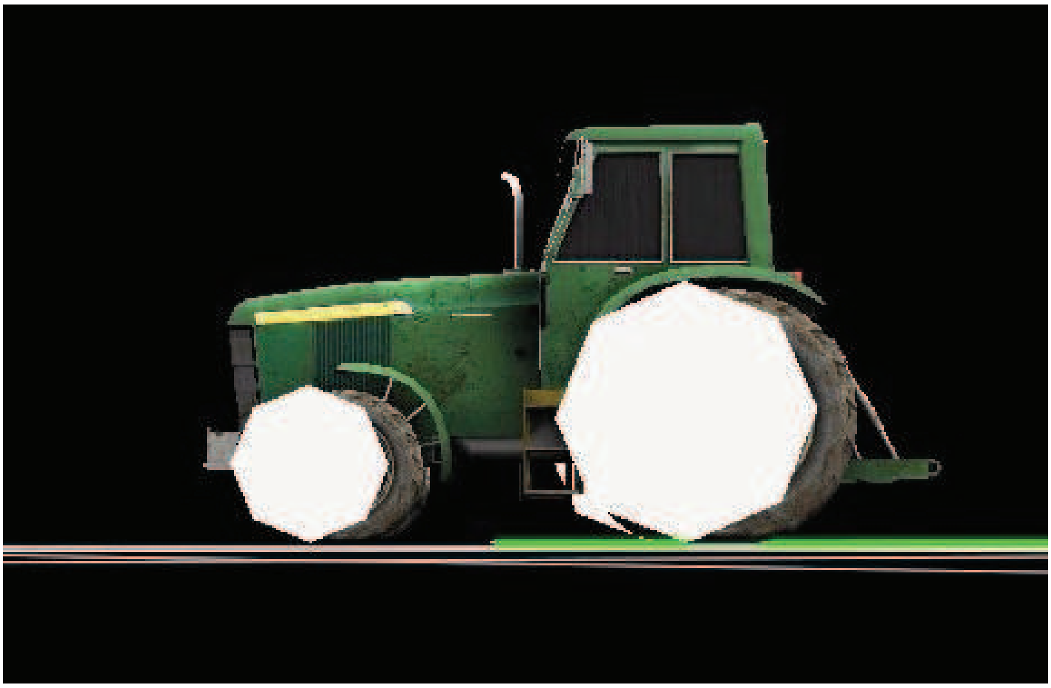

Fig. 3.10 Tractor in dynamic simulation.

The dynamic simulation platform used in this thesis was built in C++ based on [72]. To model terrain uncertainty, a parametric noise map is introduced into the wheel-ground system in the form of simplex noise. Under each wheel, the contact surface is determined by evaluating the noise function across a small region of the contact patch, which is used to determine contact and slip forces in the wheel model based on the surface's up-vector direction [73]. Note that these noises are configurable in the dynamic platform, where slips and disturbances are changing within a bounded range.

In the dynamic simulation, the reference path used in the dynamic simulation was exactly the same as that in the kinematic simulation, which is shown in Figure 3.3. Figure 3.11 shows the comparison of path offset and heading offset between AMM-MPC (red line) and classical MPC (blue line). The largest error of classical MPC in the path offset figure was almost 30 cm occurring at the sharpest corner and the second largest error was even more than 23 cm at the third corner while errors of AMM-MPC was less than 5 cm throughout the whole path tracking. Besides, the performance in the last straight segments was slightly improved. As to heading offset, the largest error was decreased from 30° to 20° by AMM-MPC and the overall indicated adequate improvement.

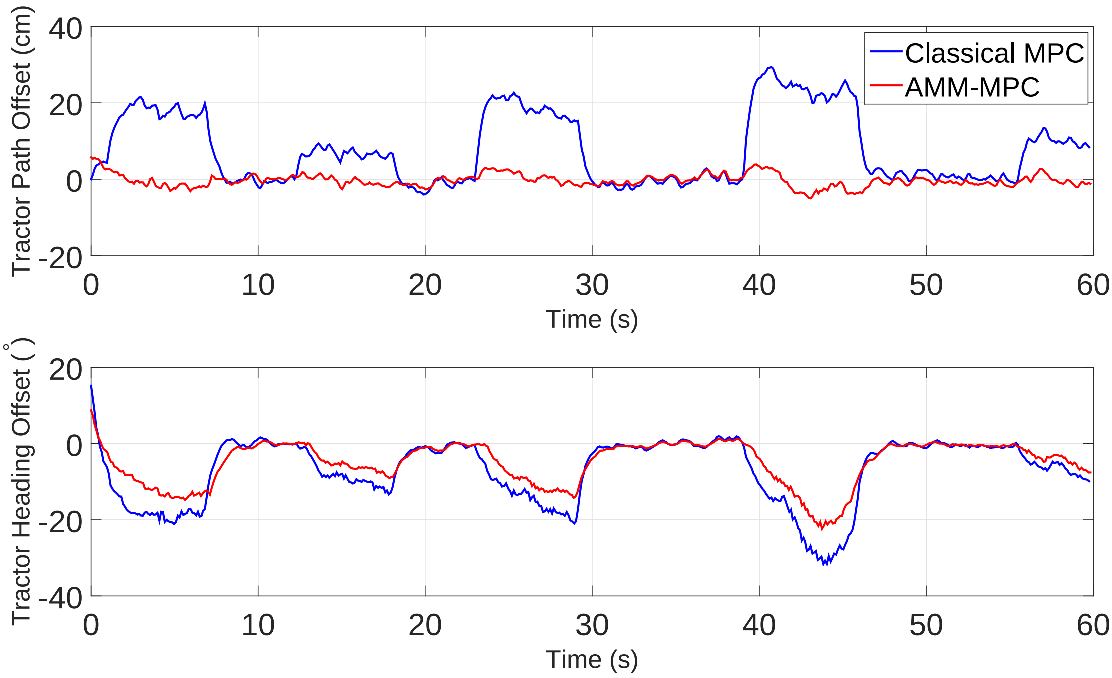

Fig. 3.11 Dynamic simulation: path offset and heading offset comparison between AMM-MPC and classical MPC. AMM-MPC shows improvement in path offset and heading offset, compared with classical MPC.

Box plots shown in Figure 3.12 and Figure 3.13 confirmed the significant improvement brought about by the proposed AMM-MPC. Especially, by looking at the quartile, a majority of path offsets produced from AMM-MPC were within the range from -2 cm to 2 cm.

3.4.6 Field testing

The AMM-MPC algorithm was tested on a tractor in two different experiments involving two different reference paths with different terrain. The tractor used in these two tests is a John Deere 4210 Compact Utility Tractor and was made an autonomous vehicle at the University of New South Wales, Australia (Figure 3.14). More details about software

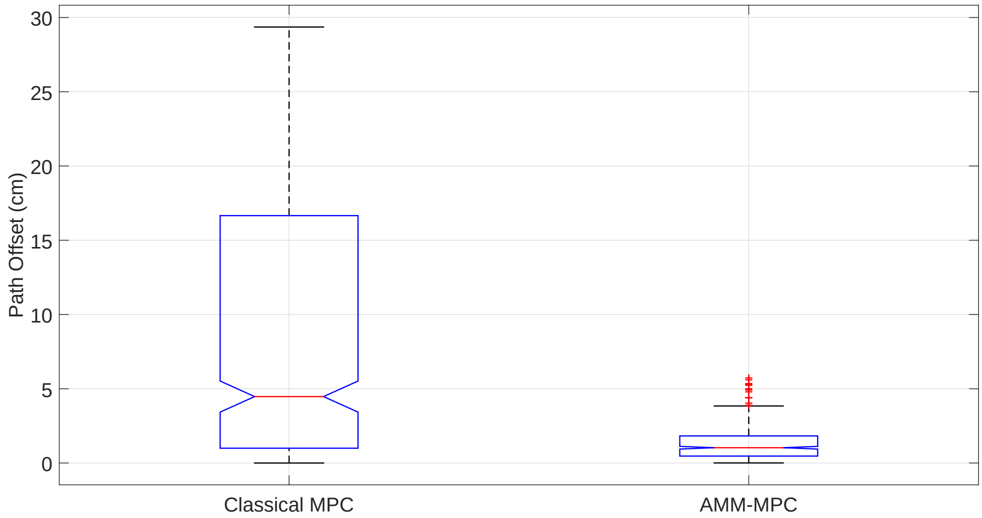

Fig. 3.12 Dynamic simulation: box plot of path offset comparison between AMM-MPC and classical MPC. AMM-MPC shows improvement in path offset, compared with classical MPC.

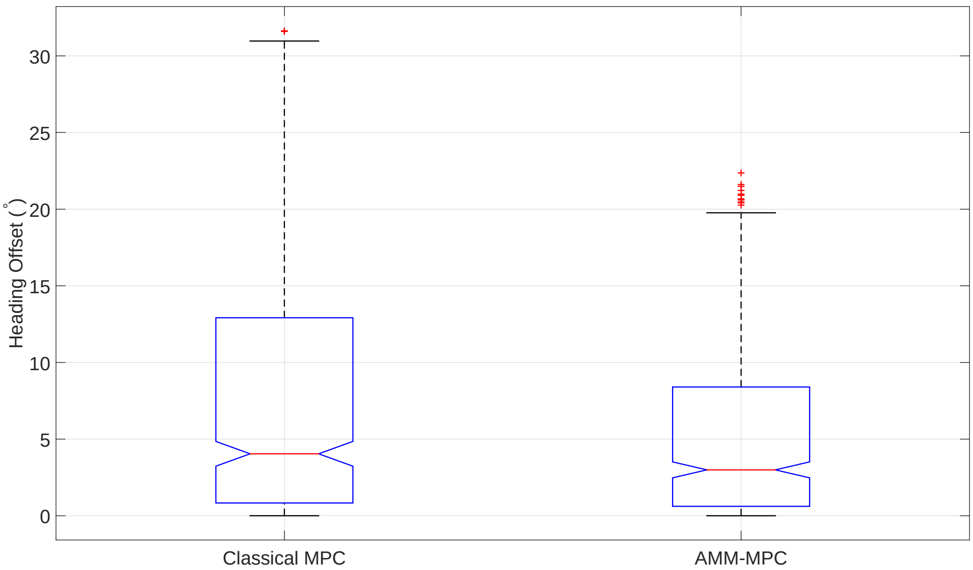

Fig. 3.13 Dynamic simulation: box plot of heading offset comparison between AMM-MPC and classical MPC. AMM-MPC shows improvement in heading offset, compared with classical MPC.

and hardware of the tractor can be found in [19, 50, 73]. The two tests demonstrated the proposed algorithm's effectiveness at reducing path-tracking errors.

Fig. 3.14 John Deere 4210 Compact Utility Tractor used in field experiments.

Comparison of AMM-MPC with Classical MPC

The first experiment was performed at Elizabeth Macarthur Agricultural Institute Farm Square in Menangle, New South Wales, Australia (Figure 3.15). The experimental terrain was plain overall but with some sand as well as grass and small slopes. The tractor autonomously followed the reference path at the fixed speed (1 m/s) with two kinds of controllers, AMM-MPC and classical MPC.

Figure 3.16 shows plots of path offset of AMM-MPC (red solid line) and classical MPC (blue dashed line). Unlike results in both simulations, classical MPC in this experiment showed large errors in straight lines with more than 10 cm while AMM-MPC still showed minor errors in straight lines. Those large errors occurring in straight lines are actually caused by the slip phenomenon in straight lines, and this is the point we do not consider in

Fig. 3.15 Experimental site 1 according to Google Earth.

the simulation. At corners, the largest error from classical MPC reached even 50 cm which was then decreased by a factor of 2 by AMM-MPC. Figure 3.17 plots the comparison of heading offset between classical MPC and AMM-MPC, indicating improvement brought by AMM-MPC at all corners.

Box plots presented the superior performance of AMM-MPC, especially in reducing path offset. Figure 3.18 shows path offset of AMM-MPC and classical MPC, from which most errors of classical MPC were distributed within the range from 8 cm to 18 cm and the median was 12.5 cm. However, most errors of AMM-MPC ranged from 2 cm to 6 cm and the median was 2.5 cm. Figure 3.19 proved slight improvement in heading accuracy. As a consequence, compared to classical MPC, the accuracy of path tracking was significantly improved by AMM-MPC based on above results. AMM-MPC can perform more accurately and robustly in both curved and straight segments of the path. In addition, AMM-MPC dealt

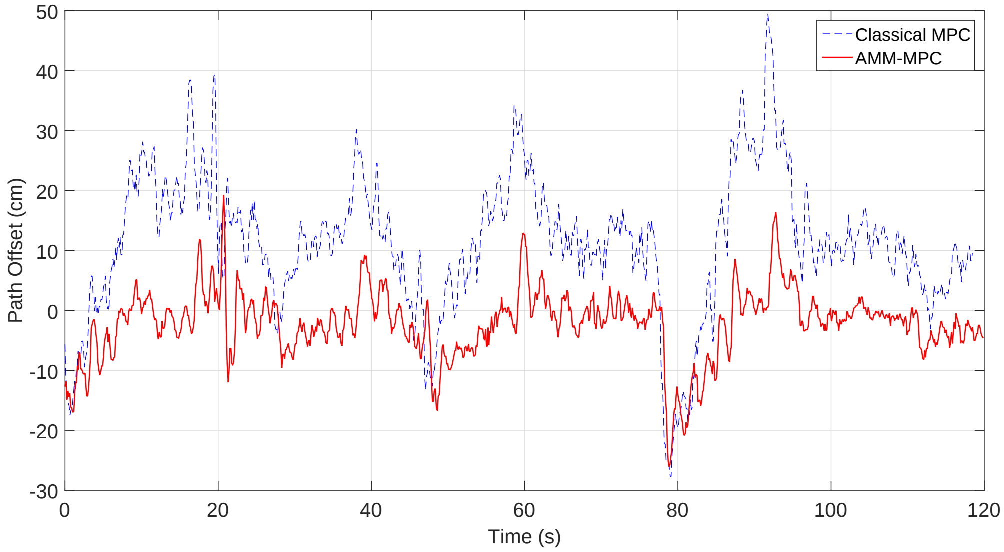

Fig. 3.16 Field experiment 1: path offset comparison between AMM-MPC and classical MPC. AMM-MPC shows improvement in path offset, compared with classical MPC.

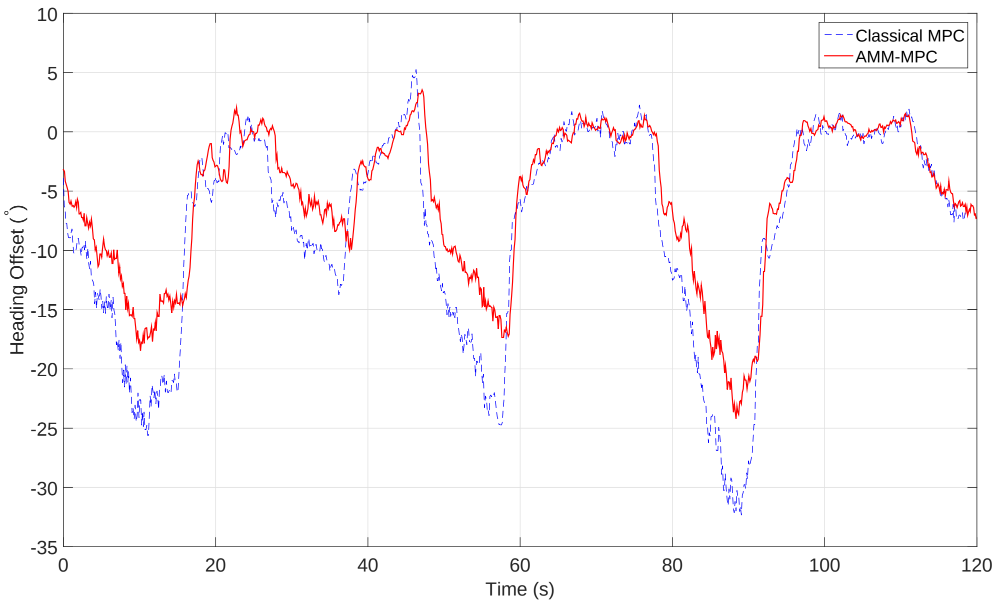

Fig. 3.17 Field experiment 1: heading offset comparison between AMM-MPC and classical MPC. AMM-MPC shows improvement in heading offset, compared with classical MPC.

with slip adaptively, without requiring slip estimation, which is the main advantage of the proposed method.

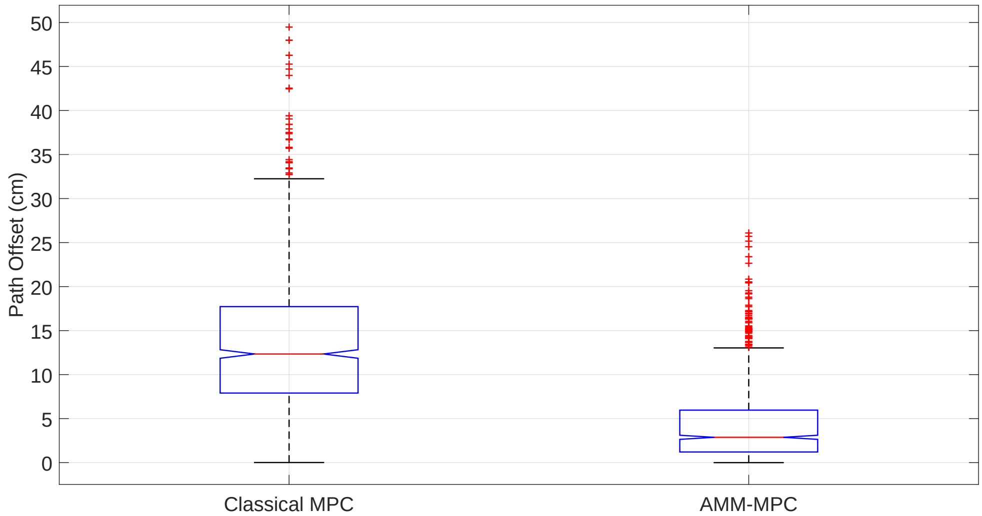

Fig. 3.18 Field experiment 1: box plot of path offset comparison between AMM-MPC and classical MPC. AMM-MPC shows improvement in path offset, compared with classical MPC.

Comparison of AMM-MPC with SMC and BSC

Although simulation as well as the first experiment has proven that AMM-MPC has the capability to deal with wheel slip compared with MPC. However, as mentioned before, MPC is not known as an inherently robust control approach and therefore validation of AMM-MPC needs further comparison with classical robust controllers which have the inherent ability to deal with the slip phenomenon. In this experiment, sliding mode control and backstepping control are chosen because they are two well-performing robust control methods. According to the literature, SMC (Sliding mode control) and BSC (Backstepping control) are very famous robust controllers, based on Lyapunov's second method of stability analysis. They have remarkable features of accuracy and robustness and both approaches can be comprehensively used for autonomous guidance of non-holonomic mobile vehicles. In this case,

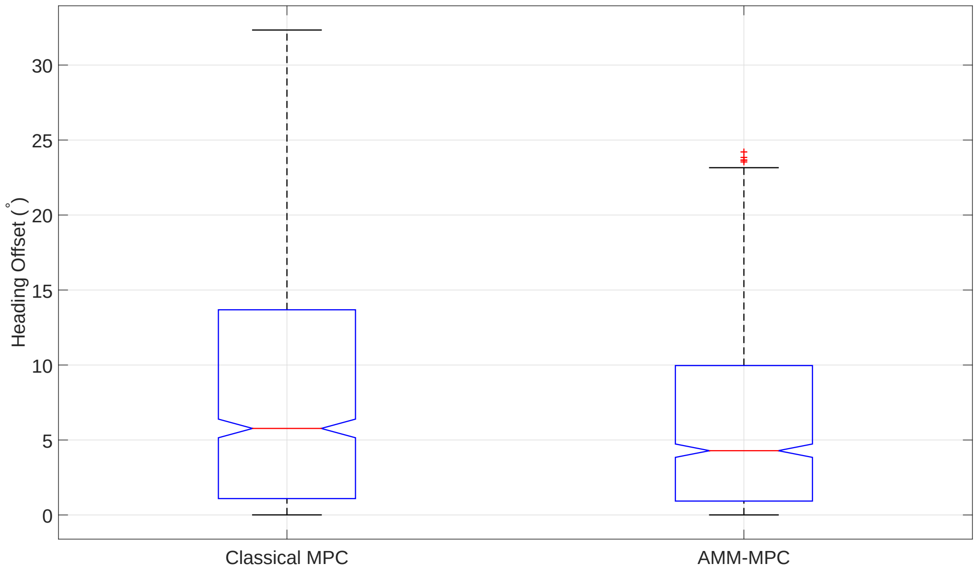

Fig. 3.19 Field experiment 1: box plot of heading offset comparison between AMM-MPC and classical MPC. AMM-MPC shows improvement in heading offset, compared with classical MPC.

the proposed AMM-MPC was compared with a successful SMC implementation, which is presented under the title 'Robust Adaptive Controller Design' in [21], and a BSC reported in literature [31] that showed good performance. The second experiment was performed at Elizabeth Macarthur Agricultural Institute for Robotics and Autonomous Systems Farmland in Menangle, New South Wales, Australia (Figure 3.20) where the terrain was hasher with sand, grass, wheel tracks, inclines, and slopes (Figure 3.21), which means higher wheel slip.

The second experiment was performed at Elizabeth Macarthur Agricultural Institute for Robotics and Autonomous Systems Farmland in Menangle, New South Wales, Australia (Figure 3.20) where the terrain was hasher with sand, grass, wheel tracks, inclines, and slopes (Figure 3.21), which means higher wheel slip.

Three controllers were used to control the tractor to drive from a parking area to the field and then to follow the reference path (Figure 3.22) under the same conditions. The results were recorded and shown in Figure 3.23 and 3.24, where SMC was plotted as a blue dot

Fig. 3.20 Experimental site 2 according to Google Earth.

Fig. 3.21 Experimental site 2 terrain.

dashed line, BSC was plotted as a red dashed line and AMM-MPC was plotted as a black solid dashed line. In Figure 3.23, the most noticeable improvement was found from 180 to 240 seconds where AMM-MPC reduced the error from more than 150 cm to 50cm. In two parallel lines of the path, the accuracy of AMM-MPC was significant whereas errors of SMC and BSC were 25cm and 20cm. Figure 3.24 indicated that the heading accuracy of three controllers were almost the same.

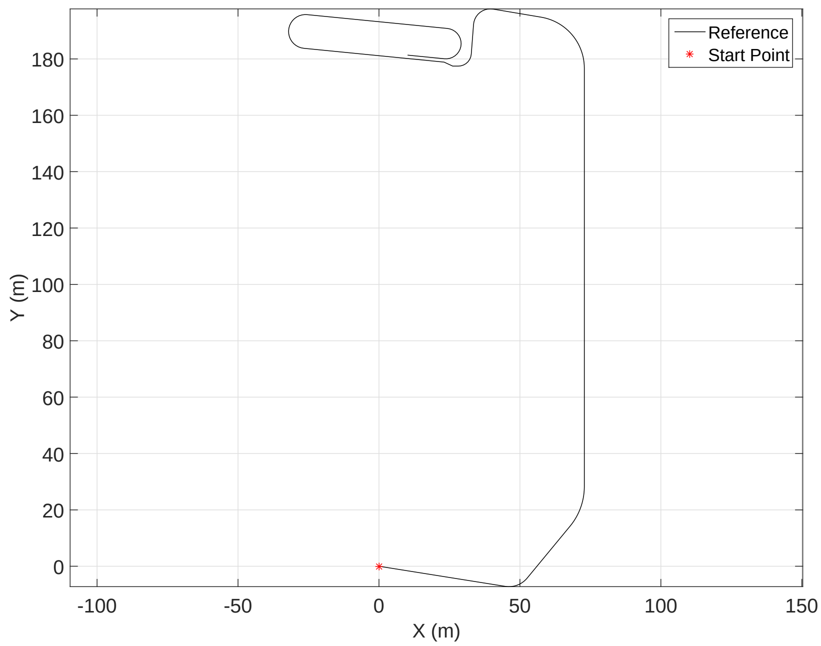

Fig. 3.22 The reference path used in the field experiment 2 in comparison of AMM-MPC with SMC and BSC.

For a more compact quantitative comparison, box plots and root mean square(RMS) values as well as standard deviation (SD) values for the three controllers were presented. RMS value for path offset for AMM-MPC is about 12 cm that is significantly better than the path offset of BSC which is 26 cm and the path offset of SMC is 30 cm. For the heading offset the difference is not significant. However, the heading accuracy is also better in AMM-MPC with RMS value of 10.44 ° and SD of 10.1 ° compared to those of SMC and BSC shown in Tables 3.3 and 3.4. The accuracy is enough for some agricultural applications.

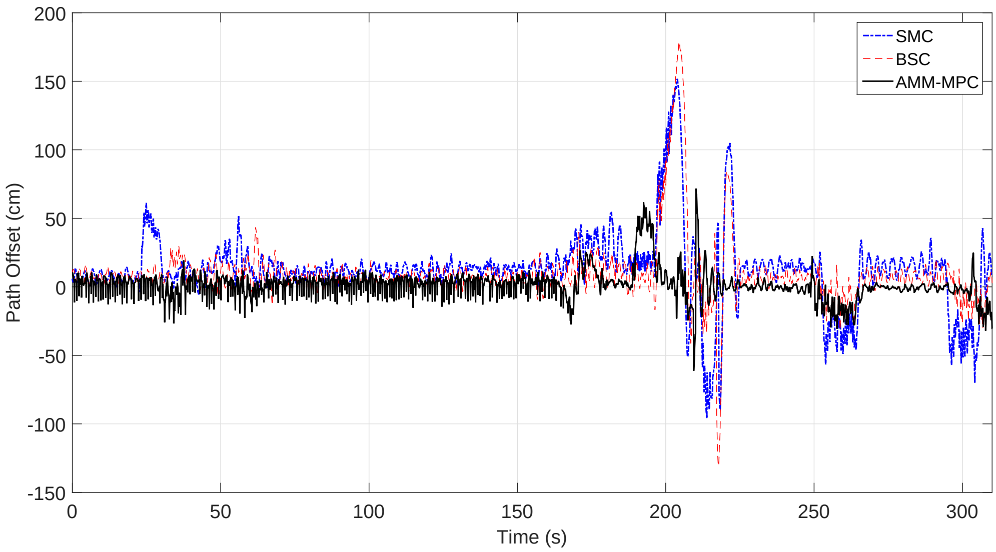

Fig. 3.23 Field experiment 2: path offset comparison among AMM-MPC, SMC and BSC.

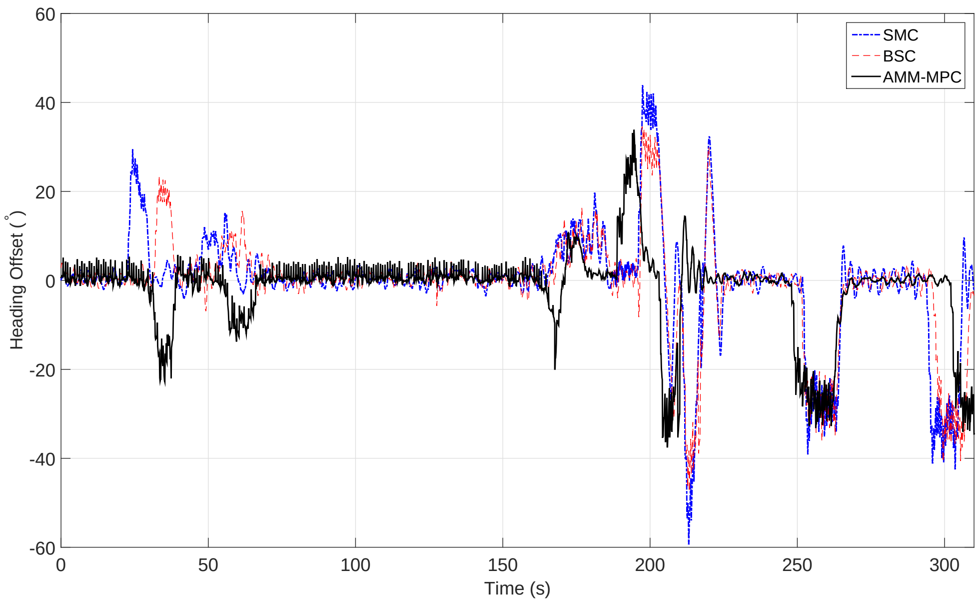

Fig. 3.24 Field experiment 2: heading offset comparison among AMM-MPC, SMC and BSC.

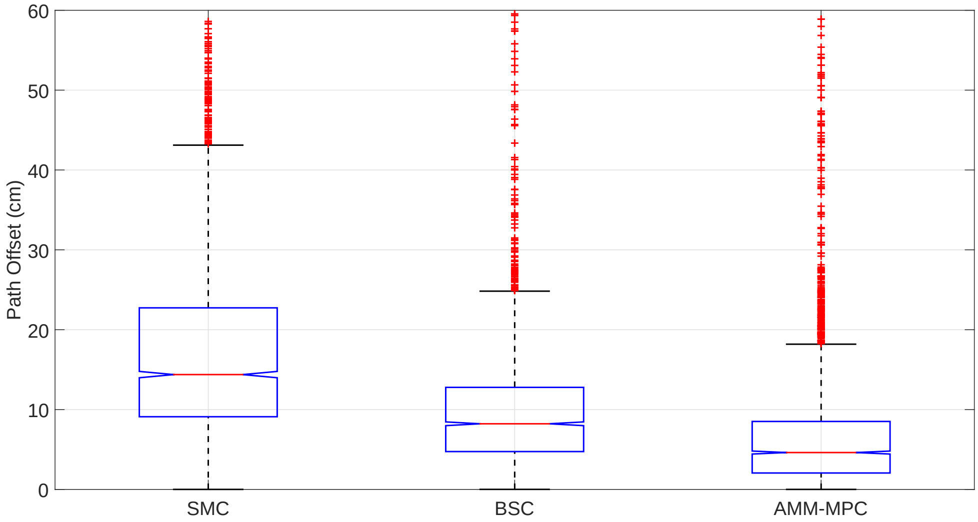

Fig. 3.25 Field experiment 2: box plot of path offset comparison among AMM-MPC, SMC and BSC.

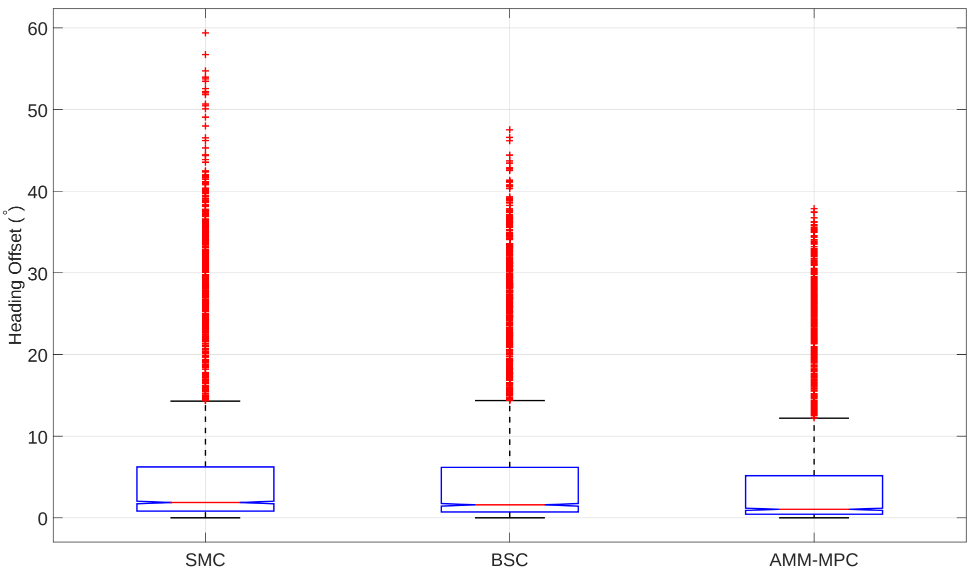

Fig. 3.26 Field experiment 2: box plot of heading offset comparison among AMM-MPC, SMC and BSC.

Table 3.3 RMS values and SD values of path offset.

Path Offset (cm)	SMC	BSC	AMM-MPC
RMS	30.33	26.88	11.42
SD	27.74	25.04	11.39

Table 3.4 RMS values and SD values of heading offset.

Heading Offset (°)	SMC	BSC	AMM-MPC
RMS	12.48	11.50	10.44
SD	12.47	11.46	10.10

3.5 Summary

This chapter proposed a very novel and promising adaptive min-max model predictive controller for path tracking control of a farm tractor in the presence of slip. The proposed controller's derivation was presented in detail. The performance of the proposed controller was evaluated with extensive simulation incorporating kinematic simulation, dynamic simulation and real field experiments in which the performance of the AMM-MPC was compared with classical MPC's performance. Moreover, the proposed controller was compared with two successful implementations of other forms of robust nonlinear controllers, namely, a sliding mode controller and a back stepping controller in field experiments on a typical farm. The results obtained show substantial improvements in the accuracy in path offsets and heading offsets, especially at the segments with higher curvatures, where slip is greater than slips for the straight segments. It is sufficiently proven that AMM-MPC not only provided robustness but also dealt with wheel slip adaptively without requiring slip measurement or estimation.

Chapter 4

AMM-MPC for Tractor-trailer Path Tracking

The system of a tractor pulling a trailer has become popular in agriculture due to widespread potential of implements. The tractor and the trailer are mechanically coupled together so that the tractor can pull the trailer carrying on more agricultural tasks in an efficient and cost effective manner, such as ploughing and seeding. However, the tractor-trailer system usually only steer the tractor and the trailer is passive, despite the fact that the implement is the one that carries on the actual agricultural tasks. Moreover, the implement is significantly affected by the ground contact forces and that easily makes the trailer to drift away. Finally, it is rather difficult to control the accuracy of the non-steerable trailer as the controller will only directly work on the tractor. As a result, it is essential to design a controller for the trailer.

This chapter presents a path tracking control algorithm for a tractor pulling a steerable trailer. Based on good performance of AMM-MPC verified in Chapter 3, the same control approach was assumed to apply to the trailer in this chapter. The breakdown of sections in this chapter was as follows. In Section 4.1, a kinematic model and its offset model of a trailer were built. In Section 4.2 feedback linearisation was used to linearise its offset model. In Section 4.3, AMM-MPC for a tractor-trailer system was derived while comparative simulation as well as discussion were presented to validate the proposed control law in the following section. Finally, this chapter is concluded in Section 4.4.

4.1 System Modelling and Description

A tractor-trailer system is described in Figure 4.1 and correlative notations are defined as shown in Table 4.1. The tractor is represented by a bicycle model which is the same as the one depicted in last chapter. The trailer is a steerable trailer and steered by rear wheels which are represented by single wheel. Note that the whole system is driven by rear wheels of tractor. In this chapter, it is assumed that the tractor-trailer follow the reference path in a clockwise direction and always moves forward.

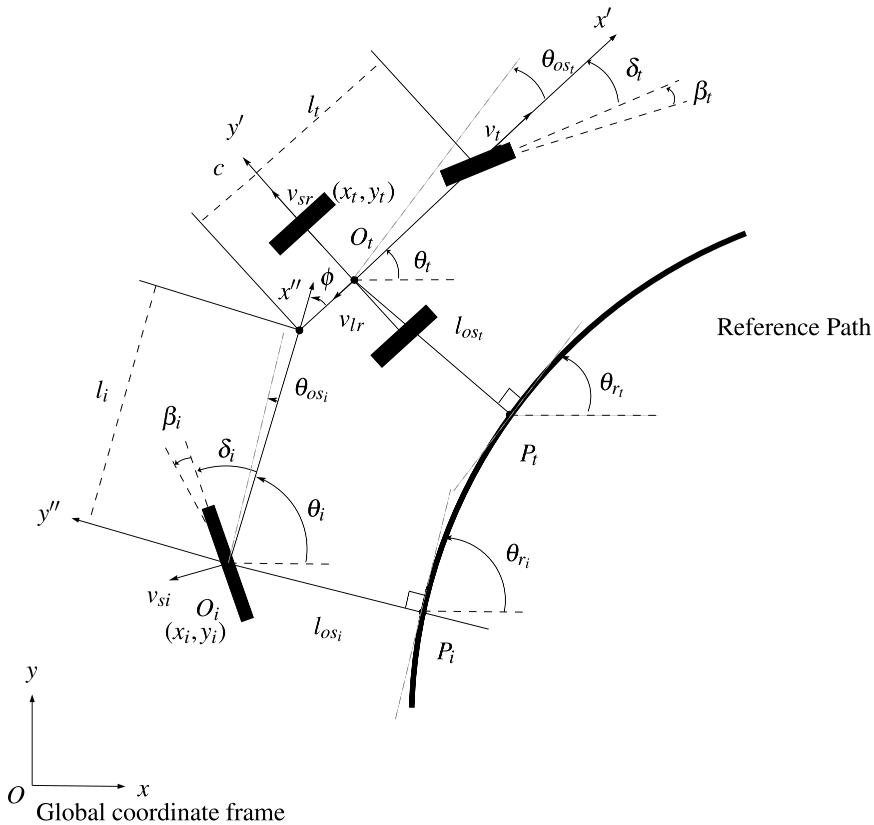

Fig. 4.1 Kinematic model of the tractor-trailer system

Table 4.1 Notations in the tractor-trailer model.

Notations	Description for Tractor
x_t, y_t	position of O_t in the xOy coordinate
θ_t	heading of the tractor in the xOy coordinate
δ_t	steering angle
v_t	longitudinal velocity at O_t
v_{sr}	lateral slip velocity at O_t
v_{lr}	longitudinal slip velocity at O_t
β_t	front wheel slip angle
l_t	tractor wheelbase
P_t	point at normal distance from o_t to the reference path
c_{d_t}	curvature of the reference path at point P_t
θ_{r_t}	reference heading angle for the tractor
l_{os_t}	path offset of tractor
θ_{os_t}	heading offset of tractor
Notations	**Description for Trailer**
x_i, y_i	position of O_i in the xOy coordinate
θ_i	heading of the trailer in the xOy coordinate
δ_i	steering angle
l_i	length of trailer
ϕ	hitch angle
c	hitch length
P_i	point at normal distance from O_i to the reference path
c_{d_i}	curvature of the reference path at point P_i
β_i	side slip angle at O_i
v_{si}	lateral slip velocity at O_i
θ_{r_i}	reference heading angle for the trailer
l_{os_i}	path offset of the trailer
θ_{os_i}	heading offset of the trailer

Tractor

The tractor's state is given by $\mathbf{p}_t = [x_t, y_t, \theta_t]^T$, where (x_t, y_t) is the position of O_t in the xOy global coordinate. The tractor is then controlled by a steering angle δ_t. The kinematic model of the tractor in the presence of slip is as follow,

$$\begin{aligned}
\dot{x}_t &= (v_t - v_{lr})\cos\theta_t - v_{sr}\sin\theta_t, \\
\dot{y}_t &= (v_t - v_{lr})\sin\theta_t + v_{sr}\cos\theta_t, \\
\dot{\theta}_t &= \frac{v_t - v_{lr}}{l_t}\tan(\delta_t + \beta_t) + \frac{v_{sr}}{l_t}.
\end{aligned} \tag{4.1}$$

In (4.1), v_{sr}, v_{lr} and β_t are lateral slip velocity at tractor's rear wheels, longitudinal slip velocity at tractor's rear wheels and side slip angle at the tractor's front wheels, respectively.

Trailer

The trailer's state is given by $\mathbf{p}_i = [x_i, y_i, \theta_i]^T$, where (x_i, y_i) is the position of O_i in the xOy global coordinate. The trailer is controlled by a steering angle δ_i. The kinematic equations for the trailer in the presence of slip are presented as,

$$\begin{aligned}
\dot{x}_i &= \dot{x}_t + \dot{\theta}_t c\sin\theta_t + \dot{\theta}_i l_i \sin\theta_i, \\
\dot{y}_i &= \dot{y}_t - \dot{\theta}_t c\cos\theta_t - \dot{\theta}_i l_i \cos\theta_i, \\
\dot{\theta}_i &= \frac{1}{n}(m_1 + m_2 + m_3' + m_4),
\end{aligned} \tag{4.2}$$

where

$$
\begin{aligned}
n &= l_i \sin\phi \cos\delta_i, \\
m_1 &= -(v - v_{lr}) \sin(\delta_i + \phi) \sin\phi, \\
m_2 &= v_{sr} \sin\phi \cos(\delta_i + \phi), \\
m_3 &= -\dot{\theta}_t \sin\phi (a\cos(\delta_i + \phi) + l_i \cos\delta_i), \\
m_3' &= -c\dot{\theta}_t \sin\phi \cos(\delta_i + \phi), \\
m_4 &= -v_{si} \sin\phi, \\
\dot{\theta}_t &= \frac{v_t - v_{lr}}{l_t} \tan(\delta_t + \beta_t) + \frac{v_{sr}}{l_t}.
\end{aligned}
$$

In (4.2), v_{si} is lateral slip velocity and located at the trailer's rear wheels.

Offset model

The offset model of the tractor is the same as the one in last chapter, represented as

$$
\begin{aligned}
\dot{l}_{os_t} &= (v_t - v_{lr}) \sin\theta_{os_t} + v_{sr} \cos\theta_{os_t}, \\
\dot{\theta}_{os_t} &= \frac{v - v_{lr}}{l_t} \tan(\delta + \beta_f) + \frac{v_{sr}}{l_t} \\
&\quad + (v_t - v_{lr}) \frac{c_{d_t} \cos\theta_{os_t}}{1 + c_{d_t} l_{os_t}} - v_{sr} \frac{c_{d_t} \sin\theta_{os_t}}{1 + c_{d_t} l_{os_t}}.
\end{aligned}
\tag{4.3}
$$

Path tracking errors of the trailer are path offset l_{os_i} and heading offset θ_{os_i}. The differentiation of l_{os_i} is the rate of change of O_iP_i. From Figure 4.1, change of O_iP_i is affected by two velocities v and v_{si} in the O_iP_i direction, so $\dot{l}_{os_i}$ can be obtained as follow,

$$
\dot{l}_{os_i} = v_t \cos\phi \sin\theta_{os_i} + v_{si} \cos(\delta_i - \theta_{os_i}). \tag{4.4}
$$

Based on [30], the equation of θ_{os_i} is

$$\begin{aligned}\dot{\theta}_{os_i} = &\frac{1}{l_i \cos\theta_i}\{-(v_t - v_{lr})\sin(\delta_i+\phi) + v_{sr}\cos(\delta_i+\phi)\\ &-\left(\frac{v_t - v_{lr}}{l_t}\tan(\delta_t+\beta_t) + \frac{v_{sr}}{l_t}\right)\times(c\cos(\delta_i+\phi)+l_i\cos\delta_i) - v_{si}\bigg\}.\end{aligned} \tag{4.5}$$

4.2 Feedback Linearisation

As can be seen in last section, offset models of the tractor-trailer system are highly nonliear. Thus, the nonlinear tractor-trailer system cannot be directly used to design the AMM-MPC controller. In this case, it is essential to use feedback linearisation to first transform the nonlinear system to the equivalent state-space model by changing some variables.

Before feedback linearisation, the offset models (4.3) (4.4) and (4.5) can be simplified based on Assumption 2, written as,

$$\begin{aligned}\dot{l}_{os_t} &= v_t \sin\theta_{os_t} + d_{1_t},\\ \dot{\theta}_{os_t} &= \frac{v_t}{l_t}\tan\delta_t + v_t\frac{c_{d_t}\cos\theta_{os_t}}{1+c_{d_t}l_{os_t}} + d_{2_t},\end{aligned} \tag{4.6}$$

where

$$\begin{aligned}d_{1_t} &= -v_{lr}\sin\theta_{os_t} + v_{sr}\cos\theta_{os_t},\\ d_{2_t} &= -\frac{v_{lr}}{l_t}\tan\delta_t + \frac{v_t - v_{lr}}{l_t}\tan\beta_t + \frac{v_{sr}}{l_t}\\ &\quad - v_{lr}\frac{c_d\cos\theta_{os}}{1+c_d l_{os}} + v_{sr}\frac{c_d\sin\theta_{os}}{1+c_d l_{os}},\end{aligned} \tag{4.7}$$

and

$$\begin{aligned}\dot{l}_{os_i} &= v_t\cos\phi\sin\theta_{os_i} + d_{1_i},\\ \dot{\theta}_{os_i} &= -\frac{v_t\sin(\delta_i+\phi)}{l_i\cos\theta_i}\\ &\quad -\frac{v_t\tan\delta_t\times(c\cos(\delta_i+\phi)+l_i\cos\delta_i)}{l_i l_t\cos\theta_i} + d_{2_i},\end{aligned} \tag{4.8}$$

where

$$
\begin{aligned}
d_{1_i} &= v_{si}\cos(\delta_i - \theta_{os_i}),\\
d_{2_i} &= \frac{1}{l_i\cos\theta_i}\{v_{lr}\sin(\delta_i+\phi) + v_{sr}\cos(\delta_i+\phi)\\
&\quad -\left(\frac{v_t - v_{lr}}{l_t}\tan\beta_t - \frac{v_{lr}}{l_t}\tan\delta_t + \frac{v_{sr}}{l_t}\right)\times(c\cos(\delta_i+\phi)+l_i\cos\delta_i) - v_{si}\Big\}.
\end{aligned}
\tag{4.9}
$$

Then the linearisation of the tractor model and the trailer model is implemented separately. For cancelling the nonlinearity in (4.6), two new state variables z_{1_t}, z_{2_t} and a new control input is defined as u_{k_t}, represented as,

$$
\begin{aligned}
z_{1_t} &= l_{os_t},\\
z_{2_t} &= v_t\sin\theta_{os_t},\\
u_{k_t} &= v_t\cos\theta_{os_t}\Big(\frac{v_t}{l_t}\tan\delta + v_t\frac{c_{d_t}\cos\theta_{os_t}}{1+c_{d_t}l_{os_t}}\Big).
\end{aligned}
\tag{4.10}
$$

With this definition, the offsets model (4.6) is described by the new system,

$$
\begin{aligned}
\dot{z}_{1_t} &= z_{2_t} + \omega_{1_t},\\
\dot{z}_{2_t} &= u_{k_t} + \omega_{2_t},
\end{aligned}
\tag{4.11}
$$

where

$$
\begin{aligned}
\omega_{1_t} &= d_{1_t},\\
\omega_{2_t} &= v_t\cos\theta_{os_t}d_{2_t}.
\end{aligned}
\tag{4.12}
$$

Then, the state-space model is expressed by defining two vectors $\mathbf{z}_{k_t} = [z_{1_t}\ z_{2_t}]^T$, $\omega_{k_t} = [\omega_{1_t}\ \omega_{2_t}]^T$ and an output y_{k_t}

$$
\begin{aligned}
\dot{\mathbf{z}}_{k_t} &= \mathbf{A}_{\mathbf{t}c}\mathbf{z}_{k_t} + \mathbf{B}_{\mathbf{t}c}u_{k_t} + \mathbf{D}_{\mathbf{t}c}\omega_{k_t},\\
y_{k_t} &= \mathbf{C}_{\mathbf{t}c}\mathbf{z}_{k_t}.
\end{aligned}
\tag{4.13}
$$

where

$$
\begin{aligned}
\mathbf{A_t}_c &= \begin{bmatrix} 0 & 1 \\ 0 & 0 \end{bmatrix}, \\
\mathbf{B_t}_c &= \begin{bmatrix} 0 \\ 1 \end{bmatrix}, \\
\mathbf{C_t}_c &= \begin{bmatrix} \alpha\,\mathrm{sign}(l_{os_t}) & \gamma\,\mathrm{sign}(\theta_{os_t}) \end{bmatrix}, \\
\mathbf{D_t}_c &= \begin{bmatrix} 1 \\ 1 \end{bmatrix}.
\end{aligned}
$$

In (4.13), $\mathbf{z}_{k_t}$, u_{k_t} and ω_{k_t} are the current state, the control input and the disturbance in the state-space model respectively, and $\mathbf{A_t}_c$, $\mathbf{B_t}_c$ and $\mathbf{D_t}_c$ are corresponding matrices. y_{k_t} in (4.13) represents path tracking errors as the output, where y_{k_t} are related to the values of α and γ.

After feedback linearisation of the tractor, that of the trailer is followed by the same approach. Two new state variables z_{1_i}, z_{2_i} and a new control input is defined as u_{k_i} in order to proceed the linearisation of (4.8),

$$
\begin{aligned}
z_{1_i} &= l_{os_i}, \\
z_{2_i} &= v_t \cos\phi \sin\theta_{os_i}, \\
u_{k_i} &= a_i(b_i \tan\delta_i + c_i)
\end{aligned}
\tag{4.14}
$$

where

$$
\begin{aligned}
a_i &= {v_t}^2 \cos\phi \cos\theta_{os_i}, \\
b_i &= -\frac{1}{l_i}\cos\phi + \frac{c}{l_t l_i}\tan\delta_t \sin\phi, \\
c_i &= -\frac{1}{l_i}\sin\phi + \frac{c}{l_t l_i}\tan\delta_t \cos\phi - \frac{1}{l_t}\tan\delta_t.
\end{aligned}
\tag{4.15}
$$

With this definition, the offsets model (4.8) is described by the new system,

$$\dot{z}_{1_i} = z_{2_i} + \omega_{1_i},$$
$$\dot{z}_{2_i} = u_{k_i} + \omega_{2_i}, \tag{4.16}$$

where

$$\omega_{1_i} = d_{1_i},$$
$$\omega_{2_i} = v_t \cos\phi\, \theta_{os_i} d_{2_i}. \tag{4.17}$$

Then, the state-space model is expressed by defining two vectors $\mathbf{z}_{k_i} = [z_{1_i}\ z_{2_i}]^T$, $\omega_{k_i} = [\omega_{1_i}\ \omega_{2_i}]^T$ and an output y_{k_i}

$$\dot{\mathbf{z}}_{k_i} = \mathbf{A}_{\mathbf{i}c}\mathbf{z}_{k_i} + \mathbf{B}_{\mathbf{i}c}u_{k_i} + \mathbf{D}_{\mathbf{i}c}\omega_{k_i},$$
$$y_{k_i} = \mathbf{C}_{\mathbf{i}c}\mathbf{z}_{k_i}. \tag{4.18}$$

where

$$\mathbf{A}_{\mathbf{t}c} = \begin{bmatrix} 0 & 1 \\ 0 & 0 \end{bmatrix},$$
$$\mathbf{B}_{\mathbf{t}c} = \begin{bmatrix} 0 \\ 1 \end{bmatrix},$$
$$\mathbf{C}_{\mathbf{t}c} = \begin{bmatrix} \alpha\, \mathrm{sign}(l_{os_i}) & \gamma\, \mathrm{sign}(\theta_{os_i}) \end{bmatrix},$$
$$\mathbf{D}_{\mathbf{t}c} = \begin{bmatrix} 1 \\ 1 \end{bmatrix}.$$

In (4.13), $\mathbf{z}_{k_i}$, u_{k_i} and ω_{k_i} are the current state, the control input and the disturbance respectively, and $\mathbf{A}_{\mathbf{i}c}$, $\mathbf{B}_{\mathbf{i}c}$ and $\mathbf{D}_{\mathbf{i}c}$ are corresponding matrices. The output is y_{k_i}, and α and γ which are gains on l_{os_i} and θ_{os_i}.

4.3 Control Design for Tractor-trailer Path Tracking

The process of control design for the tractor is the same as the process in Chapter 3. For details, please see Section 3.4. In this section, we mainly focus on the derivation of AMM-MPC for the trailer.

In order to design the AMM-MPC algorithm, the model in (4.18) is first discretized with respect time to sampling interval Δt as,

$$\begin{aligned} \mathbf{z}_{k_i+1} &= \mathbf{A_i}_d \mathbf{z}_{k_i} + \mathbf{B_i}_d u_{k_i} + \mathbf{D_i}_d \omega_{k_i}, \\ y_{k_i} &= \mathbf{C_i}_d \mathbf{z}_{k_i}. \end{aligned} \tag{4.19}$$

where $\mathbf{A_i}_d$, $\mathbf{B_i}_d$, $\mathbf{C_i}_d$ and $\mathbf{D_i}_d$ are discrete counterparts of $\mathbf{A_i}_c$, $\mathbf{B_i}_c$, $\mathbf{C_i}_c$ and $\mathbf{D_i}_c$.

The differences between last sampling time and current sampling time are defined as

$$\begin{aligned} \Delta \mathbf{z}_{k_i} &= \mathbf{z}_{k_i} - \mathbf{z}_{k_i-1}, \\ \Delta u_{k_i} &= u_{k_i} - u_{k_i-1}, \\ \Delta \omega_{k_i} &= \omega_{k_i} - \omega_{k_i-1} \end{aligned} \tag{4.20}$$

and then the augmented model is obtained,

$$\begin{aligned} \begin{bmatrix} \Delta \mathbf{z}_{k_i+1} \\ y_{k_i+1} \end{bmatrix} &= \begin{bmatrix} \mathbf{A_i}_d & \mathbf{o}_d^T \\ \mathbf{C_i}_d \mathbf{A_i}_d & 1 \end{bmatrix} \begin{bmatrix} \Delta \mathbf{z}_{k_i} \\ y_{k_i} \end{bmatrix} + \begin{bmatrix} \mathbf{B_i}_d \\ \mathbf{C_i}_d \mathbf{B_i}_d \end{bmatrix} \Delta u_{k_i} + \begin{bmatrix} \mathbf{D_i}_d \\ \mathbf{C_i}_d \mathbf{D_i}_d \end{bmatrix} \Delta \omega_{k_i}, \\ y_{k_i} &= \begin{bmatrix} \mathbf{o}_d & 1 \end{bmatrix} \begin{bmatrix} \Delta \mathbf{z}_{k_i} \\ y_{k_i} \end{bmatrix}, \end{aligned} \tag{4.21}$$

where $\mathbf{o}_d = [0\ 0]$.

To simplify, the vector $\mathbf{x}_{k_i} = [\Delta\mathbf{z}_{k_i}^T \ y_{k_i}]^T$ is defined and (4.21) is rewritten as,

$$\begin{aligned} \mathbf{x}_{k_i+1} &= \mathbf{A_i}\mathbf{x}_k + \mathbf{B_i}\Delta u_{k_i} + \mathbf{D_i}\Delta\omega_{k_i}, \\ y_k &= \mathbf{C_i}\mathbf{x}_{k_i}, \end{aligned} \tag{4.22}$$

where

$$\begin{aligned} \mathbf{A_i} &= \begin{bmatrix} \mathbf{A_i}_d & \mathbf{o}_d^T \\ \mathbf{C_i}_d\mathbf{A_i}_d & 1 \end{bmatrix}, \\ \mathbf{B_i} &= \begin{bmatrix} \mathbf{B_i}_d \\ \mathbf{C_i}_d\mathbf{B_i}_d \end{bmatrix}, \\ \mathbf{C_i} &= \begin{bmatrix} \mathbf{o}_d & 1 \end{bmatrix}, \\ \mathbf{D_i} &= \begin{bmatrix} \mathbf{D_i}_d \\ \mathbf{C_i}_d\mathbf{D_i}_d \end{bmatrix}. \end{aligned} .$$

In (4.22), $\mathbf{x}_{k_i} \in \mathbb{R}^{3\times1}$, $y_{k_i} \in \mathbb{R}^{1\times1}$, $\Delta u_{k_i} \in \mathbb{R}^{1\times1}$, $\Delta\omega_{k_i} \in \mathbb{R}^{2\times1}$ denote the state, the controlled output, the augmented control input and the external disturbances, respectively.(check size)

Then the future state vector $\mathbf{X_i}$, the future output vector $\mathbf{Y_i}$, the input vector $\Delta\mathbf{U_i}$ and the disturbance vector $\Delta\mathbf{W_i}$ are defined as,

$$\begin{aligned} \mathbf{X_i} &= \left(\mathbf{x}_{k_i+1|k_i} \ \mathbf{x}_{k_i+2|k_i} \ \mathbf{x}_{k_i+3|k_i} \ \cdots \ \mathbf{x}_{k_i+N_p|k_i}\right)^T \\ \mathbf{Y_i} &= \left(y_{k_i+1|k_i} \ y_{k_i+2|k_i} \ y_{k_i+3|k_i} \ \cdots \ y_{k_i+N_p|k_i}\right)^T \\ \Delta\mathbf{U_i} &= \left(\Delta u_{k_i|k_i} \ \Delta u_{k_i+1|k_i} \ \Delta u_{k_i+2|k_i} \ \cdots \ \Delta u_{k_i+N_c-1|k_i}\right)^T \\ \Delta\mathbf{W_i} &= \left(\Delta\omega_{k_i|k_i} \ \Delta\omega_{k_i+1|k_i} \ \Delta\omega_{k_i+3|k_i} \ \cdots \ \Delta\omega_{k_i+N_p-1|k_i}\right)^T. \end{aligned} \tag{4.23}$$

By calculation, the simple form can be obtained,

$$\mathbf{Y_i} = \mathbf{F_i x}_{k_i} + \mathbf{\Phi}_i \Delta \mathbf{U_i} + \mathbf{\Lambda}_i \Delta \mathbf{W_i}, \tag{4.24}$$

where

$$\mathbf{F_i} = \begin{bmatrix} \mathbf{C_i A_i} \\ \mathbf{C_i A_i}^2 \\ \mathbf{C_i A_i}^3 \\ \vdots \\ \mathbf{C_i A_i}^{N_p} \end{bmatrix},$$

$$\mathbf{\Phi}_i = \begin{bmatrix} \mathbf{C_i B_i} & 0 & 0 & \cdots & 0 \\ \mathbf{C_i A_i B_i} & \mathbf{CB} & 0 & \cdots & 0 \\ \mathbf{C_i A_i}^2 \mathbf{B_i} & \mathbf{C_i A_i B_i} & \mathbf{C_i B_i} & \cdots & 0 \\ \vdots & \vdots & \vdots & \ddots & \vdots \\ \mathbf{C_i A_i}^{N_p-1} \mathbf{B_i} & \mathbf{CA}^{N_p-2} \mathbf{B_i} & \mathbf{C_i A_i}^{N_p-3} \mathbf{B_i} & \cdots & \mathbf{C_i A_i}^{N_p-N_c} \mathbf{B_i} \end{bmatrix},$$

$$\mathbf{\Lambda}_i = \begin{bmatrix} \mathbf{C_i D_i} & 0 & 0 & \cdots & 0 \\ \mathbf{C_i A_i D_i} & \mathbf{C_i D_i} & 0 & \cdots & 0 \\ \mathbf{C_i A_i}^2 \mathbf{D_i} & \mathbf{C_i A_i D_i} & \mathbf{C_i D_i} & \cdots & 0 \\ \vdots & \vdots & \vdots & \ddots & \vdots \\ \mathbf{C_i A_i}^{N_p-1} \mathbf{D_i} & \mathbf{C_i A_i}^{N_p-2} \mathbf{D_i} & \mathbf{C_i A_i}^{N_p-3} \mathbf{D_i} & \cdots & \mathbf{C_i D_i} \end{bmatrix}.$$

The crucial point in AMM-MPC is using the bounds of the disturbances. In the trailer model (4.8), there are four slips, trailer lateral slip velocity v_{si}, tractor side slip angle β_f, tractor lateral slip velocity v_{sr} and tractor longitudinal slip velocity v_{lr}. All slips are physical variables, so the bounds of these slips exist,

$$\sup||v_{lr}|| \leq v_{lr}^*,$$
$$\sup||v_{sr}|| \leq v_{sr}^*,$$
$$\sup||\beta_f|| \leq \beta_f^*,$$
$$\sup||v_{si}|| \leq v_{si}^*,$$

wherev_{lr}^*, v_{sr}^*, β_f^* and v_{si}^* are the bounds of the uncertainties.

Now, these bounds are substituted into (4.12) and (4.9), and then equations can be obtained

$$\sup||\omega_{1_i}|| \leq \omega_{1_i}^*,$$
$$\sup||\omega_{2_i}|| \leq \omega_{2_i}^*,$$
$$\omega_{k_i} \in \omega_{k_i}^*,$$
$$\Delta\omega_{k_i} \in \Delta\omega_{k_i}^*,$$
$$\Delta\mathbf{W_i} \in \Delta\mathbf{W_i}^*,$$

where $\omega_{k_i}^*$ and $\Delta\omega_{k_i}^*$ are bounded vectors of disturbances, and $\Delta\mathbf{W_i}^*$ is normally taken as a constant matrix that corresponds to the worst case scenario.

Then, the cost function J in AMM-MPC is represented as,

$$\begin{aligned} &\min_{\Delta\mathbf{U_i}} \max_{\Delta\mathbf{W_i}} \mathbf{Y_i}^T\mathbf{Y_i} + \Delta\mathbf{U_i}^T\bar{\mathbf{R}}_\mathbf{i}\Delta\mathbf{U_i} \ \text{ subject to} \\ &\Delta\mathbf{U_i} \in \Delta\mathbf{U_i}^*, \\ &\Delta\mathbf{W_i} \in \Delta\mathbf{W_i}^*. \end{aligned} \tag{4.25}$$

Then, $\Delta\mathbf{W}^*$ is assumed to relate to: (i) the curvature of the reference path to provide robustness, (ii) the amount of errors in offset values to provide adaptation, represented as follow,

$$\Delta\mathbf{W_i}^* = \overbrace{[1\ 1\ \cdots\ 1]}^{N_p}{}^T (k_p c_d + k_q + k_t l_{os_i}), \tag{4.26}$$

where k_p is a value based on the worst case scenario when the curvature is not zero. The parameter k_q is a small positive constant at the worst case scenario representing zero curvature. The worst case scenario is decided by the bounds of v_{lr}, v_{sr}, β_f and v_{si}.

Through minimization of J, the control trajectory vector $\Delta\mathbf{U}$ can be obtained, and only the first control increment $\Delta u_{k|k}$ is applied as per MPC method, while other control inputs are ignored. Therefore,

$$\begin{aligned} \Delta u_{k_i} &= \overbrace{[1\ 0\ \cdots\ 0]}^{N_c}{}^T \Delta\mathbf{U_i} \\ &= -\mathbf{K}_1 \mathbf{x}_{k_i} - K_2, \end{aligned} \tag{4.27}$$

where

$$\mathbf{K}_1 = \overbrace{[1\ 0\ \cdots\ 0]}^{N_c}{}^T (\mathbf{\Phi}_i{}^T \mathbf{\Phi}_i + \bar{\mathbf{R}}_\mathbf{i})^{-1} (\mathbf{\Phi}_i^T \mathbf{F_i}), \tag{4.28}$$

$$K_2 = \overbrace{[1\ 0\ \cdots\ 0]}^{N_c}{}^T (\mathbf{\Phi}_i{}^T \mathbf{\Phi}_i + \bar{\mathbf{R}}_\mathbf{i})^{-1} (\mathbf{\Phi}_i{}^T \mathbf{\Lambda}_i \Delta\mathbf{W_i}). \tag{4.29}$$

Finally, from (4.10) and (4.20), the steering angle δ which is the actual control input is calculated as,

$$\begin{aligned} u_{k_i} &= \Delta u_{k_i} + u_{k_i - 1}, \\ \delta_i &= \arctan\{\frac{u_{k_i}}{a_i b_i} - \frac{c_i}{b_i}\}, \end{aligned} \tag{4.30}$$

where

$$\begin{aligned} a_i &= v_t{}^2 \cos\phi \cos\theta_{os_i}, \\ b_i &= -\frac{1}{l_i}\cos\phi + \frac{c}{l_t l_i}\tan\delta_t \sin\phi, \\ c_i &= -\frac{1}{l_i}\sin\phi + \frac{c}{l_t l_i}\tan\delta_t \cos\phi - \frac{1}{l_t}\tan\delta_t. \end{aligned} \tag{4.31}$$

4.4 Simulation and Discussion

As it is seen from the previous chapter, the dynamic platform is more realistic than the kinematic platform. Thus, the validation of AMM-MPC for the trailer was directly carried out in the dynamic environment in the presence of slip forces. In the simulation, the proposed AMM-MPC was used to control a tractor-trailer shown in Figure 4.2 to follow the reference shown in Figure 3.3, comparing with (i) MPC and (ii) the trailer with no controller which means the trailer is only passively towed by the tractor through the hitch. The parameters of the controllers and the vehicles were listed in Table 4.2.

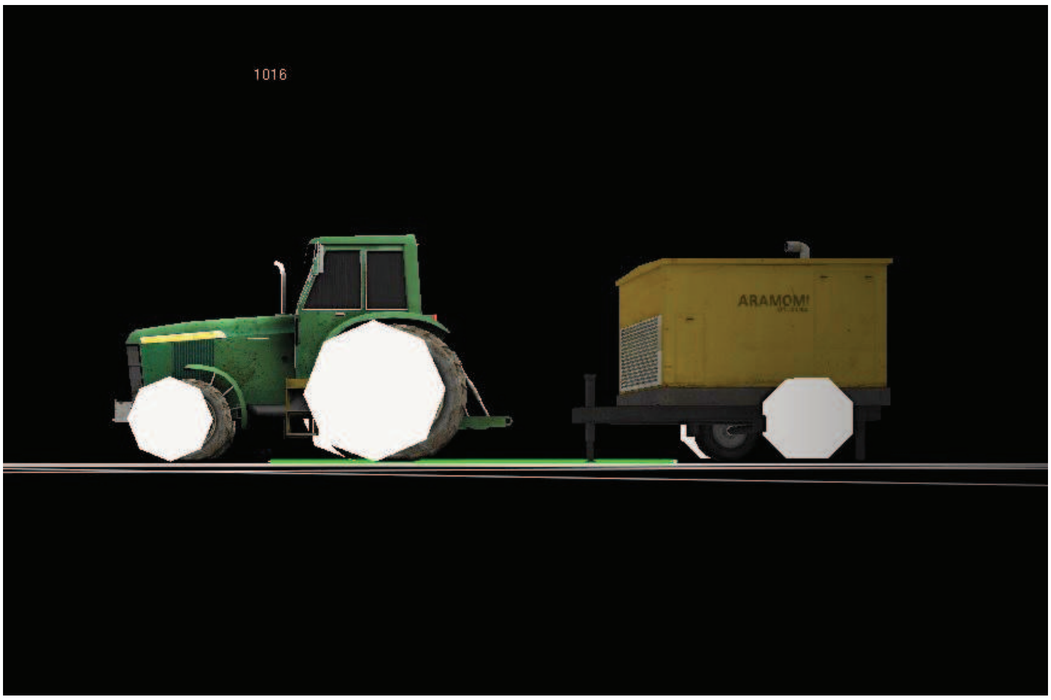

Fig. 4.2 The tractor-trailer model used in the dynamic simulation platform.

Table 4.2 Parameters for simulation

Parameters	Value
Tractor wheelbase l_t	1.70 m
Trailer wheelbase l_i	2.8 m
Hitch length c	0.88 m
Maximum steering angle of tractor $\delta_{t_{max}}$	$\pm 45°$
Maximum steering angle of trailer $\delta_{i_{max}}$	$\pm 45°$
Prediction horizon N_p	20
Control horizon N_c	4
Tuning parameter r_w	0.1

Figure 4.3 and Figure 4.4 show path offset and heading offset of the trailer. Path offset of No Controller and MPC were depicted in a blue solid line and a red solid line, respectively, while path offset of AMM-MPC is shown in a black solid line. Heading offsets of the three controllers are shown in a similar way. From Figure 4.5, very obviously, the performance of No controller was the worst, with the biggest value of path offset reaching almost 95 cm in the sharpest corner. In terms of performance of straight lines MPC is better than No Controller, almost the same as AMM-MPC, whereas AMM-MPC shows better performance than MPC when it comes to the curve segments which contains more significant slip. However, these two controllers showed the opposite by looking at Figure 4.4. This is because we chose the value of α is as twice as the value of γ, as in path tracking, path offset is a more important factor than heading offset. As a result, this controller is feasible for those agricultural applications where path offset plays a more important role than heading offset. However, for the wide implement like a boom sprayer, this controller needs further investigation.

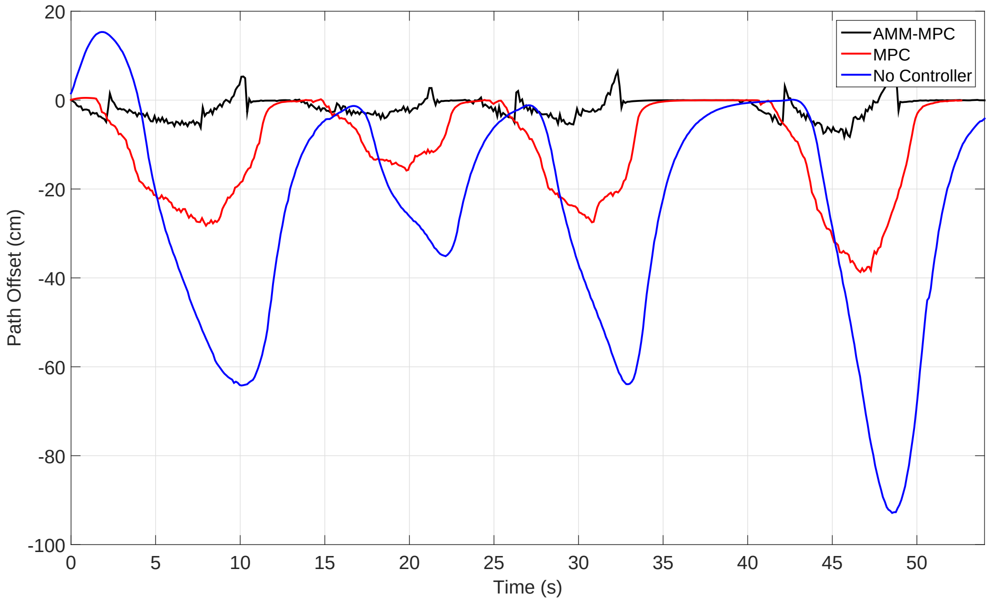

Fig. 4.3 Dynamic simulation: path offset comparison of the trailer among AMM-MPC, MPC and No Controller. AMM-MPC shows improvement in path offset, compared with other two controllers.

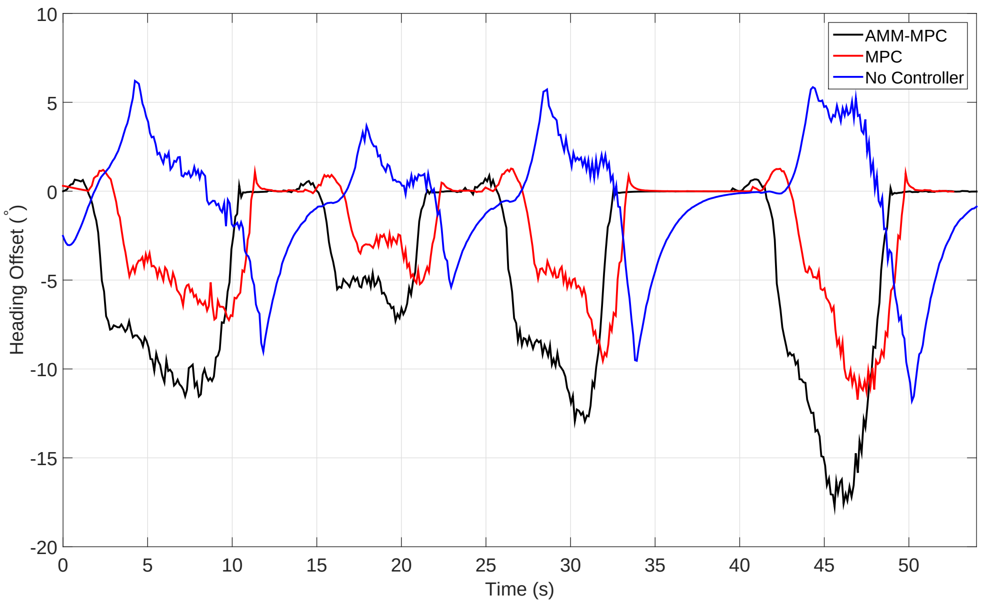

Fig. 4.4 Dynamic simulation: heading offset comparison of the trailer among AMM-MPC, MPC and No Controller.

To provide a better statistical quantitative comparison, box plots are shown for the absolute value of path offset and heading offset in Figure 4.5 and Figure 4.6, respectively. The plots confirmed the significant improvements brought about by the proposed AMM-MPC in the aspect of path following. The root mean square (RMS) values were listed in Table 4.3. The RMS of MPC was 15.15 cm while the RMS of AMM-MPC was 2.755 cm, showing significant improvement.

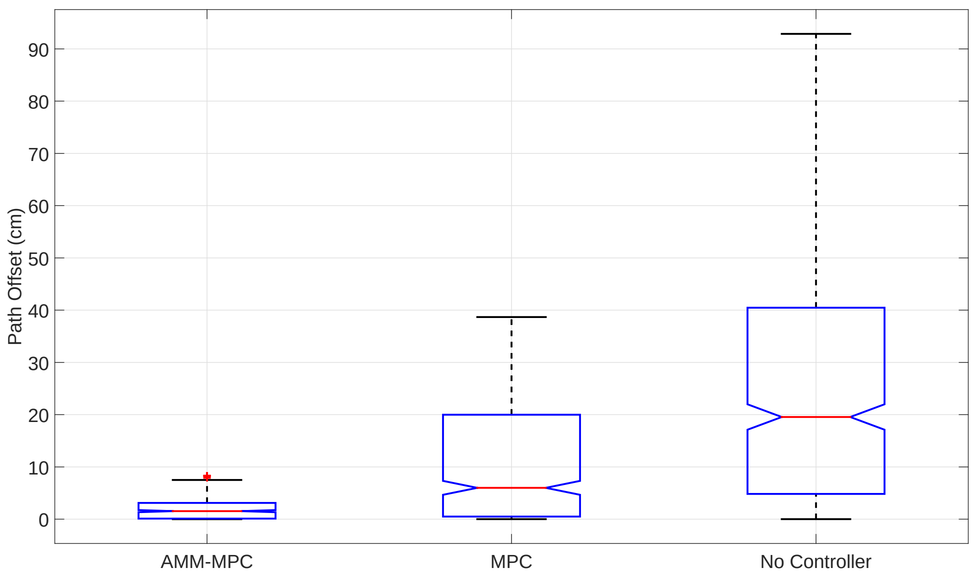

Fig. 4.5 Dynamic simulation: box plot of path offset comparison among AMM-MPC, MPC and No Controller. AMM-MPC shows improvement in path offset, compared with other two controllers.

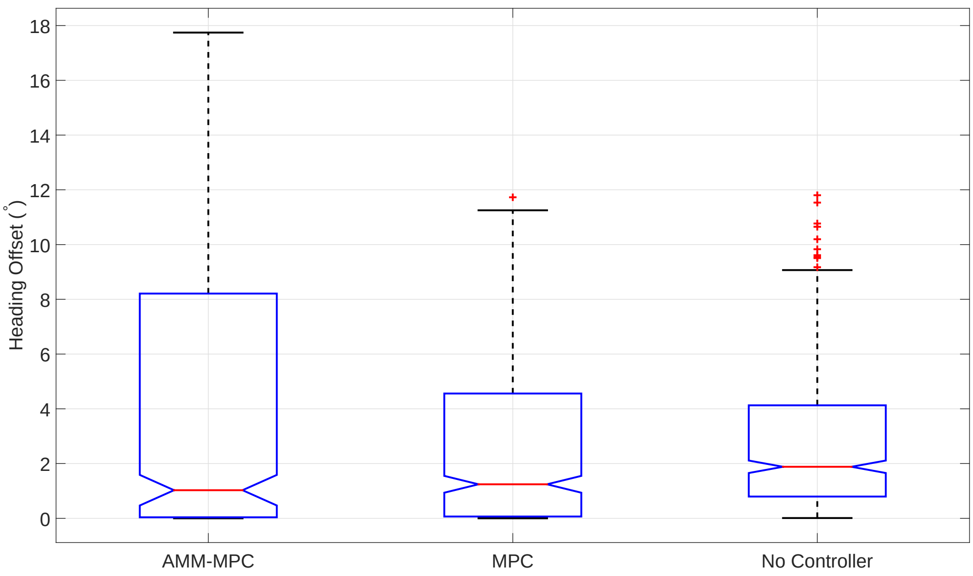

Fig. 4.6 Dynamic simulation: box plot of heading offset comparison among AMM-MPC, MPC and No Controller.

Table 4.3 RMS values of path offset.

Path Offset (cm)	No Controller	MPC	AMM-MPC
RMS	35.21	15.15	2.755

4.5 Summary

Given the superior performance of AMM-MPC in the preceding chapter, the AMM-MPC is extended and applied to a tractor-trailer system in this chapter with a view to achieve increased accuracy and robustness in the control of the trailer in autonomous farming. The controller for the tractor part is the same as the controller described in Chapter 3, while the controller for the trailer part is designed based on the linearised offset model of the trailer by using feedback linearisation. The proposed controller is validated by comparing its performance with the performance of the classical model predictive controller as well as the performance of the trailer in the absence of controller. Although the control of the trailer met more challenges due to the fact that the trailer is subject to more slip than the tractor, the AMM-MPC for the trailer still demonstrated a superior performance in its capability to deal with uncertain but bounded slip.

Chapter 5

AMM-MPC for Tracked Vehicle-trailer Path Tracking

In the previous two chapters, a 2WD2WS tractor is used as the leading vehicle in path tracking. Recently, the use of a tracked vehicle is on the increase as tracked vehicles have uniform weight distributions along the tracks which decrease the ground compaction. Moreover, the two tracks on both sides provide higher traction to weight ratios and robustness in comparison to a standard wheeled vehicle, for example a tractor. On the other side, this chapter further resolved the combination of two offsets by using an error angle model.

This chapter presents a path tracking control algorithm for a tracked vehicle pulling a steerable trailer by using an error angle model. In Section 5.1, kinematic models of the tracked vehicle as well as the trailer were presented, followed by error models of them. In Section 5.2, AMM-MPC for tracked vehicle-trailer the trailer was derived . In section 5.3, the proposed controller was verified in simulation and the results were discussed. Finally, this chapter was summarized in Section 5.4.

5.1 System Modelling and Description

5.1.1 Tracked vehicle

The schematic representation of the tracked vehicle-steerable trailer is shown in Figure 5.1, and related parameters are listed in Table 5.1. The tracked vehicle's states are described by a vector $\mathbf{p}_t = [x_t, y_t, \theta_t]^T$, where (x_t, y_t) is the position of the tracked vehicle in the XOY global coordinate and θ_t is the heading angle of the tracked vehicle. The tracked vehicle is controlled by two angular velocities ω_r and ω_l. The longitudinal velocity v and the angular velocity of the longitudinal axis ω are represented as,

$$\begin{aligned} v &= \frac{r}{2}(\omega_r + \omega_l), \\ \omega &= \frac{r}{b}(\omega_r - \omega_l), \end{aligned} \tag{5.1}$$

where r is the sprocket radius and b is the wheel base.

Then the kinematic equations in the presence of slip based on [72] are presented as,

$$\begin{aligned} \dot{x}_t &= v\cos\theta_t + v_{dx}, \\ \dot{y}_t &= v\sin\theta_t + v_{dy}, \\ \dot{\theta}_t &= \omega + \omega_d, \end{aligned} \tag{5.2}$$

where v_{dx}, v_{dy} and ω_d are slip parameters and described as,

$$\begin{aligned} v_{dx} = &-v\sin\theta_t\tan\alpha_t - \frac{r}{2}(\omega_r s_l + \omega_l s_r)\cos\theta_t \\ &+ \frac{r}{2}(\omega_r s_l + \omega_l s_r)\sin\theta_t\tan\alpha_t, \\ v_{dy} = &-v\cos\theta_t\tan\alpha_t - \frac{r}{2}(\omega_r s_l + \omega_l s_r)\sin\theta_t \\ &+ \frac{r}{2}(\omega_r s_l + \omega_l s_r)\cos\theta_t\tan\alpha_t, \\ \omega_d = &\frac{r}{b}(-\omega_r s_l + \omega_l s_r), \end{aligned} \tag{5.3}$$

where s_l, s_r and α_t are the longitudinal slip at right track, the longitudinal slip at left track and the side slip angle α_t. Note that slip at two tracks is unit-less.

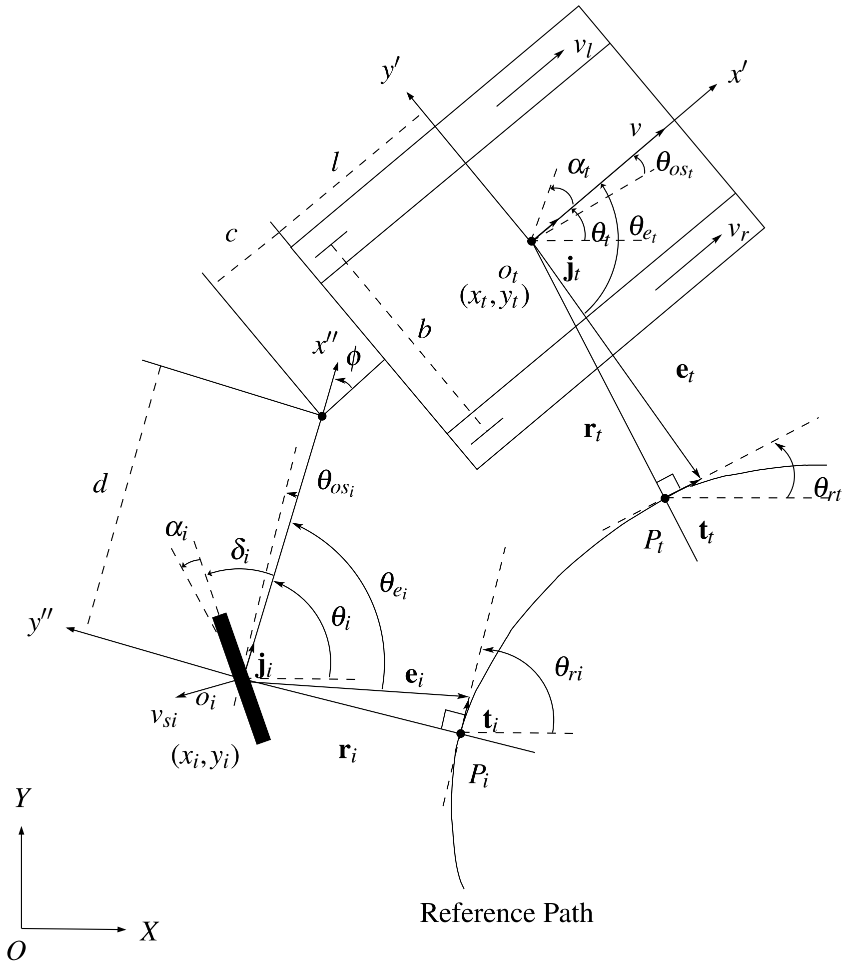

Fig. 5.1 Kinematic model of the tracked vehicle-trailer system

5.1.2 Steerable trailer

The steerable trailer is steered by rear wheels, the same as the trailer in last Chapter. The state of the trailer is described by a vector $\mathbf{q}_t = [x_i, y_i, \theta_i]^T$, where (x_i, y_i) is the position of the trailer in the global coordinate frame XOY and θ_i is the heading angle of the trailer in the global coordinate frame XOY. And the trailer is controlled by a steering angle δ_i. The

Table 5.1 Notations in the kinematic model.

Notations	Description for Tracked Vehicle
x_t, y_t	position of o_t in the XOY coordinate
θ_t	heading of the tracked vehicle in the XOY coordinate
v	longitudinal velocity at o_t
v_r	velocity at the right track
v_l	velocity at the left track
r	sprocket radius of tracked vehicle
ω_r / ω_l	sprocket angular velocity at the right/left track
s_r / s_l	longitudinal slip at the right/left track
α_t	side slip angle at o_t
b	wheel base of the tracked vehicle
l	half of track length
P_t	point at normal distance from o_t to the reference path
θ_{r_t}	desired heading angle for tracked vehicle
$\mathbf{j_t}$	unit vector in direction of tracked vehicle's heading
$\mathbf{t_t}$	unit vector aligned with tangent line to reference path at P_t
$\mathbf{r_t}$	path offset vector of the tracked vehicle
θ_{os_t}	heading offset of the tracked vehicle
$\mathbf{e_t}$	error vector of tracked vehicle
θ_{e_t}	error angle between $\mathbf{e_t}$ and $\mathbf{j_t}$ for tracked vehicle
Notations	**Description for Trailer**
x_i, y_i	position of o_i in the XOY coordinate
θ_i	heading of the trailer in the XOY coordinate
δ_i	steering angle of the trailer
ϕ	hitch angle
d	length of the trailer
c	hitch length
P_i	point at normal distance from o_i to the reference path
α_i	side slip angle at o_i
v_{si}	lateral slip velocity at o_i
θ_{r_i}	desired heading angle for the trailer
$\mathbf{j_i}$	unit vector in direction of the trailer's heading
$\mathbf{t_i}$	unit vector aligned with tangent line to the reference path at P_i
$\mathbf{r_i}$	path offset vector of the trailer
θ_{os_i}	heading offset of the trailer
$\mathbf{e_i}$	error vector of the trailer
θ_{e_i}	error angle between $\mathbf{e_i}$ and $\mathbf{j_i}$ for trailer

kinematic equations based on [10] are presented as,

$$\begin{aligned}
\dot{x}_i &= \dot{x}_t + \dot{\theta}_t \sin\theta_t + \dot{\theta}_i \sin\theta_i, \\
\dot{y}_i &= \dot{y}_t - \dot{\theta}_t \cos\theta_t - \dot{\theta}_i \cos\theta_i, \\
\dot{\theta}_i &= \frac{1}{n}(m_1 + m_2 + m_3' + m_4),
\end{aligned} \tag{5.4}$$

where

$$\begin{aligned}
n &= d\cos\delta_i, \\
m_1 &= -\frac{r}{2}\left[\omega_l(1-s_l) + \omega_r(1-s_r)\right]\sin(\delta_i + \phi), \\
m_2 &= \frac{r}{2}\left[\omega_l(1-s_l) + \omega_r(1-s_r)\right]\cos(\delta_i + \phi)\tan\alpha_t, \\
m_3' &= -c\cos(\delta_i + \phi)\dot{\theta}_t, \\
m_4 &= -v_{si}.
\end{aligned} \tag{5.5}$$

5.1.3 Virtual error vector model

Now, recalling the previous two chapters, the objective is to make path offset and heading offset as small as possible and two tuning parameters α and γ were used to decide which offset was playing an more important role during the control task. However, sometimes there may be a problem for choosing two parameter values and how to match them. As a result, there is a necessity to think about a method to solve this problem. In this Chapter, these two offset of each vehicle are combined to one offset which is an error angle based on [72]. In Figure 5.1, the error angle of the tracked vehicle is θ_{e_t} while the error angle of the trailer is θ_{e_i}. If the error angle is zero, it means that both path offset and heading offsets are zero.

As shown in Figure5.1, the vector $\mathbf{t_t}$ is a unit vector aligned with tangent line to the reference path at P_t and the vector $\mathbf{r_t}$ is the path offset the tracked vehicle with respect to the reference. Then, the vector e_t which is formed by $\mathbf{r_t}$ and $\mathbf{t_t}$ is the error vector of the tracked vehicle. Moreover, there is a vector $\mathbf{j_t}$ that is a unit vector in direction of tracked vehicle's heading. As a consequence, the angle between $\mathbf{e_t}$ and $\mathbf{j_t}$ is the error angle θ_{e_t}. If the error vector θ_{e_t} is zero, it means that both path offset $\mathbf{r_t}$ and heading offset θ_{os_t} are zero. In other words, the error angle shows the amount of error with respect to the reference path and the pose of the vehicle.

Then, two new virtual states related the error vector angle θ_{e_t} were defined,

$$\begin{aligned} x_{1_t} &= \int \frac{\theta_{e_t}}{k_t} dt, \\ x_{2_t} &= \frac{\theta_{e_t}}{k_t}, \end{aligned} \tag{5.6}$$

where k_t is a tuning parameter for the tracked vehicle.

Similarly, for the trailer two states are defined as same as (5.6)

$$\begin{aligned} x_{1_i} &= \int \frac{\theta_{e_i}}{k_i} dt, \\ x_{2_i} &= \frac{\theta_{e_i}}{k_i}, \end{aligned} \tag{5.7}$$

where k_i is a tuning parameter for the trailer.

Then, the state-space model of the tracked vehicle was obtained according to (5.6),

$$\begin{aligned} \dot{x}_{1_t} &= x_{2_t}, \\ \dot{x}_{2_t} &= \frac{1}{k_t}(\omega - \dot{\theta}_{t_t} + \omega_d), \end{aligned} \tag{5.8}$$

where k_t is a gain and the reference path is assumed as twice differentiable.

Similarly, virtual error vector model of the trailer was derived as follows,

$$\begin{aligned} \dot{x}_{1_i} &= x_{2_i}, \\ \dot{x}_{2_i} &= \frac{1}{k_i}(\mathfrak{T} - \dot{\theta}_{t_i} + \mathfrak{T}_d), \end{aligned} \tag{5.9}$$

where k_i is a gain, and

$$\begin{aligned}
\mathfrak{T} &= -\frac{v}{d}(\sin\phi + \tan\delta_i \sin\phi) - \frac{c\omega}{d}(\cos\phi - \tan\delta_i \sin\phi), \\
\mathfrak{T}_d &= \frac{1}{n}\big(m_2 + m_4 + \frac{r}{2}(\omega_l s_l + \omega_r s_r)\sin(\delta_i + \phi) - c\omega_d \cos(\delta_i + \phi)\big).
\end{aligned} \tag{5.10}$$

5.2 Control Design for Tracked Vehicle-trailer Path Tracking

In this section, AMM-MPC for tracked vehicle-trailer was derived based on [80]. Two state-space model (5.8) and (5.9) for the tracked vehicle and the trailer can be presented in a general form as

$$\begin{aligned}
\dot{\chi}_1 &= \chi_2, \\
\dot{\chi}_2 &= \mathfrak{u} + \mathfrak{h} + \mathfrak{h}_d,
\end{aligned} \tag{5.11}$$

where $\mathfrak{h}_d$ is the sum of disturbance, $\mathfrak{h}$ is the known parts in models and $\mathfrak{u}$ is the input to the system. In this case, for the tracked vehicle,

$$\begin{aligned}
\mathfrak{u} &= \frac{\omega}{k_t}, \\
\mathfrak{h} &= -\frac{\dot{\theta}_{t_t}}{k_t}, \\
\mathfrak{h}_d &= \frac{\omega_d}{k_t}.
\end{aligned} \tag{5.12}$$

Similarly, for the trailer,

$$\begin{aligned}
\mathfrak{u} &= \frac{\mathfrak{T}}{k_i}, \\
\mathfrak{h} &= -\frac{\dot{\theta}_{t_i}}{k_i}, \\
\mathfrak{h}_d &= \frac{\mathfrak{T}_d}{k_i}.
\end{aligned} \tag{5.13}$$

Then a vector $\mathbf{z} = [\chi_1 \ \chi_2]^T$ was defined and the model in (5.11) was discretised as,

$$\begin{aligned} \mathbf{z}_{k+1} &= \mathbf{A}_d \mathbf{z}_k + \mathbf{B}_d u_k + \mathbf{D}_d \mathbf{w}_k, \\ y_k &= \mathbf{C}_d \mathbf{z}_k, \end{aligned} \tag{5.14}$$

where $\mathbf{A}_d$, $\mathbf{B}_d$, $\mathbf{C}_d$, and $\mathbf{D}_d$ are matrices after discretisation.

Then, we convert the state-space model (5.14) to an augmented model with an embedded integrator based on [79]. We define $\Delta \mathbf{z}_k = \mathbf{z}_k - \mathbf{z}_{k-1}$, $\Delta u_k = u_k - u_{k-1}$, $\Delta \mathbf{w}_k = \mathbf{w}_k - \mathbf{w}_{k-1}$, and obtain the augmented model as

$$\begin{aligned} \begin{bmatrix} \Delta \mathbf{z}_{k+1} \\ y_{k+1} \end{bmatrix} &= \begin{bmatrix} \mathbf{A}_d & \mathbf{o}_d^T \\ \mathbf{C}_d \mathbf{A}_d & 1 \end{bmatrix} \begin{bmatrix} \Delta \mathbf{z}_k \\ y_k \end{bmatrix} + \begin{bmatrix} \mathbf{B}_d \\ \mathbf{C}_d \mathbf{B}_d \end{bmatrix} \Delta u_k + \begin{bmatrix} \mathbf{D}_d \\ \mathbf{C}_d \mathbf{D}_d \end{bmatrix} \Delta \mathbf{w}_k, \\ y_k &= \begin{bmatrix} \mathbf{o}_d & 1 \end{bmatrix} \begin{bmatrix} \Delta \mathbf{z}_k \\ y_k \end{bmatrix}, \end{aligned} \tag{5.15}$$

where $\mathbf{o}_d = [0 \ 0]$. To simplify, we define $\mathbf{x}_k = [\Delta \mathbf{z}_k^T \ y_k]^T$ and rewrite (5.15) as,

$$\begin{aligned} \mathbf{x}_{k+1} &= \mathbf{A}\mathbf{x}_k + \mathbf{B}\Delta u_k + \mathbf{D}\Delta \mathbf{w}_k, \\ y_k &= \mathbf{C}\mathbf{x}_k, \end{aligned} \tag{5.16}$$

where

$$\mathbf{A} = \begin{bmatrix} \mathbf{A}_d & \mathbf{o}_d^T \\ \mathbf{C}_d \mathbf{A}_d & 1 \end{bmatrix}, \mathbf{B} = \begin{bmatrix} \mathbf{B}_d \\ \mathbf{C}_d \mathbf{B}_d \end{bmatrix}, \mathbf{C} = \begin{bmatrix} \mathbf{o}_d & 1 \end{bmatrix}, \mathbf{D} = \begin{bmatrix} \mathbf{D}_d \\ \mathbf{C}_d \mathbf{D}_d \end{bmatrix}.$$

In (5.16), $\mathbf{x}_k \in \mathbb{R}^{3\times 1}$, $y_k \in \mathbb{R}^{1\times 1}$, $\Delta u_k \in \mathbb{R}^{1\times 1}$, $\Delta \mathbf{w}_k \in \mathbb{R}^{2\times 1}$ denote the state, the controlled output, the augmented control input and the external disturbances, respectively.

To obtain a convenient notation, we introduce vectors to denote future states $\mathbf{X}$, future outputs $\mathbf{Y}$, future control inputs $\Delta\mathbf{U}$ and unknown disturbances $\Delta\mathbf{W}$ as,

$$\begin{aligned}
\mathbf{X} &= \left(\mathbf{x}_{k+1|k}\ \mathbf{x}_{k+2|k}\ \mathbf{x}_{k+3|k}\ \cdots\ \mathbf{x}_{k+N_p|k}\right)^T \\
\mathbf{Y} &= \left(y_{k+1|k}\ y_{k+2|k}\ y_{k+3|k}\ \cdots\ y_{k+N_p|k}\right)^T \\
\Delta\mathbf{U} &= \left(\Delta u_{k|k}\ \Delta u_{k+1|k}\ \Delta u_{k+2|k}\ \cdots\ \Delta u_{k+N_c-1|k}\right)^T \\
\Delta\mathbf{W} &= \left(\Delta\mathbf{w}_{k|k}\ \Delta\mathbf{w}_{k+1|k}\ \Delta\mathbf{w}_{k+3|k}\ \cdots\ \Delta\mathbf{w}_{k+N_p-1|k}\right)^T.
\end{aligned}$$

Then, we can obtain,

$$\mathbf{Y} = \mathbf{F}\mathbf{x}_{k|k} + \mathbf{Q}\Delta\mathbf{U} + \mathbf{L}\Delta\mathbf{W}, \tag{5.17}$$

where

$$\mathbf{F} = \begin{bmatrix} \mathbf{CA} & \mathbf{CA}^2 & \mathbf{CA}^3 & \cdots & \mathbf{CA}^{N_p} \end{bmatrix}^T,$$

$$\mathbf{Q} = \begin{bmatrix} \mathbf{CB} & 0 & 0 & \cdots & 0 \\ \mathbf{CAB} & \mathbf{CB} & 0 & \cdots & 0 \\ \mathbf{CA}^2\mathbf{B} & \mathbf{CAB} & \mathbf{CB} & \cdots & 0 \\ \vdots & \vdots & \vdots & \ddots & \vdots \\ \mathbf{CA}^{N_p-1}\mathbf{B} & \mathbf{CA}^{N_p-2}\mathbf{B} & \mathbf{CA}^{N_p-3}\mathbf{B} & \cdots & \mathbf{CA}^{N_p-N_c}\mathbf{B} \end{bmatrix},$$

$$\mathbf{L} = \begin{bmatrix} \mathbf{CD} & 0 & 0 & \cdots & 0 \\ \mathbf{CAD} & \mathbf{CD} & 0 & \cdots & 0 \\ \mathbf{CA}^2\mathbf{D} & \mathbf{CAD} & \mathbf{CD} & \cdots & 0 \\ \vdots & \vdots & \vdots & \ddots & \vdots \\ \mathbf{CA}^{N_p-1}\mathbf{D} & \mathbf{CA}^{N_p-2}\mathbf{D} & \mathbf{CA}^{N_p-3}\mathbf{D} & \cdots & \mathbf{CD} \end{bmatrix}$$

Assumption 3 *The disturbance $\mathfrak{h}_d$ in the model (5.11) is bounded so that we have,*

$$sup||\mathfrak{h}_d|| \le \mathfrak{h}_d^*,\ \Delta\mathbf{w}_k \in \Delta\mathbf{w}_k^*,\ \Delta\mathbf{W} \in \Delta\mathbf{W}^*. \tag{5.18}$$

The cost function J can be represented as,

$$\begin{gathered}\min_{\Delta\mathbf{U}}\max_{\Delta\mathbf{W}}\ (\mathbf{R}_s-\mathbf{Y})^T(\mathbf{R}_s-\mathbf{Y})+\Delta\mathbf{U}^T\bar{\mathbf{R}}\Delta\mathbf{U}\ \text{ subject to}\\ \Delta\mathbf{U}\in\Delta\mathbf{U}^*,\ \Delta\mathbf{W}\in\Delta\mathbf{W}^*.\end{gathered}\tag{5.19}$$

where $\Delta\mathbf{U}^*$ is the constraint set, $\mathbf{Y}\in\mathbb{R}^{N_p\times 1}$ and $\Delta\mathbf{U}\in\mathbb{R}^{N_c\times 1}$. For path tracking, $\mathbf{R}_s$ is always set to 0, as the error vector angle is driven to zero. Moreover, the diagonal matrix $\bar{\mathbf{R}}$ is defined as $\bar{\mathbf{R}}=r_w\mathbf{I}_{Nc\times Nc}$ where $r_w\geq 0$ is a tuning parameter for penalizing the control input. However, $\Delta\mathbf{W}^*$ is normally taken as a constant matrix that corresponds to the worst case scenario, which will cause overcompensation in most cases as the worst case cannot occur all the time.

Then, $\Delta\mathbf{W}^*$ is defined as,

$$\Delta\mathbf{W}^*=\overbrace{[1\ 1\ \cdots\ 1]}^{N_p}{}^T(k_pc_d+k_q+k_o\theta_{e_t}),\tag{5.20}$$

where k_p is a value based on the worst case scenario when the curvature is not zero. The parameter k_q is a small constant at the worst case scenario representing zero curvature. The parameter k_o brings adaptive behaviour, which is based on the error vector angle.

Through minimization of J, the control trajectory vector $\Delta\mathbf{U}$ is obtained, however, only the first control increment $\Delta u_{k|k}$ is applied as per MPC method, while other control inputs are ignored. Therefore,

$$\Delta u_k=\overbrace{[1\ 0\ \cdots\ 0]}^{N_c}{}^T\Delta\mathbf{U}=-\mathbf{K}_1\mathbf{x}_k-K_2,\tag{5.21}$$

where

$$\begin{aligned}\mathbf{K}_1&=\overbrace{[1\ 0\ \cdots\ 0]}^{N_c}{}^T(\mathbf{Q}^T\mathbf{Q}+\bar{\mathbf{R}})^{-1}(\mathbf{Q}^\mathbf{T}\mathbf{F}),\\ K_2&=\overbrace{[1\ 0\ \cdots\ 0]}^{N_c}{}^T(\mathbf{Q}^T\mathbf{Q}+\bar{\mathbf{R}})^{-1}(\mathbf{Q}^T\mathbf{L}\Delta\mathbf{W}).\end{aligned}\tag{5.22}$$

Finally, ω_r and ω_l are calculated using the model in (5.1).

5.3 Simulation and Discussion

In Chapter 3, SMC and BSC have been chosen to compare with AMM-MPC for evaluation. However, BSC and SMC are both based on Lyapunov's function and might be considered as a repetition. In this simulation, BSC is replaced by Min-max MPC which is another inherently robust controller. Moreover, AMM-MPC is a method improved from Min-max MPC. As a result, in this section, AMM-MPC is compared with SMC and Min-max MPC inspired by [13].

In the simulation, the proposed AMM-MPC is used to control the tracked vehicle coupled to the steerable trailer to follow a predefined path. Vehicle slips are a result of inadequate reactionary forces exerted by the ground at the wheels. To simulate this realistic situation, a dynamic simulation environment incorporating the reactionary forces and the vehicle dynamic model was created based on [72] instead of the kinematic simulation environment. The performance of the controllers were investigated using the dynamic simulation environment in the presence of vehicle slips.

The reference path used in the simulation is shown in Figure 3.3. The parameters of the controllers and the vehicles are listed in Table 5.2. Note that parameter values come from the experimental model built at UNSW Mechatronics Lab.

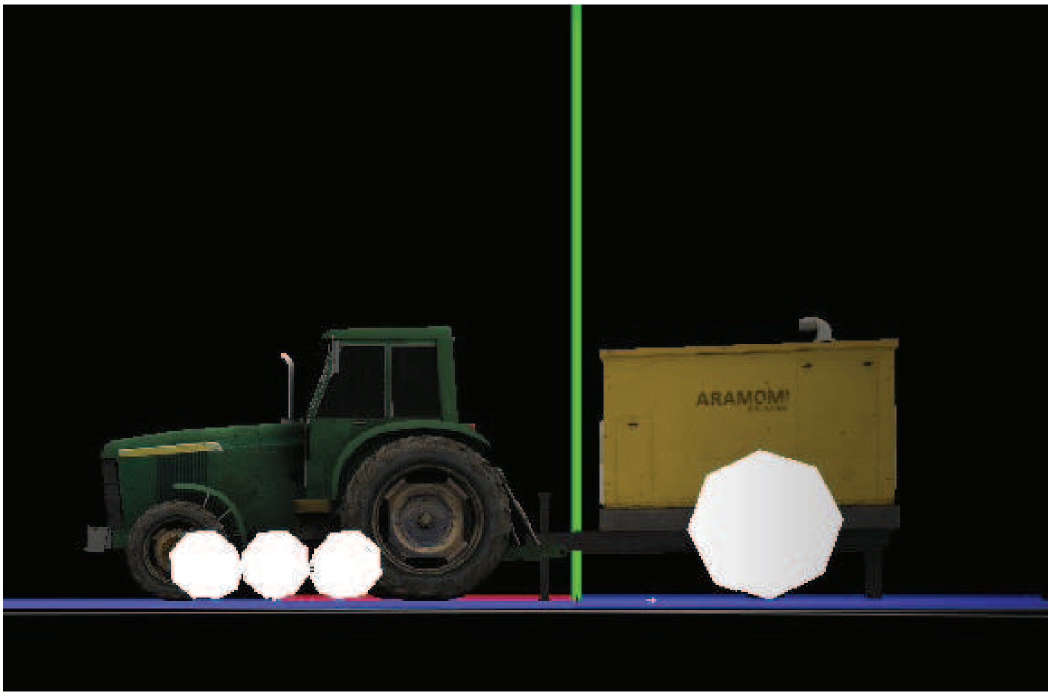

Fig. 5.2 The tracked vehicle-trailer model used in dynamic simulation platform [72].

Table 5.2 Parameters for simulation

Parameters	Value
Sprocket radius of the tracked vehicle r	0.25 m
Hitch length c	0.7 m
Wheel base of tracked vehicle b	2 m
Half of the tracked length l	0.86 m
Length of the trailer d	2 m
Virtual model tuning parameter k_t	1.03 m
Maximum angular velocity of the tracked vehicle ω_{max}	5.0 rad/s
Maximum steering angle of the trailer $\delta_{i_{max}}$	$\pm 22°$
Prediction horizon N_p	20
Control horizon N_c	4
Tuning parameter r_w	0.1

Figure 5.3 and Figure 5.4 show path offset and heading offset of the tracked vehicle. Path offset of Min-max MPC and SMC are depicted in a red dashed line and a blue dotted dashed line, respectively, while path offset of AMM-MPC is shown in black solid line. Heading offsets of the three controllers are shown in a similar way. In the path tracking of autonomous farming vehicles, path offset is a more important factor than heading offset. As seen in Figure 5.3, for path offsets, Min-max MPC shows overcompensation all the time except at curved segment 4 which is regarded as the worst case in the reference path. The path offset is about 10 cm for most of the path and it reaches 13 cm at curved segment 4. Meanwhile, AMM-MPC shows more accurate and robust performance than SMC, especially in the straight segments and curved segments 2,3, and 4. Path offset for AMM-MPC stays in an acceptable range with less than ± 4 cm during the curves while it is negligible during the straight segments. Moreover, in Figure 5.4, Min-max MPC and AMM-MPC show almost the same performance in heading offsets, while SMC provides relatively better heading offset accuracy. In general, SMCs are good and reliable robust nonlinear controllers, and they are widely used in path tracking controllers [70]. As a result, AMM-MPC brings the best performance, when we consider that path offset plays a more important role.

Similarly, the trailer's path offsets and heading offsets for three different controllers (Min-max MPC, SMC, and AMM-MPC) are shown in Figure 5.5 and Figure 5.6, respectively. The path offset accuracy of AMM-MPC is still better than those of SMC and Min-max MPC. The path offsets for AMM-MPC are less than 6 cm during the curve segments and are insignificant during the straight segments while the path offsets for the other two controllers grew over 11 cm. For heading offset, the three controllers showed very similar performance. As mentioned for the case of the tracked vehicle, during path tracking control by the trailer, path offset accuracy is more important than heading offset.

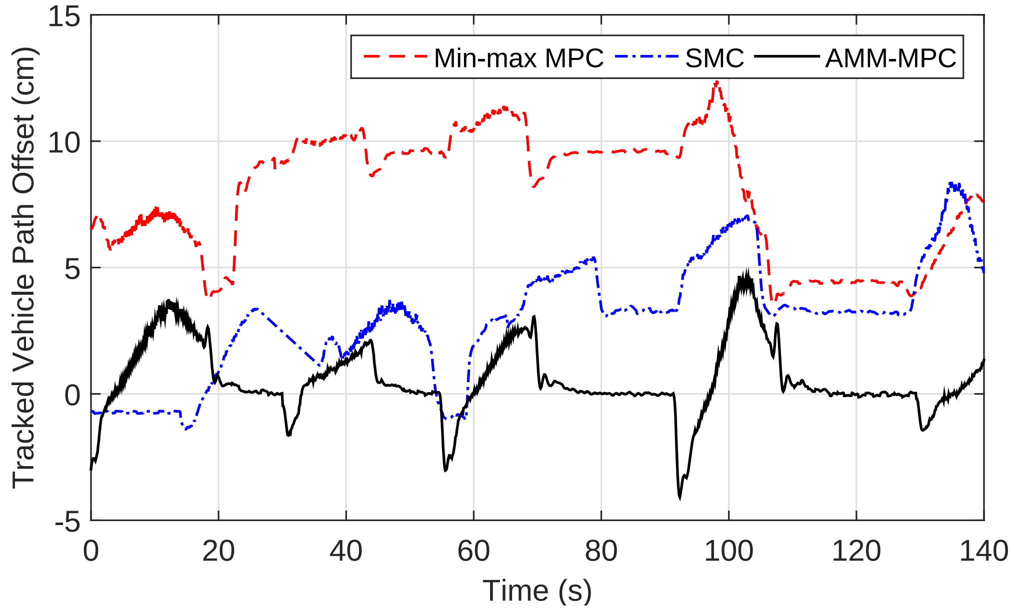

Fig. 5.3 Dynamic simulation: path offset comparison of the tracked vehicle among Min-max MPC, SMC, and AMM-MPC.

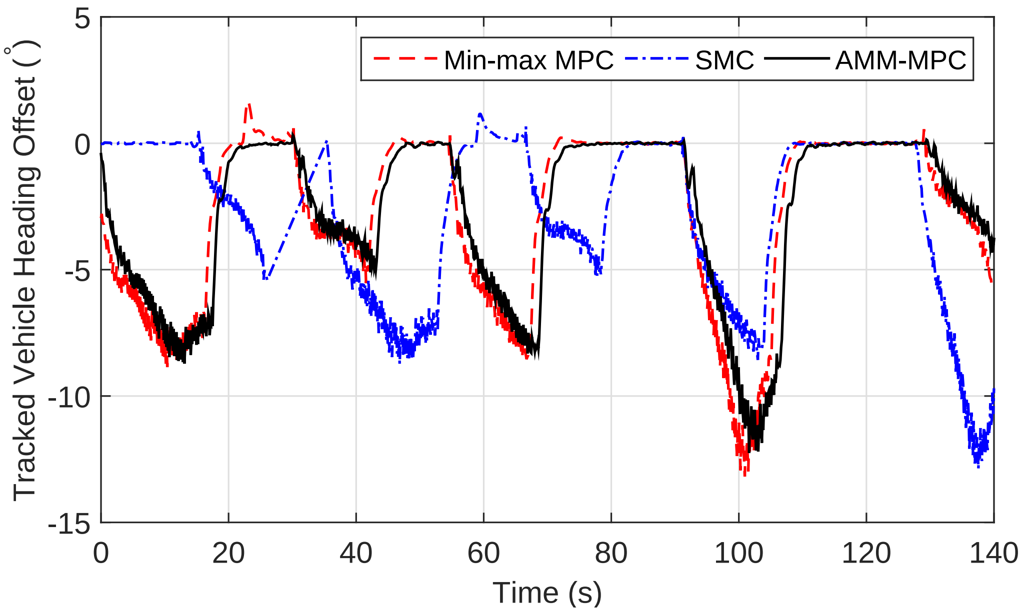

Fig. 5.4 Dynamic simulation: heading offset comparison of the tracked vehicle among Min-max MPC, SMC, and AMM-MPC.

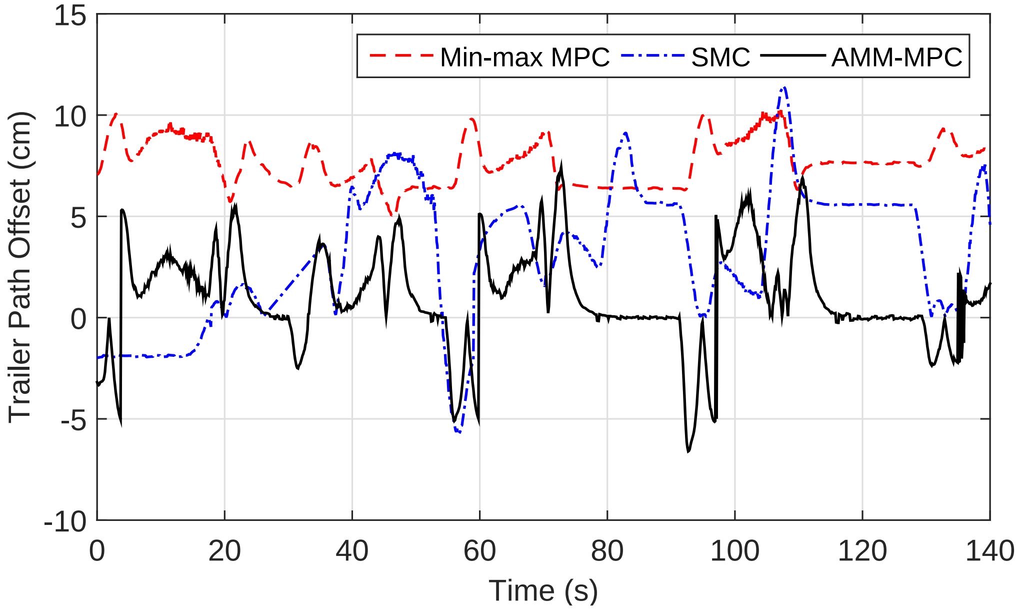

Fig. 5.5 Dynamic simulation: path offset comparison of the trailer among Min-max MPC, SMC, and AMM-MPC.

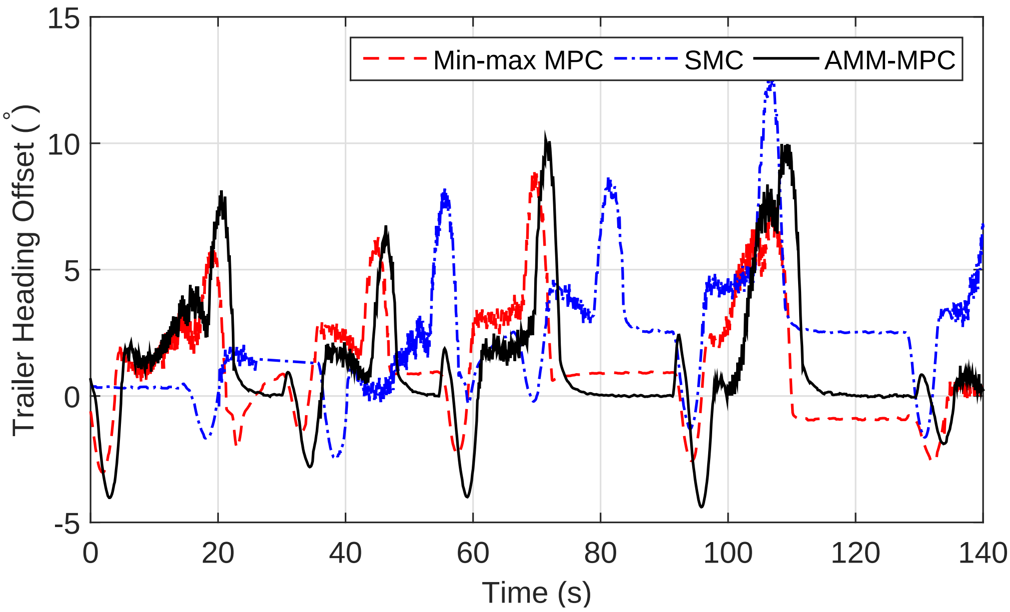

Fig. 5.6 Dynamic simulation: heading offset comparison of the trailer among Min-max MPC, SMC, and AMM-MPC.

To provide a better statistical quantitative comparison, box plots are shown for the absolute value of path offsets of the tracked vehicle and the trailer in Figure 5.7 and 5.8, respectively. The plots confirmed the significant improvements brought about by the proposed AMM-MPC.

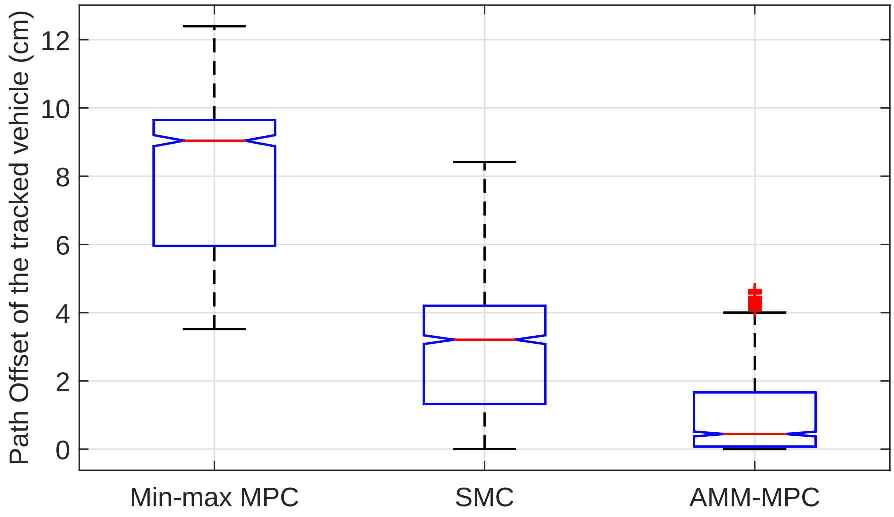

Fig. 5.7 Dynamic simulation: box plot of path offset comparison of the tracked vehicle among Min-max MPC, SMC, and AMM-MPC.

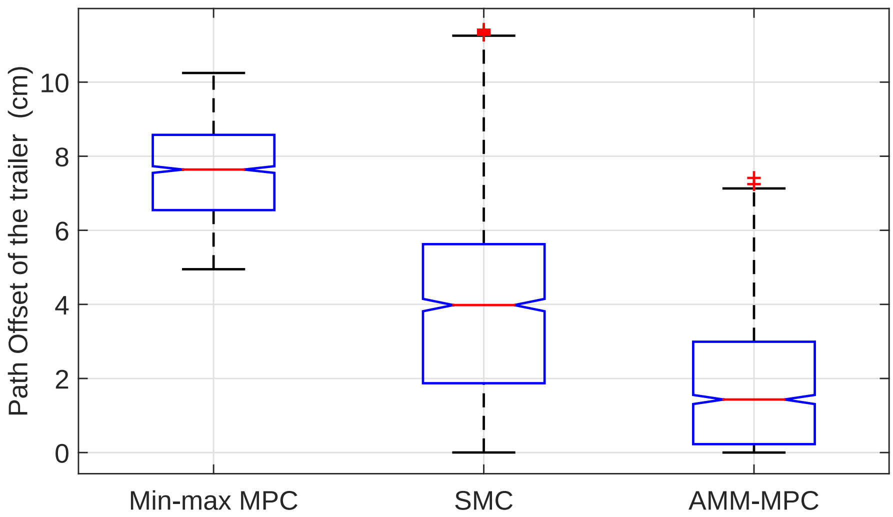

Fig. 5.8 Dynamic simulation: box plot of path offset comparison of the trailer among Min-max MPC, SMC, and AMM-MPC.

5.4 Summary

This chapter proposes a robust and adaptive MPC controller for path tracking control of a tracked vehicle pulling a steerable trailer in the presence of slip. Compared with min-max MPC and SMC, the proposed controller presents a superior improvement in its capability to deal with uncertain but bounded slip. The stability analysis is also presented and proved using the terminal state criteria. Then, instead of kinematic simulation, a more realistic dynamic simulation platform was used to evaluate the performance of the proposed controller that is compared with min-max MPC and SMC. The results obtained show significant improvements in the accuracy in path tracking for the tracked vehicle as well as the trailer, especially at the segments with higher curvatures, where slips are greater than slips for the straight segments. On the other hand, the AMM-MPC design for the tracked vehicle-trailer system is developed by only changing some parameters with respect to previous two chapters. This proves that AMM-MPC can be applied in a lot of systems and only needs small changes.

Chapter 6

Conclusion

The final chapter begins with a summary of major contributions presented in this thesis, followed by suggestion of future work.

6.1 Major Contributions

Wheel slip has been a significant issue in path tracking of UAGVs. The challenge of this problem is that UAGVs are affected by the high-level uncertainties and disturbances of the farmland when UAGVs traverse through the field. Therefore, this requires the controller to perform both robustly and accurately. An accurate vehicle model with slip accounted will also assist the controller to improve performance significantly. This thesis has mainly addressed the wheel slip problem in path tracking control of UAGVs, including UAGVs modelling, control design, kinematic as well as dynamic simulation and field experiments. The key contributions in this thesis are listed as follows:

- A novel robust model predictive control for UAGVs guidance in the presence of significant slip was proposed to guarantee both robustness and accuracy. One of the novelties lies on the receding min-max optimization which minimizes the worst case scenario of the path tracking. The worst case is characterized as curvature-varying since the slip in the straight path is far less significant than slip in the curve path. Based on above, a very novel and promising adaptive min-max model predictive controller for path tracking control of farm vehicles in the presence of slip was proposed in Chapter 3. This new controller not only maintains the good performance in straight paths that can be achieved by classical MPC but also improves the performance in curved paths affected by significant slip. Another contribution of this controller is that AMM-MPC dealt with wheel slip adaptively without requiring slip measurement or estimation, but solely by utilizing the bound of slip.

- The kinematic model-based controller was tested in dynamic simulation and field experiments. In the kinematic simulation, the condition that slip considered as velocity was not true in the real world. Thus, the proposed controller was validated in more realistic platforms, dynamic and field experiments where slip occurs in the form of slip forces. Moreover, in field experiments, the proposed controller was not only compared with classical MPC but also with two other well-performing robust controllers - SMC and BSC through which the superiority of the performance based on the proposed controller has been achieved. Finally, all conditions such as terrain and path used in the second experiment were set the same as they were in the commercial application of seeding.

- The proposed controller can be used in three typical farm vehicles and expected to be extended to many applications. The proposed controller can be easily applied in tractor, tractor-trailer, tracked vehicle-trailer by simply changing some related parameters, which brings UAGVs close to commercialization in the farm system worldwide. According to different farm tasks, the type of farm vehicle can be chosen. The controller can be applied to both the leading vehicle and the implement, which significantly improves the precision farming as it is usually the implement which carries out farming tasks. Besides above, the proposed controller is expected to be used in other applications such as mining and defence using the results obtained in this thesis.

- The linearisation of highly nonlinear kinematic models is simple but proved to be very effective with appropriate assumptions. Also, the derivation of the augmented model with disturbances in model predictive control was presented in detail and made it more understandable to the reader.

6.2 Future Work

The suggestions of future work are given as follows:

- The controller designed in this thesis only requires the farm vehicle to follow the reference path in a geometric way so this controller is not available for some farm work which requires the vehicle to move to a specific position with a specific timing law, such as trajectory tracking. However, such task is not easy because the speed keeps changing while tracking the reference path.

References

[1] Al-Mayyahi, A., Wang, W., and Birch, P. (2015). Path tracking of autonomous ground vehicle based on fractional order PID controller optimized by PSO. In *2015 IEEE 13th International Symposium on Applied Machine Intelligence and Informatics (SAMI)*, pages 109–114.

[2] Arimoto, S. (1984). Stability and robustness of pid feedback control for robot manipulators of sensory capability. In *Robotics Research, 1st Int. Symp.*, pages 783–799. MIT Press.

[3] Arnold, M. and Andersson, G. (2011). Model predictive control of energy storage including uncertain forecasts. In *Power Systems Computation Conference (PSCC), Stockholm, Sweden*.

[4] Astolfi, A., Bolzern, P., and Locatelli, A. (2004). Path-tracking of a tractor-trailer vehicle along rectilinear and circular paths: a lyapunov-based approach. *Robotics and Automation, IEEE Transactions on*, 20(1):154–160.

[5] Astrand, B. and Baerveldt, A. J. (2005). A vision based row-following system for agricultural field machinery. *Mechatronics*, 15(2):251–269.

[6] Backman, J., Oksanen, T., and Visala, A. (2009). Parallel guidance system for tractor-trailer system with active joint. In *7^{th} European Conference on Precision Agriculture, Wageningen, Netherlands, July 6-8*, pages 615–622.

[7] Backman, J., Oksanen, T., and Visala, A. (2010). Nonlinear model predictive trajectory control in tractor-trailer system for parallel guidance in agricultural field operations. *Agricontrol 2010*.

[8] Bagnell, J. A., Bradley, D., Silver, D., Sofman, B., and Stentz, A. (2010). Learning for autonomous navigation. *Robotics & Automation Magazine, IEEE*, 17(2):74–84.

[9] Bouvet, D. and Garcia, G. (2000). Improving the accuracy of dynamic localization systems using rtk gps by identifying the gps latency. In *Proceedings 2000 ICRA. Millennium Conference. IEEE International Conference on Robotics and Automation. Symposia Proceedings (Cat. No.00CH37065)*, volume 3, pages 2525–2530 vol.3.

[10] Briquet-Kerestedjian, N., Taghia, J., and Katupitiya, J. (2014). Derivation of error models incorporating slippage for a tracked vehicle coupled to a steerable trailer. In *2014 IEEE/ASME International Conference on Advanced Intelligent Mechatronics*, pages 1054–1060.

[11] Bushnell, L. G., Tilbury, D. M., and Sastry, S. S. (1995). Steering three-input nonholonomic systems. the fire truck example. *International Journal of Robotics Research*, 14(4):366–381.

[12] Campion, G., Bastin, G., and Dandrea-Novel, B. (1996). Structural properties and classification of kinematic and dynamic models of wheeled mobile robots. *IEEE Transactions on Robotics and Automation*, 12(1):47–62.

[13] Campo, P. J. and Morari, M. (1987). Robust model predictive control. In *American Control Conference*, pages 1021–1026. IEEE.

[14] Corradini, M. and Orlando, G. (2002). Control of mobile robots with uncertainties in the dynamical model: a discrete time sliding mode approach with experimental results.

Control Engineering Practice, 10(1):23 – 34. Modelling and Control in Biomedical Systems.

[15] DeSantis, R. (1994). Path-tracking for a tractor-trailer-like robot: Communication. *The International Journal of Robotics Research*, 13(6):533–544.

[16] DeSantis, R. M., Bourgeot, J. M., Todeschi, J. N., and Hurteau, R. (2002). Path-tracking for tractor-trailers with hitching of both the on-axle and the off-axle kind. In *Proceedings of the IEEE Internatinal Symposium on Intelligent Control*, pages 206–211.

[17] Duff, E. S., Roberts, J. M., and Corke, P. I. (2003). Automation of an underground mining vehicle using reactive navigation and opportunistic localization. In *Intelligent Robots and Systems, 2003.(IROS 2003). Proceedings. 2003 IEEE/RSJ International Conference on*, volume 4, pages 3775–3780. IEEE.

[18] Eaton, R., Katupitiya, J., Pota, H., and Siew, K. W. (2009). Robust sliding mode control of an agricultural tractor under the influence of slip. In *Advanced Intelligent Mechatronics, 2009. AIM 2009. IEEE/ASME International Conference on*, pages 1873–1878. IEEE.

[19] Eaton, R., Katupitiya, J., Siew, K., and Dang, K. (2008a). Precision guidance of agricultural tractors for autonomous farming. In *2nd Annual IEEE Systems Conference, Montreal, Canada*, pages 1–8.

[20] Eaton, R., Katupitiya, J., Siew, K. W., and Howarth, B. (2008b). Autonomous farming: Modeling and control of agricultural machinery in a unified framework. In *2008 15th International Conference on Mechatronics and Machine Vision in Practice*, pages 499–504.

[21] Fang, H. (2004). Automatic guidance of farm vehicles in presence of sliding effects. A scientific report for the post-doc research project of all-terrain autonomous vehicle control, Le LASMEA.

[22] Fang, H., Fan, R., Thuilot, B., and Martinet, P. (2006). Trajectory tracking control of farm vehicles in presence of sliding. *Robotics and Autonomous Systems*, 54(10):828–839. cited By (since 1996) 23.

[23] Fao, U. et al. (2009). How to feed the world in 2050. In *Rome: High-Level Expert Forum*.

[24] Gan-Mor, S., Clark, R. L., and Upchurch, B. L. (2007). Implement lateral position accuracy under rtk-gps tractor guidance. *Computers and Electronics in Agriculture*, 59(1–2):31 – 38.

[25] Garcia, C. E., Prett, D. M., and Morari, M. (1989). Model predictive control: theory and practice-—a survey. *Automatica*, 25(3):335–348.

[26] Garcia, O., Ferreira, J. V., and Neto, A. M. (2014). Design and simulation for path tracking control of a commercial vehicle using mpc. In *Proceedings of the 2014 Joint Conference on Robotics: SBR-LARS Robotics Symposium and Robocontrol*, SBR-LARSROBOCONTROL '14, pages 61–66, Washington, DC, USA. IEEE Computer Society.

[27] Grüne, L. and Pannek, J. (2011). *Nonlinear Model Predictive Control: Theory and Algorithms*. Communications and Control Engineering. Springer, 1st ed. edition.

[28] Ha, Q., Rye, D., and Durrant-Whyte, H. (1999). Fuzzy moving sliding mode control with application to robotic manipulators. *Automatica*, 35(4):607 – 616.

[29] Han, G., Chen, L., Shao, J., and Sun, Z. (2005). Study of fuzzy pid controller for industrial steam turbine governing system. In *IEEE International Symposium on Communications and Information Technology, 2005. ISCIT 2005.*, volume 2, pages 1275–1279.

[30] Huynh, V., Katupitiya, J., Kwok, N., and Eaton, R. (2010). Derivation of an error model for tractor-trailer path tracking. In *Intelligent Systems and Knowledge Engineering (ISKE), 2010 International Conference on*, pages 60 –66.

[31] Huynh, V., Smith, R., Kwok, N. M., and Katupitiya, J. (2012). A nonlinear PI and backstepping-based controller for tractor-steerable trailers influenced by slip. In *International Conference on Robotics and Automation, IEEE*, pages 245–252.

[32] Kalmari, J., Backman, J., and Visala, A. (2014). Nonlinear model predictive control of hydraulic forestry crane with automatic sway damping. *Computers and Electronics in Agriculture*, 109(Complete):36–45.

[33] Keymasi Khalaji, A. and Moosavian, S. A. A. (2015). Adaptive sliding mode control of a wheeled mobile robot towing a trailer. *Proceedings of the Institution of Mechanical Engineers, Part I: Journal of Systems and Control Engineering*, 229(2):169–183.

[34] Khalil, H. K. (2002). *Nonlinear Systems*. Prentice Hall, Upper Saddle River, New Jersey, 3rd edition.

[35] Kokotović, P. and Arcak, M. (2001). Constructive nonlinear control: A historical perspective. *Automatica*, 37(5):637–662.

[36] Kothare, M., Balakrishnan, V., and Morai, M. (1994). Robust constrained model predictive control using linear matrix inequalities. In *American Control Conference, 1994*, volume 1, pages 440–444 vol.1.

[37] Krstic, M., Kokotovic, P. V., and Kanellakopoulos, I. (1995). *Nonlinear and Adaptive Control Design, first ed.* John Wiley & Sons, Inc., New York, NY, USA.

[38] Kuhne, F., Lages, W. F., and da Silva Jr, J. M. G. (2004). Model predictive control of a mobile robot using linearization. In *Proceedings of mechatronics and robotics*, pages 525–530.

[39] Kumar, V., Nakra, B., and Mittal, A. (2011). A review on classical and fuzzy pid controllers. *International Journal of Intelligent Control and Systems*, 16(3):170–181.

[40] Langson, W., Chryssochoos, I., Raković, S., and Mayne, D. Q. (2004). Robust model predictive control using tubes. *Automatica*, 40(1):125–133.

[41] Lenain, R., Thuilot, B., Cariou, C., and Martinet, P. (2003). Adaptive control for car like vehicles guidance relying on rtk gps: rejection of sliding effects in agricultural applications. In *2003 IEEE International Conference on Robotics and Automation (Cat. No.03CH37422)*, volume 1, pages 115–120 vol.1.

[42] Lenain, R., Thuilot, B., Cariou, C., and Martinet, P. (2004). Non-linear control for car like mobile robots in presence of sliding: Application to guidance of farm vehicles using a single rtk gps.

[43] Lenain, R., Thuilot, B., Cariou, C., and Martinet, P. (2005). Model predictive control for vehicle guidance in presence of sliding: application to farm vehicles path tracking. In *International Conference on Robotics and Automation, IEEE*, pages 885–890.

[44] Lenain, R., Thuilot, B., Cariou, C., and Martinet, P. (2006). High accuracy path tracking for vehicles in presence of sliding: Application to farm vehicle automatic guidance for agricultural tasks. *Autonomous Robots*, 21(1):79–97.

[45] Löfberg, J. (2003). *Minimax approaches to robust model predictive control, PhD thesis*. Linköping University.

[46] Madani, T. and Benallegue, A. (2006). Backstepping control for a quadrotor helicopter. In *Intelligent Robots and Systems, 2006 IEEE/RSJ International Conference on*, pages 3255–3260. IEEE.

[47] MAILONLINE, T. Y. F. (2017). Meet 'little orange', the cutest warehouse worker: Self-charging robots can sort 20,000 parcels an hour at a chinese courier firm. *Daily Mail*.

[48] Marsland, S., Nehmzow, U., and Shapiro, J. (2005). On-line novelty detection for autonomous mobile robots. *Robotics and Autonomous Systems*, 51(2):191–206.

[49] Martins-Filho, L. S. and Macau, E. E. (2007). Trajectory planning for surveillance missions of mobile robots. In *Autonomous Robots and Agents*, pages 109–117. Springer.

[50] Matveev, A. S., Hoy, M., Katupitiya, J., and Savkin, A. V. (2013). Nonlinear sliding mode control of an unmanned agricultural tractor in the presence of sliding and control saturation. *Robotics and Autonomous Systems*, 61(9):973 – 987.

[51] Micaelli, A. and Samson, C. (1993). Trajectory tracking for unicycle-type and two-steering-wheels mobile robots. INRIA Technical Report No. 2097.

[52] Morari, M. and Lee, J. H. (1999). Model predictive control: past, present and future. *Computers & Chemical Engineering*, 23(4):667–682.

[53] Normey-Rico, J. E., Alcalá, I., Gómez-Ortega, J., and Camacho, E. F. (2001). Mobile robot path tracking using a robust {PID} controller. *Control Engineering Practice*, 9(11):1209 – 1214. {PID} Control.

[54] OConnor, M., Bell, T., Elkaim, G., and Parkinson, B. (1996). Automatic steering of farm vehicles using gps.

[55] Palacin, J., Salse, J. A., Valganon, I., and Clua, X. (2004). Building a mobile robot for a floor-cleaning operation in domestic environments. *IEEE Transactions on Instrumentation and Measurement*, 53(5):1418–1424.

[56] Peng, S.-T., Sheu, J.-J., and Chang, C.-C. (2004). A control scheme for automatic path tracking of vehicles subject to wheel slip constraint. In *Proceedings of the 2004 American Control Conference*, volume 1, pages 804–809 vol.1.

[57] Qin, S. J. and Badgwell, T. A. (2003). A survey of industrial model predictive control technology. *Control Engineering Practice*, 11(7):733–764.

[58] Richalet, J. (1993). Industrial applications of model based predictive control. *Automatica*, 29(5):1251–1274.

[59] Richards, A. and How, J. (2004). A decentralized algorithm for robust constrained model predictive control. In *American Control Conference, 2004. Proceedings of the 2004*, volume 5, pages 4261–4266. IEEE.

[60] Richards, A. and How, J. (2005). Robust model predictive control with imperfect information. In *American Control Conference, 2005. Proceedings of the 2005*, pages 268–273. IEEE.

[61] Ridley, P. and Corke, P. (2003). Load haul dump vehicle kinematics and control. *Journal of Dynamic Systems, Measurement and Control, Transactions of the ASME*, 125(1):54–59.

[62] Roberts, J. M., Duff, E. S., and Corke, P. I. (2002). Reactive navigation and opportunistic localization for autonomous underground mining vehicles. *Information Sciences*, 145(1–2):127 – 146.

[63] Rocco, P. (1996). Stability of pid control for industrial robot arms. *IEEE Transactions on Robotics and Automation*, 12(4):606–614.

[64] Rozali, S. M., Rahmat, M., Wahab, N. A., Ghazali, R., and Zulfatman (2010). Pid controller design for an industrial hydraulic actuator with servo system. In *2010 IEEE Student Conference on Research and Development (SCOReD)*, pages 218–223.

[65] Ryu, J.-C., Agrawal, S. K., and Franch, J. (2008). Motion planning and control of a tractor with a steerable trailer using differential flatness. *Journal of Computational and Nonlinear Dynamics*, 3(3):031003.

[66] Samson, C. (1993). Mobile robot control part 2: control of chained systems and application to path following and time-varying point-stabilization of wheeled vehicles. INRIA Technical Report No. 1994.

[67] Scokaert, P. and Mayne, D. (1998). Min-max feedback model predictive control for constrained linear systems. *IEEE Transactions on Automatic Control*, 43(8):1136–1142.

[68] Slotine, J. and Li, W. (1991). *Applied Nonlinear Control*. Prentice Hall.

[69] Taghia, J. and Katupitiya, J. (2013a). A sliding mode controller with disturbance observer for a farm vehicle operating in the presence of wheel slip. In *Advanced Intelligent Mechatronics (AIM), 2013 IEEE/ASME International Conference on*, pages 1534–1539.

[70] Taghia, J. and Katupitiya, J. (2013b). A sliding mode controller with disturbance observer for a farm vehicle operating in the presence of wheel slip. In *Advanced Intelligent Mechatronics (AIM), 2013 IEEE/ASME International Conference on*, pages 1534–1539. IEEE.

[71] Taghia, J. and Katupitiya, J. (2013c). Wheel slip identification and its use in the robust control of articulated off-road vehicles. In *International Conference on Robotics and Automation, IEEE, Sydney, Australia*.

[72] Taghia, J., Lam, S., and Katupitiya, J. (2015a). Path following control of an off-road track vehicle towing a steerable driven implement. In *Advanced Intelligent Mechatronics (AIM), 2015 IEEE International Conference on*, pages 713–718. IEEE.

[73] Taghia, J., Wang, X., Lam, S., and Katupitiya, J. (2015b). A sliding mode controller with a nonlinear disturbance observer for a farm vehicle operating in the presence of wheel slip. *Autonomous Robots*, pages 1–18.

[74] Thuilot, B., Cariou, C., Cordesses, L., and Martinet, P. (2001). Automatic guidance of a farm tractor along curved paths, using a unique cp-dgps. In *Proceedings 2001 IEEE/RSJ International Conference on Intelligent Robots and Systems. Expanding the Societal Role of Robotics in the the Next Millennium (Cat. No.01CH37180)*, volume 2, pages 674–679 vol.2.

[75] Thuilot, B., Cariou, C., Martinet, P., and Berducat, M. (2002). Automatic guidance of a farm tractor relying on a single cp-dgps. *Autonomous robots*, 13(1):53–71.

[76] Van Henten, E., Hemming, J., Van Tuijl, B., Kornet, J., Meuleman, J., Bontsema, J., and Van Os, E. (2002). An autonomous robot for harvesting cucumbers in greenhouses. *Autonomous Robots*, 13(3):241–258.

[77] Van Henten, E., Van Tuijl, B. v., Hemming, J., Kornet, J., Bontsema, J., and Van Os, E. (2003). Field test of an autonomous cucumber picking robot. *Biosystems engineering*, 86(3):305–313.

[78] Volos, C., Kyprianidis, I., and Stouboulos, I. (2012). A chaotic path planning generator for autonomous mobile robots. *Robotics and Autonomous Systems*, 60(4):651 – 656.

[79] Wang, L. (2009). *Model predictive control system design and implementation using MATLAB®*. London: Springer-Verlag.

[80] Wang, X., Taghia, J., and Katupitiya, J. (2016). Robust model predictive control for path tracking of a tracked vehicle with a steerable trailer in the presence of slip. *IFAC-PapersOnLine*, 49(16):469 – 474. 5th {IFAC} Conference on Sensing, Control and Automation Technologies for Agriculture {AGRICONTROL} 2016Seattle, WA, USA, 14—17 August 2016.

[81] Werner, R., Muller, S., and Kormann, K. (2012). Path tracking control of tractors and steerable towed implements based on kinematic and dynamic modeling. In *11^{th} International Conference on Precision Agriculture, Indianapolis, Indiana, USA*, pages 15—18.

[82] Yaonan, W., Yimin, Y., Xiaofang, Y., Feng, Y., and Shuning, W. (2010). A model predictive control strategy for path-tracking of autonomous mobile robot using electromagnetism-like mechanism. In *International Conference on Electrical and Control Engineering, IEEE*, pages 96–100.

[83] Yu, X. and Kaynak, O. (2009). Sliding-mode control with soft computing: A survey. *IEEE Transactions on Industrial Electronics*, 56(9):3275–3285.

[84] z. Li, L., y. Sun, L., and Zhang, S. (2013). Direct fuzzy backstepping control for turbine main steam valve. In *Proceedings of 2013 IEEE International Conference on Vehicular Electronics and Safety*, pages 171–174.

Appendix A

Stability Analysis

The stability is proven using Lyapunov criterion based on the approach in [79].

Theorem 1 *Given that the cost function J is minimized subjected to $\Delta\mathbf{U} \in \Delta\mathbf{U}^*$ and the constraint on the final output $y_{k+N_p} = 0$ resulting from the control inputs $\Delta u_k, ...\Delta u_{k+N_p-1}$, the closed loop MPC system is asymptotically stable.*

Proof: From Subsection 3.4.3, we know that AMM-MPC is realized by receding optimization. The future control trajectory $\Delta u_k, ...\Delta u_{k+N_p-1}$ at time k is optimized by minimizing the cost function J_k, represented as,

$$J_k = \sum_{i=1}^{N_p} y_{k+i}^T y_{k+i} + \sum_{i=0}^{N_p-1} \Delta u_{k+i}^T r_w \Delta u_{k+i}, \tag{A.1}$$

where J_k is subjected to constraints and $r_w \geq 0$ is a gain.

Now, we assume the Lyapunov function $V(x_k)$ is equal to the minimum of the cost function J_k with the optimal control trajectory $\Delta u_k, ..., \Delta u_{k+N_p-1}$ and corresponding outputs

$y_{k+1},...,y_{k+N_p}$, represented as,

$$\begin{aligned} V(x_k) &= \min J_k \\ &= \sum_{i=1}^{N_p} y_{k+i}^T y_{k+i} + \sum_{i=0}^{N_p-1} \Delta u_{k+i}^T r_w \Delta u_{k+i}. \end{aligned} \tag{A.2}$$

The Lyapunov function $V(x_k)$ at sampling instant k is positive definite and $V(x_k)$ is infinite if x_k is infinite. Similar to $V(x_k)$, the Lyapunov function $V(x_{k+1})$ at time $k+1$ is the minimum of the cost function J_{k+1} with the optimal control trajectory $\Delta u_{k+1},...,\Delta u_{k+N_p}$ and corresponding outputs $y_{k+2},...,y_{k+N_p+1}$, represented as,

$$V(x_{k+1}) = \sum_{i=1}^{N_p} y_{k+1+i}^T y_{k+1+i} + \sum_{i=0}^{N_p-1} \Delta u_{k+1+i}^T r_w \Delta u_{k+1+i}. \tag{A.3}$$

Now a function $\bar{V}$ will be introduced to relate $V(x_k)$ to $V(x_{k+1})$. The optimal control trajectory of $V(x_k)$ is shifted one step forward and its last control input Δu_{k+N_P} is set to zero.

The function $\bar{V}$ is formed by evaluating $V(x_{k+1})$ at the above mentioned time shifted control trajectory, which is a non-optimal control trajectory. For any non-optimal control trajectory the objective function has to be greater or equal to $V(x_{k+1})$. Therefore,

$$V(x_{k+1}) \leq \bar{V}. \tag{A.4}$$

Based on (5.16), $\bar{V}$ has the same control trajectory with $V(x_k)$ at sampling times $k+1, k+2,\ ...\ , k+N_p-1$, thus

$$V(x_{k+1}) - V(x_k) \leq \bar{V} - V(x_k), \tag{A.5}$$

then

$$\bar{V} - V(x_k) = y_{k+N_p}^T y_{k+N_p} - y_{k+1}^T y_{k+1} - \Delta u_k^T r_w \Delta u_k. \tag{A.6}$$

Given that as per Theorem 1, $y_{k+N_p} = 0$,

$$\bar{V} - V(x_k) = -y_{k+1}^T y_{k+1} - \Delta u_k^T r_w \Delta u_k. \tag{A.7}$$

Therefore, the derivative of the Lyapunov function is,

$$V(x_{k+1}) - V(x_k) \leqslant -y_{k+1}^T y_{k+1} - \Delta u_k^T r_w \Delta u_k < 0. \tag{A.8}$$

This proves the asymptotic stability of the closed-loop system.